Coulter

AEDC-TR-80-11

Missile Motion Sensitivity to Dynamic Stability Derivatives

T. F. Langham
ARO, Inc.

September 1980

Final Report for Period October 1, 1978 – September 30, 1979

ARNOLD ENGINEERING DEVELOPMENT CENTER
ARNOLD AIR FORCE STATION, TENNESSEE
AIR FORCE SYSTEMS COMMAND
UNITED STATES AIR FORCE

NOTICES

When U. S. Government drawings, specifications, or other data are used for any purpose other than a definitely related Government procurement operation, the Government thereby incurs no responsibility nor any obligation whatsoever, and the fact that the Government may have formulated, furnished, or in any way supplied the said drawings, specifications, or other data, is not to be regarded by implication or otherwise, or in any manner licensing the holder or any other person or corporation, or conveying any rights or permission to manufacture, use, or sell any patented invention that may in any way be related thereto.

Qualified users may obtain copies of this report from the Defense Technical Information Center.

References to named commerical products in this report are not to be considered in any sense as an indorsement of the product by the United States Air Force or the Government.

This report has been reviewed by the Office of Public Affairs (PA) and is releasable to the National Technical Information Service (NTIS). At NTIS, it will be available to the general public, including foreign nations.

APPROVAL STATEMENT

This report has been reviewed and approved.

ALVIN R. OBAL, Captain, CF
Project Manager
Directorate of Technology

Approved for publication:

FOR THE COMMANDER

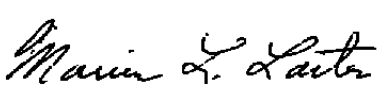

MARION L. LASTER
Director of Technology
Deputy for Operations

REPORT DOCUMENTATION PAGE		READ INSTRUCTIONS BEFORE COMPLETING FORM
1 REPORT NUMBER AEDC-TR-80-11	2. GOVT ACCESSION NO.	3 RECIPIENT'S CATALOG NUMBER
4 TITLE (and Subtitle) MISSILE MOTION SENSITIVITY TO DYNAMIC STABILITY DERIVATIVES		5 TYPE OF REPORT & PERIOD COVERED Final Report-October 1, 1978 to September 30,1979 6 PERFORMING ORG. REPORT NUMBER
7 AUTHOR(s) T. F. Langham, ARO, Inc., a Sverdrup Corporation Company		8 CONTRACT OR GRANT NUMBER(s)
9 PERFORMING ORGANIZATION NAME AND ADDRESS Arnold Engineering Development Center/DO Air Force Systems Command Arnold Air Force Station, TN 37389		10. PROGRAM ELEMENT, PROJECT, TASK AREA & WORK UNIT NUMBERS Program Element 62602F
11 CONTROLLING OFFICE NAME AND ADDRESS AFATL/DLJ Eglin Air Force Base, Florida 32542		12 REPORT DATE September 1980 13 NUMBER OF PAGES 110
14 MONITORING AGENCY NAME & ADDRESS(if different from Controlling Office)		15. SECURITY CLASS. (of this report) UNCLASSIFIED 15a DECLASSIFICATION/DOWNGRADING SCHEDULE N/A

16 DISTRIBUTION STATEMENT (of this Report)

Approved for public release; distribution unlimited.

17. DISTRIBUTION STATEMENT (of the abstract entered in Block 20, if different from Report)

18 SUPPLEMENTARY NOTES

Available in Defense Technical Information Center (DTIC)

19 KEY WORDS (Continue on reverse side if necessary and identify by block number)

dynamics	degrees of freedom	turning flight
derivatives (mathematics)	computer program	
sensitivity	static stability	
configurations	level flight	

20 ABSTRACT (Continue on reverse side if necessary and identify by block number)

A dynamic derivative sensitivity study was conducted to demonstrate the importance of dynamic derivatives in missile motion simulation studies. Generalized bank-to-turn and yaw-to-turn missile configurations were used with a six-degree-of-freedom linearized stability program. The effects of various dynamic derivatives on missile stability were investigated in both level and turning flight for several Mach numbers and altitude

DD FORM 1 JAN 73 1473 EDITION OF 1 NOV 65 IS OBSOLETE

20. ABSTRACT (Continued)

conditions. The results presented in a root locus format show that the longitudinal and lateral-directional dynamic moment derivatives C_{m_q}, $C_{m_{\dot{\alpha}}}$, C_{n_r}, C_{ℓ_p}, C_{ℓ_r}, and C_{n_p} may significantly alter the respective longitudinal and lateral-directional stability modes. Also shown is the significant coupling effect between the longitudinal and lateral-directional motions resulting from variations in the cross-coupling derivatives C_{ℓ_q}, C_{n_q}, and C_{m_p}. The force and moment derivatives C_{L_q}, $C_{L_{\dot{\alpha}}}$, C_{y_r}, C_{y_p}, and C_{m_r} are shown to have little or no effect on the missile stability modes and, therefore, are not considered important to motion simulation studies.

PREFACE

The work reported herein was conducted by the Arnold Engineering Development Center (AEDC), Air Force Systems Command (AFSC) . The results of this research were obtained by ARO, Inc., AEDC Group (a Sverdrup Corporation Company), operating contractor for the AEDC, AFSC, Arnold Air Force Station, Tennessee, under ARO Project No. P34F-31A. The research was sponsored by the Air Force Armament Laboratory. Analysis of the data was completed on September 30, 1979, and the manuscript was submitted for publication on February 1, 1980.

CONTENTS

ILLUSTRATIONS

Figure

Figure | Page

Figure Page

TABLES

APPENDIX

1.0 INTRODUCTION

Interest in highly maneuverable, aerodynamically controlled missiles has increased in recent years. Evaluation of mission capability for missiles of this category relies primarily on the missile aerodynamics. It is well known that the missile static aerodynamics are predominant in a mission analysis; what is not known is the importance of the dynamic derivatives in such an analysis. It is necessary to define the effects of these parameters so that in the future, an experimental test apparatus may be designed for their measurement and so that accurate simulations can be performed.

This subject analysis documents the effects of only those dynamic derivatives that may significantly affect the motion of highly maneuverable missiles. The derivatives investigated are the direct derivatives C_{m_q}, $C_{m_{\dot{\alpha}}}$, C_{L_q}, $C_{L_{\dot{\alpha}}}$, C_{ℓ_p}, C_{n_r}, and C_{y_r}; the cross derivatives C_{ℓ_r}, C_{n_p}, and C_{y_p}; and the cross-coupling derivatives C_{ℓ_q}, C_{n_q}, C_{m_p}, and C_{m_r}. The missile configurations used for the investigation are representative of the conventional yaw-to-turn and bank-to-turn missiles. The sensitivity of each configuration is documented with respect to derivative variations Root loci, time response, and damping ratio plots are used.

2.0 METHOD OF ANALYSIS

The sensitivity of flight vehicle motion to variations in aerodynamic and physical characteristics is reflected in the longitudinal and lateral-directional stability modes. The two longitudinal modes are short period and phugoid, and the three lateral-directional modes are roll, spiral, and dutch roll. Linearized analysis of geometrically and aerodynamically symmetric air vehicles in wings-level, nonrotating flight without sideslip does not require more than a three-degree-of-freedom program since the longitudinal and lateral-directional perturbations are truly uncoupled. However, for asymmetric geometry and nonzero-rotational rates, the perturbations from the reference conditions are all coupled. In many cases, the degree of coupling may be small; hence, a three-degree-of-freedom analysis would be adequate, but when an attempt is made to determine the actual effect of the cross-coupling between the longitudinal and lateral-directional motions, a six-degree-of-freedom analysis is required.

The Arbitrary Degree of Freedom (ADOF) computer program was modified to provide initial trim required for level and steady turning flight conditions. The program is applicable to flight vehicles either with or without feedback control systems and can be used for any set of degrees of freedom. The equations of motion and data input routines used in the program are of a general nature and are not restricted by assuming a symmetric vehicle or an equilibrium reference condition.

The modes of motion are represented by the roots of the characteristic equation formed by linearization of the six equations of motion.

Initially, all dynamic derivatives under investigation were individually assigned a value of unity and then varied over a predetermined range. All other pertinent parameters were maintained at the required trim values. The stability characteristics were recalculated for each assigned value of the derivative, thereby mapping the effects on the five primary modes of motion.

3.0 TECHNICAL DATA

3.1 MISSILE CONFIGURATIONS

Two missile configurations were selected for the dynamic derivative sensitivity study — a conventional yaw-to-turn and a bank-to-turn configuration. The selection of a specific missile for each configuration was made on the basis of current configuration design trends and available wind tunnel data.

For the bank-to-turn missile, one of the early Interlab Air-to-Air Technology (ILAAT) designs was selected and is shown in Fig. 1, along with representative full-scale dimensional characteristics. The basic configurational components consisted of nose, body, wing, and fins. The body makes a smooth transition from circular to an increasing elliptic cross section to a constant elliptical main body.

A general research model known as the Aerodynamic Data Correlation (ADC) missile was selected for the yaw-to-turn configuration. Representative full-scale dimensional characteristics are given in Fig. 2. The ADC model consists of an ogive nose section and a cylindrical body with aft mounted cruciform fins.

3.2 AERODYNAMIC DATA

3.2.1 General

The rigid-body aerodynamic data are input to the stability axis system. Data are given in table look-up form as functions of the variables shown in the equations of the Appendix. All aerodynamic coefficients for both missile configurations are referenced to body cross-sectional area and diameter.

3.2.2 Wind Tunnel Measurements

The static aerodynamic data matrices used in modeling both missile configurations were obtained from wind tunnel tests at AEDC. The static data for the bank-to-turn configuration (Fig. 1) were obtained for the Mach number range from 0.8 to 3.5 and for an angle of attack of up to 26 deg. The static data matrices for the yaw-to-turn configuration (Fig. 2) were formulated from data obtained in previous study at AEDC. The matrices include data for Mach numbers from 0.6 to 3.0 and for an angle of attack from -6 through 26 deg.

The matrices for the dynamic aerodynamic data for the yaw-to-turn configuration were formulated from data presented in Refs. 1 and 2 and in other work at AEDC. These matrices include data in the Mach number range from 0.6 to 3.0 and in the angle-of-attack range from -6 through 26 deg. The roll damping characteristics are documented in Refs. 1 and 2, and pitch and yaw damping have been documented.

3.2.3 Estimated

The dynamic stability characteristics for the bank-to-turn configuration have not been determined experimentally. Several prediction methods were reviewed for estimating flight vehicle dynamic derivatives. Both semi-empirical (Ref. 3) and unsteady panel methods (Ref. 4) were reviewed. For the methods available, a semi-empirical method known as the USAF Stability and Control Datcom (Ref. 3) appeared to be the most extensive and easiest to implement. A portion of Datcom (Digital Datcom; see Ref. 5) was used in estimating the bank-to-turn dynamic stability derivatives. The Mach number and angle-of-attack ranges for which the derivatives were estimated were, respectively, from 0.8 to 3.5 and from -6 to 26 deg. It should be noted that Datcom is valid only for the attached flow regime (low angle of attack).

The missile configuration of Fig. 1 was geometrically modified to conform to the restraints of the Digital Datcom computer code. In the Digital Datcom, flight vehicles are modeled with the use of body, wing, horizontal, and vertical tail input data. Therefore, for the computer program, fins 3 and 4 of the missile of Fig. 1 were modeled as the horizontal control surfaces, while the areas of fins 1 and 2 (also of Fig. 1), were combined as one upper vertical surface. In addition, the wing, horizontal, and vertical tail were modeled as straight tapered planforms rather than double delta planforms.

4.0 RESULTS AND DISCUSSION

4.1 GENERAL

The dynamic stability analyses for the bank-to-turn and yaw-to-turn missile configurations were conducted in trimmed level and steady turning flight. Turning flight conditions were used to simulate the missiles in maneuvering flight regime. The turning flight condition provides larger values of the angular rate terms (p, q, and r), thereby giving the aerodynamic cross-coupling moments larger values in the linearized equations of motion. This turning flight condition provides a means for ascertaining the importance of the second-order cross-coupling derivative terms.

The dynamic derivative sensitivity studies were conducted with use of flight envelopes representative of both missile categories. The specific Mach number, altitude, and g flight conditions at which the investigations were conducted are shown in Fig. 3. The trimmed flight conditions shown for each Mach number and altitude are 1-g-level, an intermediate g, and a maximum g. The maximum g at each Mach number and altitude was limited only by the control surface authority and by the maximum angle of attack of the data matrix. Tables 1 and 2 summarize the aerodynamics used for the missile flight conditions. Table 3 gives the mass, inertia, and geometric characteristics used to represent the full-scale bank-to-turn and yaw-to-turn missiles.

Figure 4 gives the range for varying the dynamic derivatives plus the associated maximum and minimum values measured in the wind tunnel and estimated by Digital Datcom. Both the direct and cross derivative ranges were arbitrarily selected at approximately twice the maximum of the measured and estimated derivatives. The range for the cross-coupling derivatives was chosen to correspond to the range for the cross derivatives. Experimental results obtained by Orlik-Ruckemann (Ref. 6) with use of a cone wing model have shown that the cross-coupling derivatives combined with the acceleration derivatives ($C_{m_{\dot{\beta}}}$, $C_{n_{\dot{\alpha}}}$, and $C_{\ell_{\dot{\alpha}}}$) approach and/or exceed those of the cross derivatives for high angles of attack. It should be noted that the dynamic derivatives for the yaw-to-turn configuration were experimentally obtained as a combination of the rate and acceleration terms (e.g., $C_{n_r} - C_{n_{\dot{\beta}}} \cos \alpha$). In the sensitivity study, these combination derivative values were used as pure rate terms.

The root locus format shown in Fig. 5 demonstrates the primary method used to show the effect of derivative variations on the vehicle modes of motion. The resultant roots (eigenvalues) of the characteristic equation are plotted in the root locus format shown as the derivatives are varied. The real part of the root represents the damping ratio, whereas the

imaginary part represents the frequency of oscillation (radian/sec). The time required for each mode to damp to one half or to diverge to double amplitude is shown below each plot; the motion period is shown vertically. The roots of the characteristic equation may be either real (aperiodic) or complex (oscillatory) and either stable or unstable.

4.2 BANK-TO-TURN CONFIGURATION

The dynamic derivative sensitivity analysis was conducted for altitudes of 10,000 and 40,000 ft for Mach numbers of 0.8., 1.1, and 3.5 for load factors of up to 25 g. The low Mach number flight conditions correspond to initial maneuvers after launch, whereas the high Mach number corresponds to supersonic terminal flight conditions.

4.2.1 Dynamic Direct Derivative Variations

Longitudinal. The missile motion sensitivity to variations in the direct rate and acceleration derivatives C_{m_q} and $C_{m_{\dot{\alpha}}}$ is shown in Figs. 6 and 7, respectively. The range ($\pm$ 1,000 per radian) for which the derivatives were varied was at least twice the magnitude of that obtained from Digital Datcom (see Fig. 4). The influences of altitude and load factor (g's) on the missile's sensitivity to derivative variations are presented for each Mach number. As previously noted, the maximum g's available at each Mach number are limited by the control surface authority and angle-of-attack limit. Only the short period, S/P, mode shows sensitivity to variations in the pitching moment caused by the C_{m_q} and $C_{m_{\dot{\alpha}}}$ derivatives. The sensitivity in the short period mode at each Mach number is essentially unaffected by the load factor, g; there is, however, a significant effect of Mach number on sensitivity of the short period mode with C_{m_q} and $C_{m_{\dot{\alpha}}}$ variations. The short period mode is less sensitive to C_{m_q} and $C_{m_{\dot{\alpha}}}$ variations at 40,000 ft than at 10,000 ft. The reduced sensitivity is primarily due to the reduction in density with increased altitude.

The motion sensitivity to the force derivatives C_{L_q} and $C_{L_{\dot{\alpha}}}$ is shown in Fig. 8. The longitudinal and lateral-directional modes of motion were totally insensitive to variations in either C_{L_q} or $C_{L_{\dot{\alpha}}}$ over the range of $\pm$ 500 per radian.

Figures 9 and 10 demonstrate, respectively, the influence of variations in C_{m_q} and $C_{m_{\dot{\alpha}}}$ on the vehicle damping ratio and motion response characteristics at Mach 3.5 and 10,000-ft altitude for a 10-g banked turn. Figures 9a and 10a show the sensitivity of the short period and damping ratio, Z, with variations in C_{m_q} and $C_{m_{\dot{\alpha}}}$ over the range of $\pm$ 1,000 per radian. As can be observed in the root locus plots, the short period damping ratio is quite sensitive to variations in C_{m_q} and $C_{m_{\dot{\alpha}}}$. The time response shown in figures 9b and 10b results from a pitch control doublet and characterizes the changes in the short period motion for three

values each for both C_{m_q} and $C_{m_{\dot{\alpha}}}$. The changes in the pitch rate response to a unit doublet in pitch control are shown for values of C_{m_q} and $C_{m_{\dot{\alpha}}}$ corresponding to the trim values, values near the point at which the short period is neutrally stable, and values near the maximum or minimum for the experimental ranges shown in Fig. 4. The changes in the time response, again, indicate the senstivity of the short period motion to the direct derivatives C_{m_q} and $C_{m_{\dot{\alpha}}}$ and quantify the significance of the root migration with derivative variation shown in Figs. 6 and 7.

Lateral-Directional. The missile motion sensitivity to variations ($\pm$ 1,000 per radian) in the direct damping derivative in yaw, C_{n_r}, is shown in Fig. 11. The only significant motion senstivity to C_{n_r} is in the dutch roll mode of motion. The sensitivity in the dutch roll mode due to C_{n_r} increases with increasing load factor (g's) for all Mach numbers at each altitude.

The effects of variations ($\pm$ 1,000 per radian) in the direct roll damping derivative, C_{ℓ_p}, on the longitudinal and lateral-directional modes of motion are shown in Fig. 12. Only the lateral-directional modes are shown here for clarity; the longitudinal modes were insensitive to C_{ℓ_p} variations.

The extreme sensitivity of both the roll and dutch roll modes to variations in C_{ℓ_p} is associated with the low moment of inertia, I_x, about the roll axis. The sensitivity in the dutch roll mode due to C_{ℓ_p} variations increases with increasing load factor (g's) for all Mach numbers at each altitude. For large negative values of C_{ℓ_p}, the dutch roll mode may migrate from a periodic spiral to a roll-spiral coupling (lateral phugoid) to, finally, an aperiodic mode at large positive values. This sensitivity is made apparent by tracing the dutch roll root migration at Mach 0.8 and 40,000-ft altitude for a 5-g banked turn. The roll mode is extremely sensitive to relatively small changes in C_{ℓ_p} as can be seen by tracing the roll root migration at M = 3.5 and altitude = 10,000 ft for 1-g level flight. The sensitivity in the roll mode due to C_{ℓ_p} increases with increasing Mach number but decreases with increasing altitude and load factor. The roll and dutch roll modes are more sensitive to the same magnitude variations in C_{ℓ_p} than to variations in C_{n_r}; this greater sensitivity to C_{ℓ_p} can be seen by comparing Figs. 11 and 12. The increased sensitivity of the roll and dutch roll modes to C_{ℓ_p} is associated with the previously mentioned low moment of inertia, I_x, about the roll axis.

Figure 8 shows the motion sensitivity to variations in the side force derivative, C_{y_r}, with variations in C_{L_q} and $C_{L_{\dot{\alpha}}}$. The longitudinal and lateral-directional modes of motion were totally insensitive to C_{y_r} over the range of $\pm$ 500 per radian.

The influence of variations in C_{n_r} on the vehicle lateral-directional damping ratio and motion response is shown in Fig. 13 at M = 0.8 and 40,000-ft altitude for a 10-g banked

turn. The sensitivity of the dutch roll and spiral mode damping ratio to variations in C_{n_r} is shown in Fig. 13a. As can be noted in the root locus plots of Fig. 11, the dutch roll damping is very sensitive to C_{n_r} variations. The yaw rate time response shown in Fig. 13b results from a yaw control doublet and characterizes the changes in the dutch roll motion for three values of C_{n_r}. The sensitivity of the dutch roll mode, as demonstrated by the yaw rate response, ranges from a highly damped motion for C_{n_r} = -1,000 per radian to a lightly damped motion that approaches a neutrally stable mode at C_{n_r} = 100 per radian. The change in the yaw rate response for the three values of C_{n_r} corresponds to the changes in the Time-to-Half-Amplitude, $T_{1/2}$, shown in Fig. 11 for the same values of C_{n_r}.

The sensitivity of the dutch roll mode damping ratio and motion response to variations in C_{ℓ_p} over the range of ±1,000 per radian is presented in Fig. 14. The flight condition presented corresponds to M = 0.8 and altitude = 10,000 ft for a 10-g banked turn. The damping ratio plot (Fig. 14a) demonstrates the sensitivity of the dutch roll to relatively small changes in C_{ℓ_p} about zero value. This sensitivity is also apparent in the roll rate time response (Fig. 14b) for C_{ℓ_p} values of -200, -100, and -62.5 (trim value) per radian. The roll rate response attributable to a unit roll control doublet changes from a motion with $T_{1/2} \sim 0.1$ sec at C_{ℓ_p} = -62.5 to a much less damped motion with $T_{1/2} \sim 0.04$ sec at C_{ℓ_p} = -200 per radian. The roll and dutch roll modes are quite sensitive to small changes in C_{ℓ_p}; this can be seen by tracing the root migrations in Fig. 12a.

Both the roll and dutch roll modes of motion have been shown to be quite sensitive to changes in C_{n_r} and C_{ℓ_p} within the value ranges estimated by Datcom (Fig. 4).

4.2.2 Dynamic Cross Derivative Variations

The missile motion sensitivity to variations in the cross derivative, C_{ℓ_r}, is shown in Fig. 15. Only the lateral-directional modes of motion are affected by a variation in C_{ℓ_r} (in the range of ±500 per radian). The sensitivity of the dutch roll mode to C_{ℓ_r} increases with increasing load factor (g's) with each Mach number, whereas the roll mode sensitivity decreases with increasing g flight at each altitude and Mach number. By comparing the dutch roll root migrations in Figs. 11 and 15, one sees that the sensitivity of the dutch roll mode to variations in C_{ℓ_r} is equal to that for variations in the direct derivative, C_{n_r}.

Variations of the yawing moment caused by the roll rate parameter, C_{n_p}, affect the damping and frequency of the roll and dutch roll modes of motion significantly, as can be seen by tracing the root migration in Fig. 16. In general, the sensitivity of the roll and dutch roll modes to C_{n_p} increases with increasing load factor (g's) and Mach number. The roll mode may go from aperiodic stable with negative values of C_{n_p} to unstable with positive

values of C_{n_p}. The dutch roll mode may go from an unstable oscillation with negative values of C_{n_p} to a stable oscillation and finally to a degenerated aperiodic mode with positive values of C_{n_p}. In general, the roll and dutch roll modes of motion are more sensitive to C_{n_p} (Fig. 16) than to C_{ℓ_r} (Fig. 15) for the flight conditions investigated.

The motion sensitivity to variations in the side force derivative, C_{y_p}, is shown in Fig. 17. As with other force derivatives, the effect of C_{y_p} on both the roll and dutch roll modes is not considered significant.

The influence of variations in C_{ℓ_r} on the vehicle dutch roll damping ratio and on the roll rate response is shown in Fig. 18 at M = 0.8 and altitude = 40,000 ft for a 10-g-banked turn. Shown in Fig. 18a is the sensitivity of the dutch roll mode damping ratio to variations in C_{ℓ_r} over the range ± 500 per radian. The roll rate time responses shown in Fig. 18b result from a yaw control doublet and demonstrate the sensitivity of the dutch roll damping to C_{ℓ_r}. The dutch roll motion, as shown by the roll rate response, ranges from highly damped motion for C_{ℓ_r} = 500 to that approaching a neutrally stable mode at C_{ℓ_r} = -50 per radian. The changes in the roll rate time responses, along with the dutch roll root migrations shown in Fig. 15, indicate that the missile's motion may be highly sensitive to variations in the cross derivative C_{ℓ_r}.

The sensitivity of the dutch roll damping ratio and yaw rate response to C_{n_p} is presented in Fig. 19 at M = 1.1 and altitude = 10,000 ft for a 10-g banked turn. The dutch roll damping ratio (Fig. 19a) is sensitive to variations in C_{n_p} over the range of ± 500 per radian. The yaw rate time response shown in Fig. 19b results from a roll control doublet and demonstrates the sensitivity of the dutch roll mode motion for three values of C_{n_p}. The changes in the yaw rate time response with C_{n_p} variations follows trends of the dutch roll mode root migrations with C_{n_p} variations as shown in Fig. 16. As with C_{ℓ_r} the bank-to-turn missile motion is sensitive to C_{n_p} variations.

The influence of variations in C_{y_p} on the dutch roll damping ratio and yaw rate response is shown in Fig. 20 at M = 3.5 and altitude = 10,000 ft for a 25-g banked turn. For variation in C_{y_p} over the range of ± 500 per radian, the change in the dutch roll damping ratio of Fig. 20a is not considered large enough to significantly alter the dutch roll motion. This is shown in the minimal change in the yaw rate response of Fig. 20b attributable to a roll control doublet for range in C_{y_p} of -500 to 500 per radian.

In general, therefore, direct damping derivatives are important in motion analysis. The sensitivity of the missile lateral-directional modes of motion to variations in the cross derivatives C_{ℓ_r} and C_{n_p} is on the order of the direct derivative C_{n_r}; therefore, C_{ℓ_r} and C_{n_p} are necessary to perform accurate missile motion simulation.

4.2.3 Dynamic Cross-Coupling Derivative Variations

In the cross-coupling derivative investigation the derivatives C_{m_r}, C_{m_p}, C_{ℓ_q}, and C_{n_q} were each initially given nominal values of 100 per radian. Then, individual variations in each derivative were performed with the remaining derivatives at their nominal values. By maintaining nominal (nonzero) values for the cross-coupling derivatives, the possible derivative interaction effects described in Ref. 7 were included.

The motion sensitivity to variations in the cross-coupling derivative C_{ℓ_q} is shown in Fig. 21 for Mach numbers of 0.8, 1.1, and 3.5. Including the cross-coupling derivatives in the linearized analysis results in a weak coupling in the longitudinal and lateral-directional axes as indicated by the migration in the short period, spiral, roll, and dutch roll modes. As observed, the sensitivity of the dutch roll mode with variations in C_{ℓ_q} depends on the flight conditions (Mach number, altitude, and load factor). Although the sensitivity of the modes of motion to C_{ℓ_q} is not as significant as it is to C_{ℓ_r} (compare Figs. 15 and 21), errors may occur in missile motion simulation if the C_{ℓ_q} derivative is not modeled when the magnitude approaches the maximum ranges utilized in Fig. 21.

The motion sensitivity with variations in the cross-coupling derivative C_{m_p} is shown in Fig. 22. The short period, roll, and dutch roll mode sensitivity to C_{m_p} is similar to that experienced with the C_{ℓ_q} derivative variations. If it is assumed that the cross-coupling derivative C_{m_p} is of a magnitude approaching that of the cross derivatives, then incorrect motion simulation may possibly result if the derivative is not included in the aerodynamic modeling.

The motion sensitivity with variations in the cross-coupling derivatives C_{m_r} and C_{n_q} is shown in Fig. 8 along with the variations in the force derivatives. The longitudinal and lateral-directional modes of motion are totally insensitive to variations in either C_{m_r} or C_{n_q} over the range of ± 500 per radian.

The sensitivities of the missile damping ratio and frequency and the roll and pitch rate to variations of C_{ℓ_q} (Fig. 23) and C_{m_p} (Fig. 24) are given for M = 3.5 and altitude = 40,000 ft for a 25-g banked turn. At this flight condition, the missile was most sensitive to variations in cross-coupling derivatives. The short period, phugoid, and dutch roll mode damping ratios are shown, in Fig. 23a, to be quite sensitive to variations in C_{ℓ_q} over the range of ± 500 per radian. The short period and dutch roll damping ratios exhibit similar sensitivity to C_{m_p} (Fig. 24b). The sensitivity of the dutch roll mode of motion to C_{ℓ_q} is shown (Fig. 23b) by the changes in the roll rate response resulting from a pitch control doublet, whereas the sensitivity of the short period mode of motion to C_{m_p} is shown (Fig. 25b) by the changes in the pitch rate response resulting from a roll control doublet.

4.3 YAW-TO-TURN CONFIGURATION

The dynamic sensitivity study for the yaw-to-turn missile was conducted at altitudes of 10,000 and 20,000 ft at Mach 1.3 and at altitudes of 10,000 and 40,000 ft for Mach 3.0. The flight conditions investigated were 1-g-level flight at Mach 1.3 and 1-g-level and 5- and 10-g turning flight at Mach 3.0. Angle of attack and/or control surface deflection required for trim flight at Mach numbers of less than 1.3 for accelerated g flight conditions exceeded the range in the available aerodynamic data matrix.

4.3.1 Dynamic Direct Derivative Variations

Longitudinal. Figures 25 and 26 show the missile motion sensitivity to variations in the direct rate and acceleration derivatives C_{m_q} and $C_{m_{\dot{\alpha}}}$. The range for which the derivatives were varied ($\pm$1,000 per radian) was slightly less than twice the magnitude obtained experimentally (see Fig. 4). Due to the absence of coupling between the longitudinal and lateral-directional planes of motion, only the longitudinal modes are shown. Only the short period mode shows sensitivity to variations in C_{m_q} and $C_{m_{\dot{\alpha}}}$. There is a significant Mach number effect on the sensitivity of the short period mode with C_{m_q} and $C_{m_{\dot{\alpha}}}$ variations. As noted for the bank-to-turn configuration, the short period mode is less sensitive at 40,000 ft to C_{m_q} and $C_{m_{\dot{\alpha}}}$ variations than at 10,000 ft because of the decrease in density with increasing altitude.

The motion sensitivity to the force derivatives C_{L_q} and $C_{L_{\dot{\alpha}}}$ is shown in Fig. 27. The missile modes of motion were totally insensitive to variations in either C_{L_q} or $C_{L_{\dot{\alpha}}}$ over the range of $\pm$500 per radian.

The influence of variations in C_{m_q} and $C_{m_{\dot{\alpha}}}$ on the vehicle longitudinal damping ratio and pitch rate response is shown respectively in Figs. 28 and 29 at M = 3.0 and altitude = 40,000 ft for 1-g-level flight. In Figs. 28a and 29a, the short period damping ratio is shown to be sensitive to variations in C_{m_q} and $C_{m_{\dot{\alpha}}}$. The pitch rate time response shown in these figures results from a pitch control doublet and demonstrates the sensitivity of the short period mode to C_{m_q} and $C_{m_{\dot{\alpha}}}$. The changes shown in the pitch rate response correspond to values of C_{m_q} and $C_{m_{\dot{\alpha}}}$ at trim, at values of zero, and at values near which the short period mode is neutrally stable.

Lateral-Directional. The missile motion sensitivity to variations ($\pm$ 1,000 per radian) in the direct damping derivatives in yaw, C_{n_r}, is shown in Fig. 30. The roll, spiral, and dutch roll modes are affected to different degrees by C_{n_r} variation. The most predominant effect is on the dutch roll mode for the flight conditions evaluated. The sensitivity of the roll and spiral

modes is more pronounced for the 1-g-level trim flight conditions. The dutch roll mode sensitivity due to C_{n_r} variations increases with increasing load factor (g's) and altitude at Mach number 3.0.

The effect of variations ($\pm$ 1,000 per radian) in the direct roll damping derivative, C_{ℓ_p}, on the lateral-directional modes of motion is shown in Fig. 31. The extreme sensitivity of the roll and spiral modes to C_{ℓ_p} is associated with the low moment of inertia, I_X, about the roll axis. The pitch, I_Y, and yaw, I_Z, moment of inertia are approximately two orders of magnitude larger (see Table 3) than the rolling moment of inertia. The dutch roll mode of motion is sensitive to variations in C_{ℓ_p}, but this sensitivity does not produce an unstable mode for the flight conditions analyzed. The roll and spiral modes are more sensitive to the same magnitude variations in C_{ℓ_p} than to C_{n_r} as can be seen by tracing the root migrations in Figs. 30 and 31.

The lateral-directional modes of motion are totally insensitive to variations ($\pm$ 500 per radian) in the side force derivative C_{y_r}; these modes are shown with the normal force derivatives C_{L_q} and $C_{L_{\dot{\alpha}}}$ in Fig. 27.

The influence of variations in C_{n_r} on the vehicle spiral and dutch roll damping and yaw rate response is shown in Fig. 32 at M = 3.0 and altitude = 10,000 ft for a 10-g banked turn. The sensitivity of the dutch roll damping ratio with variations ($\pm$ 1,000 per radian) is shown in Fig. 32a. As can be noted from the curve slope, the dutch roll damping is very sensitive to C_{n_r} variations. The time history shown in Fig. 32b results from a yaw control doublet and characterizes the effect of changes in C_{n_r} on the dutch roll motion.

The sensitivity of the roll and dutch roll damping and roll rate response to variations in C_{ℓ_p} is shown in Fig. 33 at M = 3.0 and altitude = 10,000 ft for a 10-g banked turn. The damping ratio plot (Fig. 33a) demonstrates the sensitivity of the spiral, roll, and dutch roll modes to relatively small changes in C_{ℓ_p} about zero values. This sensitivity in the dutch roll mode is apparent from the roll rate time response plot (Fig. 33b). For the same magnitude change in the derivatives, the dutch roll mode of motion is significantly more sensitive to C_{ℓ_p} than to C_{n_r}.

4.3.2 Dynamic Cross Derivative Variations

The vehicle motion sensitivity to the cross derivative C_{ℓ_r} is shown in Fig. 34. Only the lateral-directional modes of motion are affected by variations in C_{ℓ_r} over the range of $\pm$ 500 per radian. The sensitivity of the dutch roll mode to C_{ℓ_r} increases with increasing load factor (g's), whereas the spiral mode sensitivity decreases with increasing load factor. By

comparing the dutch roll root migrations with Fig. 30, it can be seen that the sensitivity of the dutch roll mode to C_{ℓ_r} is greater than that for the direct derivative C_{n_r}.

Changes in the spiral, roll, and dutch roll modes of motion with variation of C_{n_p} are shown in Fig. 35. The roll and spiral mode sensitivity to C_{n_p} increases with increasing load factor. The dutch roll mode sensitivity is also highly dependent on the load factor. In most cases, the roll and spiral modes are more sensitive to C_{n_p} than to C_{ℓ_r} as can be seen by tracing the root migrations in Figs. 34 and 35.

The lateral-directional modes of motion are insensitive to variations (± 500 per radian) in the side force parameter C_{y_p} as shown in Fig. 27. For the flight conditions investigated, the C_{y_p} parameter does not appear to be an important parameter for motion analysis.

The influence of variations in C_{ℓ_r} on the lateral-directional damping ratios and roll rate response is shown in Fig. 36 at M = 1.3 and altitude = 20,000 ft for 1-g-level flight. The damping ratio plot demonstrates the sensitivity of the spiral, roll, and dutch roll modes to variation in C_{ℓ_r} over the range of ± 500 per radian. The roll and spiral modes are quite sensitive to C_{ℓ_r} over the range of ± 500 per radian. This is shown by changes in the roots from a coupled root at large negative values to real non-oscillatory roots or modes for values less negative than -100 per radian. The roll rate time response attributable to a yaw control doublet (Fig. 36b) demonstrates the predominance of the spiral and dutch roll roots in the C_{ℓ_r} range from -100 to 200 per radian.

The sensitivity of the lateral-directional damping ratios and yaw rate time response to C_{n_p} is shown in Fig. 37 for M = 3.0 and altitude = 10,000 ft for a 10-g banked turn. Changes in the damping ratio of the dutch roll mode shown in Fig. 37a further demonstrate the sensitivity of the dutch roll roots to relatively small changes in C_{n_p} near zero. The changes in the yaw rate time response (Fig. 37b) with changes in C_{n_p} point up the significance of the root migrations shown in Fig. 35. The changes in the time response shown for values of C_{n_p} = -1.2 and 50 demonstrate the dutch roll sensitivity to C_{n_p}, whereas the changes shown for values of -1.2 and -30 demonstrate the spiral mode sensitivity.

The sensitivity of the missile lateral-directional modes of motion to variations in the cross derivatives C_{ℓ_r} and C_{n_p} is of the same magnitude as for the direct derivatives and therefore is important and necessary for accurate motion simulation.

4.3.3 Dynamic Cross-Coupling Derivative Variations

As noted for the bank-to-turn configuration, the cross-coupling derivatives C_{m_r}, C_{m_p}, C_{ℓ_q}, and C_{n_q} were assigned nominal values of 100 per radian. Each derivative was varied

separately over the range of ±500 per radian while the others were fixed at their nominal values.

The sensitivity of the longitudinal and lateral-directional modes of motion to variations in the roll due to pitch rate derivative, C_{ℓ_q}, is shown in Fig. 38. The short period, dutch roll, roll, and spiral modes are shown to be quite sensitive to C_{ℓ_q} over the range ±500 per radian for M = 3.0 flight conditions. The dutch roll mode sensitivity to C_{ℓ_q} increases with increasing load factor, whereas the roll sensitivity remains approximately the same with increasing load factor. Although the lateral-directional modes of motion are less sensitive to C_{ℓ_q} than to C_{ℓ_r}, inaccurate motion simulation may occur if the C_{ℓ_q} derivative is of a large magnitude and is not included.

The motion sensitivity with variations in the pitch attributable to roll rate derivative, C_{m_p}, is shown in Fig. 39. The mode sensitivity to C_{m_p} is almost identical to that shown for C_{ℓ_q}. Neglecting C_{m_p} in motion analysis could cause inaccuracies if the derivative is of the magnitudes over the ranges investigated in this study.

The sensitivity of the missile modes of motion to variation in C_{n_q} is shown in Fig. 40. The root locus plot for M = 1.3 flight conditions is omitted because of the insensitivity of any of the modes to C_{n_q}. For the M = 3.0 flight conditions, one can note some movement of the roots with C_{n_q} variation, but the movement is much less than that associated with C_{ℓ_q} and C_{m_p} variations.

The missile modes of motion are totally insensitive to variations in C_{m_r} and are included in Fig. 27 with the force derivatives.

The sensitivity of the missile damping ratio and roll rate time response to C_{ℓ_q} is shown in Fig. 41 at M = 3.0 and altitude = 10,000 ft for a 10-g banked turn. This flight condition represents the condition for which the mode sensitivity to C_{ℓ_q} was the most pronounced. The short period, phugoid, dutch roll, and spiral damping ratios in Fig. 41a are shown to be quite sensitive to variations in C_{ℓ_q} over the range of ±500 per radian. The roll rate time response (Fig. 41b) to a pitch control doublet demonstrates the sensitivity of the dutch roll mode to variations in C_{ℓ_q} over the range from -50 to 100 per radian.

The sensitivity of the missile damping ratio and pitch rate time response to C_{m_p} variations over the range ±500 per radian is shown in Fig. 42 at M = 3.0 and altitude = 10,000 ft for 1-g-level flight. The primary effect shown in Fig. 42a is the sensitivity of the short period damping ratio. Associated with the change in damping ratio is a corresponding change in frequency as can be seen by tracing the root migration in Fig. 39. The pitch rate

time response (Fig. 42b) demonstrates the short period sensitivity to C_{m_p} values of -500, 0, and 200 per radian. A point of particular interest is the lack of coupling between the longitudinal and lateral-directional modes for $C_{m_p} = 0.0$.

The sensitivity of the damping ratio and yaw rate time response to C_{n_q} is shown in Fig. 43 at M = 3.0 and altitude = 10,000 ft for 10-g banked turn. Little change in dutch roll and short period damping ratio is seen in Fig. 43a. The changes in the yaw rate time response (Fig. 43b) for values of C_{n_q} = -500, 0, and 200 demonstrate the dutch roll sensitivity to C_{n_q}. The missile modes of motion are much less sensitive to C_{n_q} than they are to C_{ℓ_q} or C_{m_p}.

5.0 CONCLUDING REMARKS

Based on this analysis, the following observations and conclusions may be made:

1a. Variations in the longitudinal direct derivatives C_{m_q} and $C_{m_{\dot{\alpha}}}$ significantly affect the short period mode of motion for both the bank-to-turn and yaw-to-turn missiles. The sensitivity of the short period mode of motion with variations in C_{m_q} and $C_{m_{\dot{\alpha}}}$ increases with Mach number but is relatively unchanged by load factor (g's).

b. Variations in the lateral-directional direct derivatives C_{n_r} and C_{ℓ_p} significantly alter the roll, spiral, and dutch roll modes of motion for both the bank-to-turn and yaw-to-turn missiles. The sensitivity of the dutch roll mode increases with increasing load factor (g's) and Mach number. The spiral and roll mode sensitivity may increase or decrease with increasing load factor (g's), depending on the missile configuration.

2. Variations in the lateral-directional cross derivatives C_{ℓ_r} and C_{n_p} alter the bank-to-turn and yaw-to-turn roll, spiral, and dutch roll modes of motion in a manner similar to that resulting from variations of the same magnitude in the direct derivatives. The roll and dutch roll motion sensitivity increases with increasing load factor (g's) and Mach number.

3. Large variations ($\pm$ 500 per radian) in the cross-coupling derivatives C_{ℓ_q}, C_{n_q}, and C_{m_p} alter the longitudinal and lateral-directional modes of motion for both bank-to-turn and yaw-to-turn missiles. The yawing moment caused by pitch rate, C_{n_q}, was found to be less important than either C_{ℓ_q} or C_{m_p}. The pitching moment associated with yaw derivative, C_{m_r}, appears to be insignificant in missile motion.

4. Varying the force derivatives C_{L_q}, $C_{L_{\dot{\alpha}}}$, C_{y_p}, and C_{y_r} did not produce any noticeable changes in the modes of motion for either the bank-to-turn or yaw-to-turn missile.

REFERENCES

1. Jenke, Leroy M. "Experimental Roll-Damping, Magnus, and Static-Stability Characteristics of Two Slender Missile Configurations at High Angles of Attack (0 to 90 Deg) and Mach Numbers 0.2 through 2.5." AEDC-TR-76-58 (AD-A027027), July 1976.

2. Collins, J. A. "Verification Test of the AEDC High Alpha Roll Dynamics System." AEDC-TSR-78-P50, November 1978.

3. Finck, R. D., et al. "USAF Stability and Control Datcom." McDonnell Douglas Corporation, Douglas Aircraft Division, October 1960. Revised April 1978.

4. Giesing, J. P., Kalman, T. P., and Rodden, W. P. "Subsonic Unsteady Aerodynamics for General Configurations, Part 2, Vol. 2 — Application of the Doublet-Lattice Method and the Method of Images to Lifting-Surface/Body Interference." AFFDL-TR-71-5, April 1972.

5. Williams, John E. and Vukelich, Steven R. "The USAF Stability and Control Digital Datcom, Vol. 1, Users' Manual; Vol. 2, Implementation of Datcom Method." AFFDL-TR-76-45, November 1976.

6. Orlik-Ruckemann, K. J., Hanff, E. S., and Laberge, J. G. "Direct and Cross-Coupling Subsonic Moment Derivatives Due to Oscillatory Pitching and Yawing of an Aircraft-Like Model of Angle of Attack up to 40° in Ames 6 x 6 Wind Tunnel." NAE LTR-UA-38, 1976.

7. Butler, R. W., and Langham, T. F. "Aircraft Motion Sensitivity to Variations in Dynamic Stability Parameters." AGARD Conference Preprint No. 235, Paper 35, 1978.

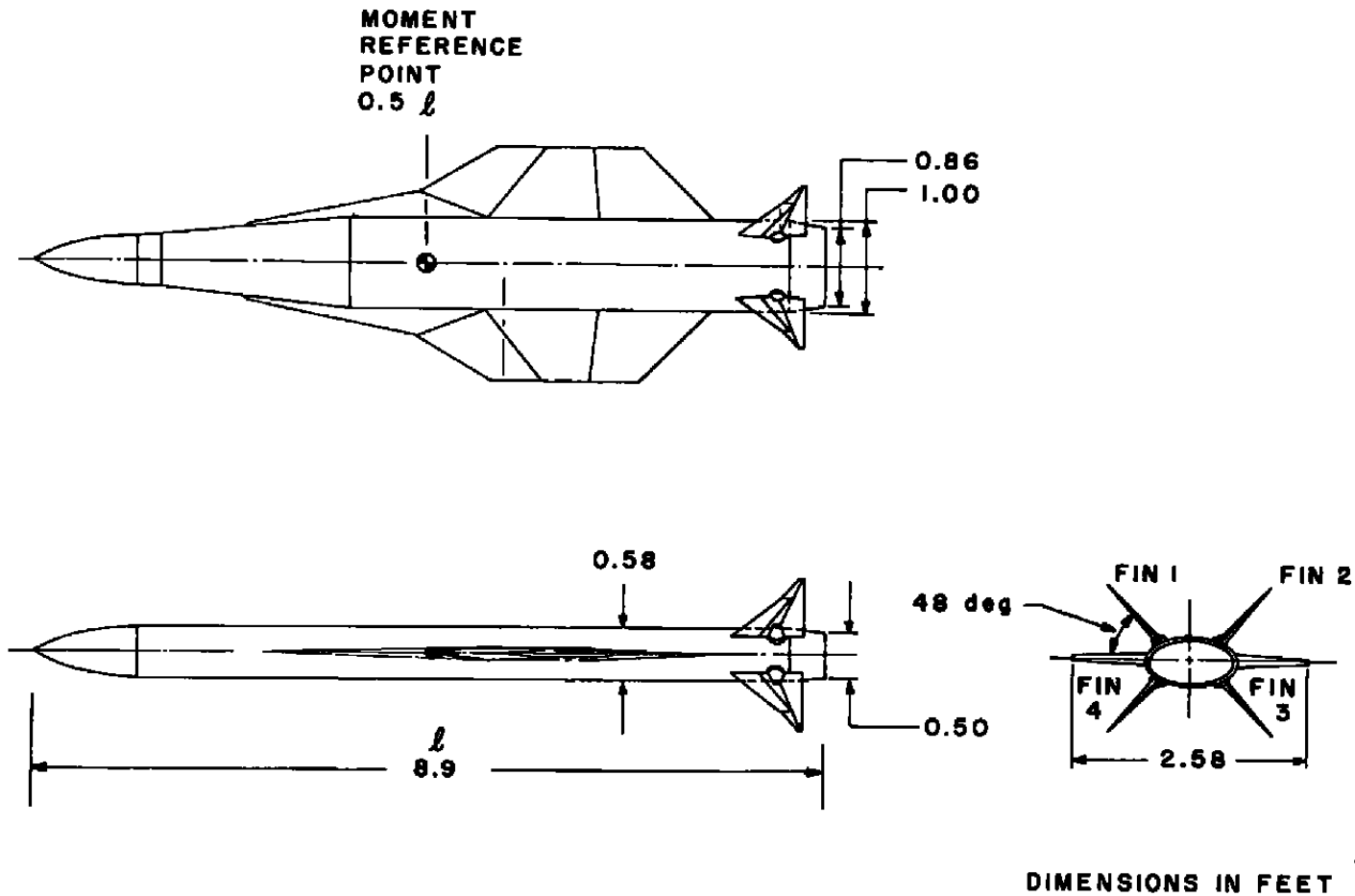

Figure 1. Bank-to-turn missile configuration.

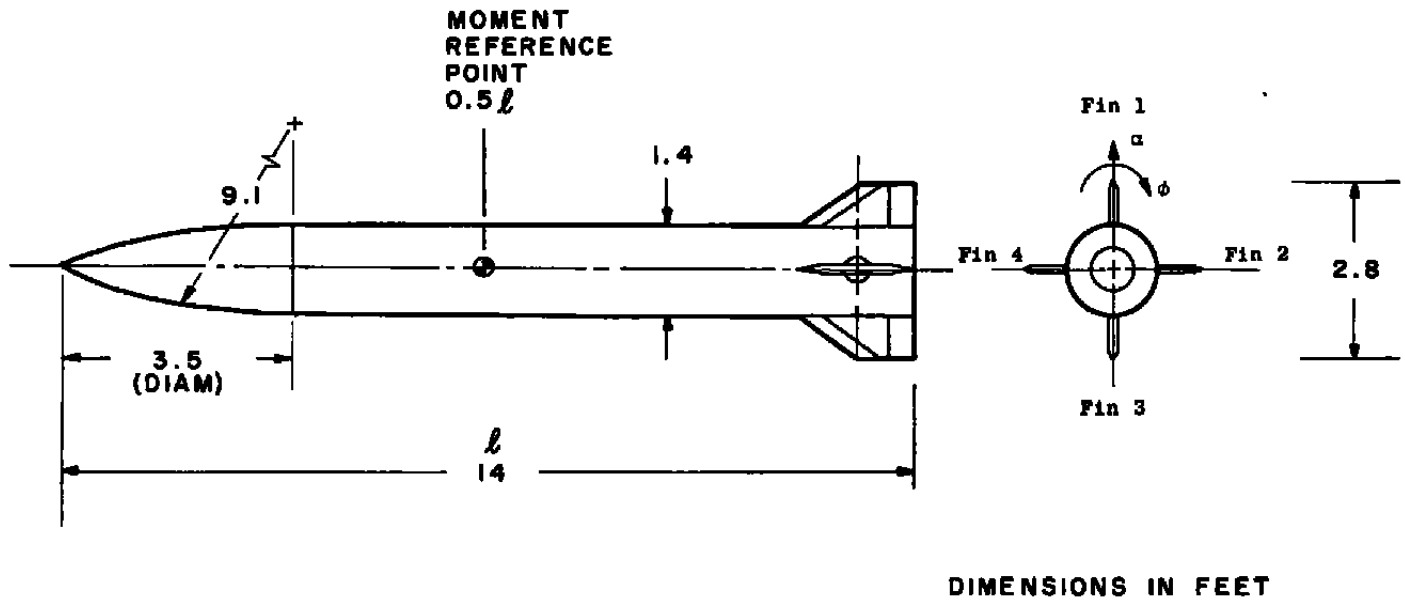

Figure 2. Yaw-to-turn missile configuration.

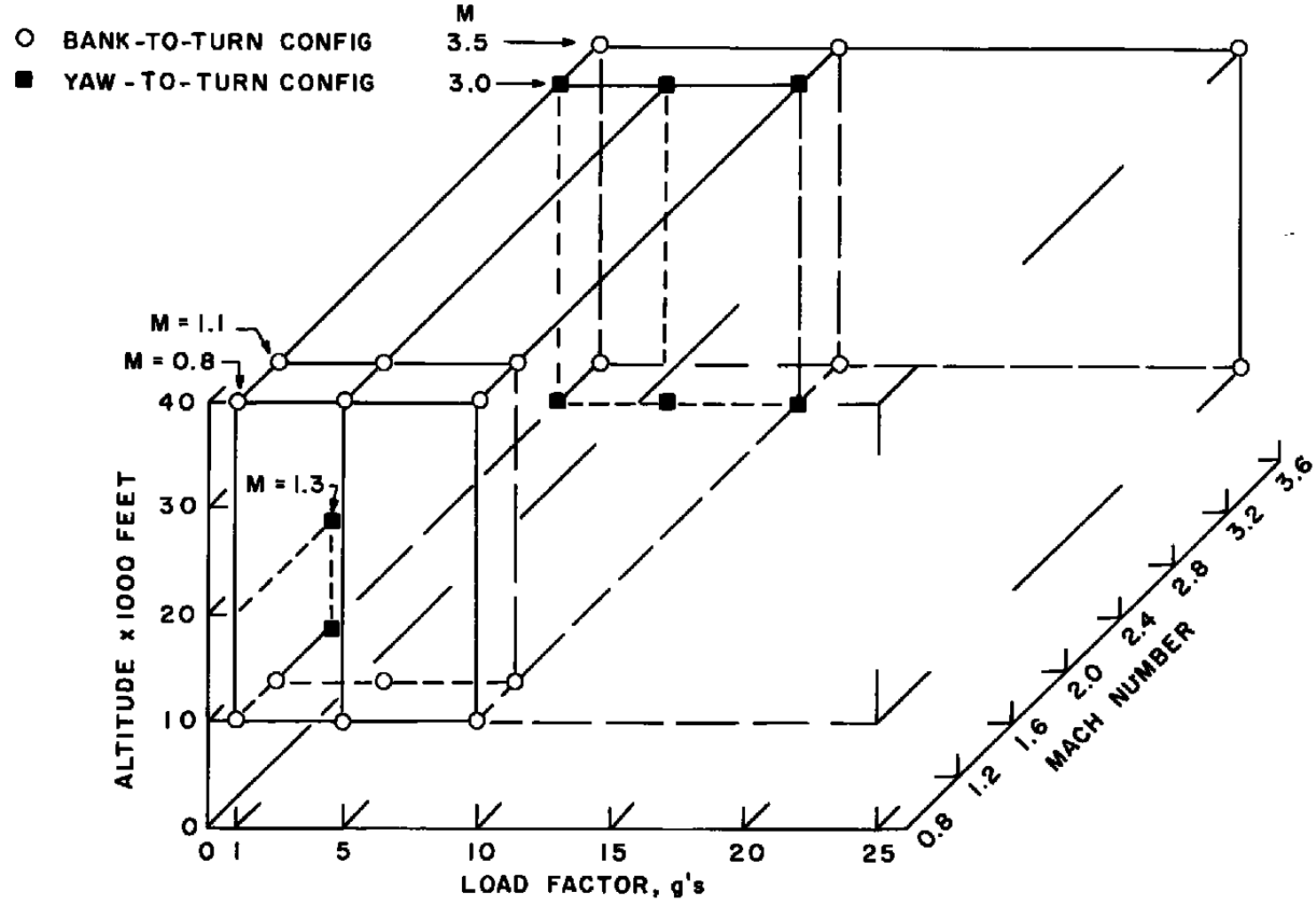

Figure 3. Missile flight envelope.

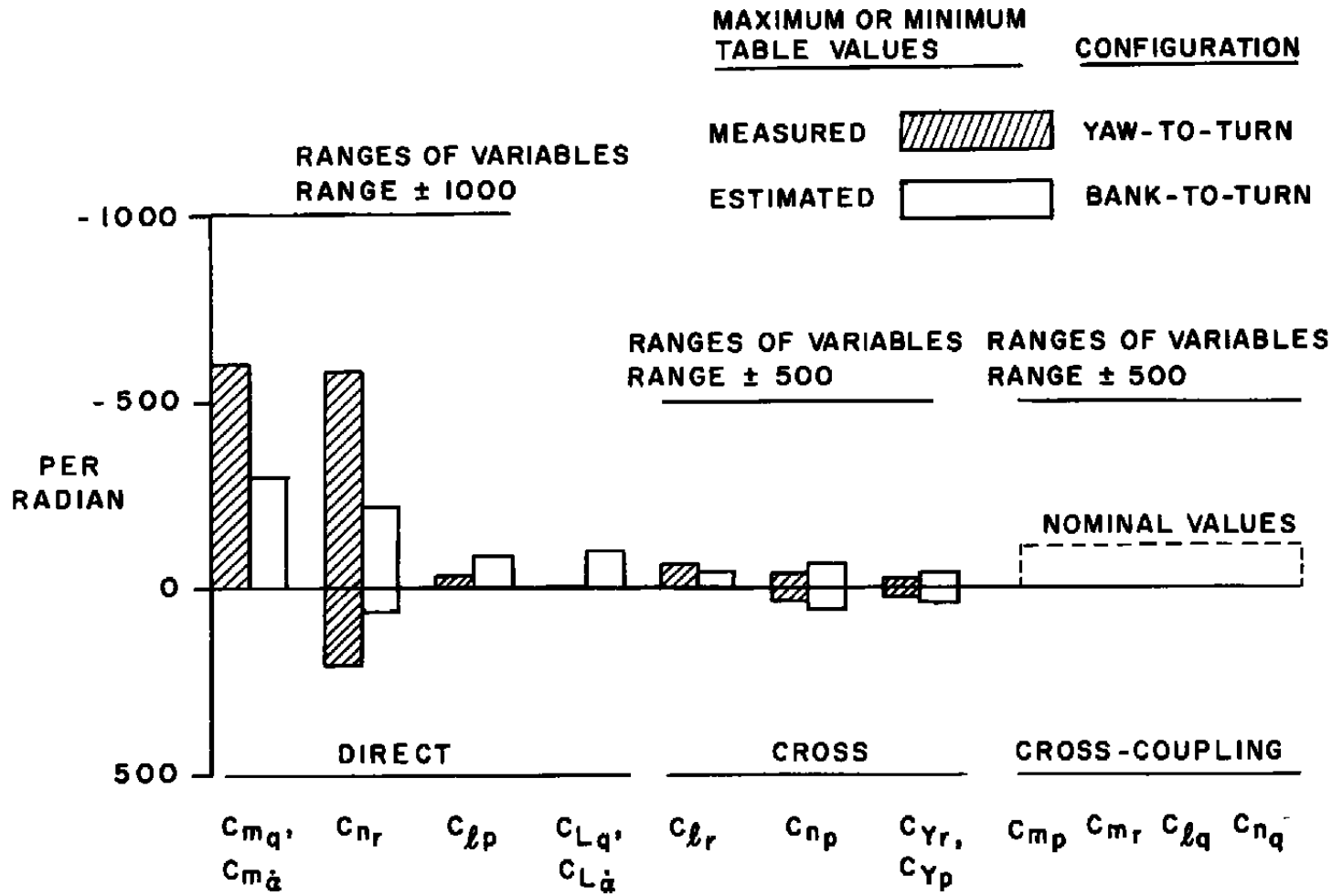

Figure 4. Range of derivative values.

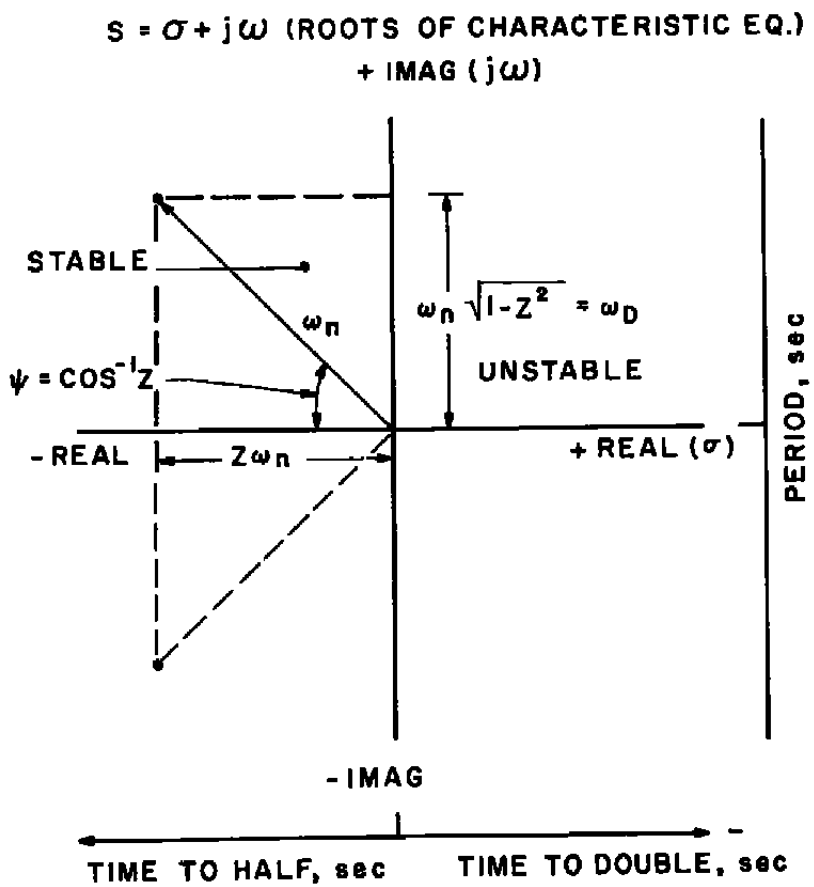

RELATIONSHIP OF TERMS

$\omega_n = \sqrt{(\sigma^2) + (\omega)^2}$

Z = DAMPING RATIO = $-\sigma/\omega_n = \sigma/\sigma_{cR}$

$T_{1/2} = -0.69315/\sigma$

P = PERIOD = $2\pi/\omega$

$C\,1/2 = \frac{\ell n(1/2)}{2\pi} \sqrt{\frac{1-Z^2}{Z^2}}$

Figure 5. Sample root locus format.

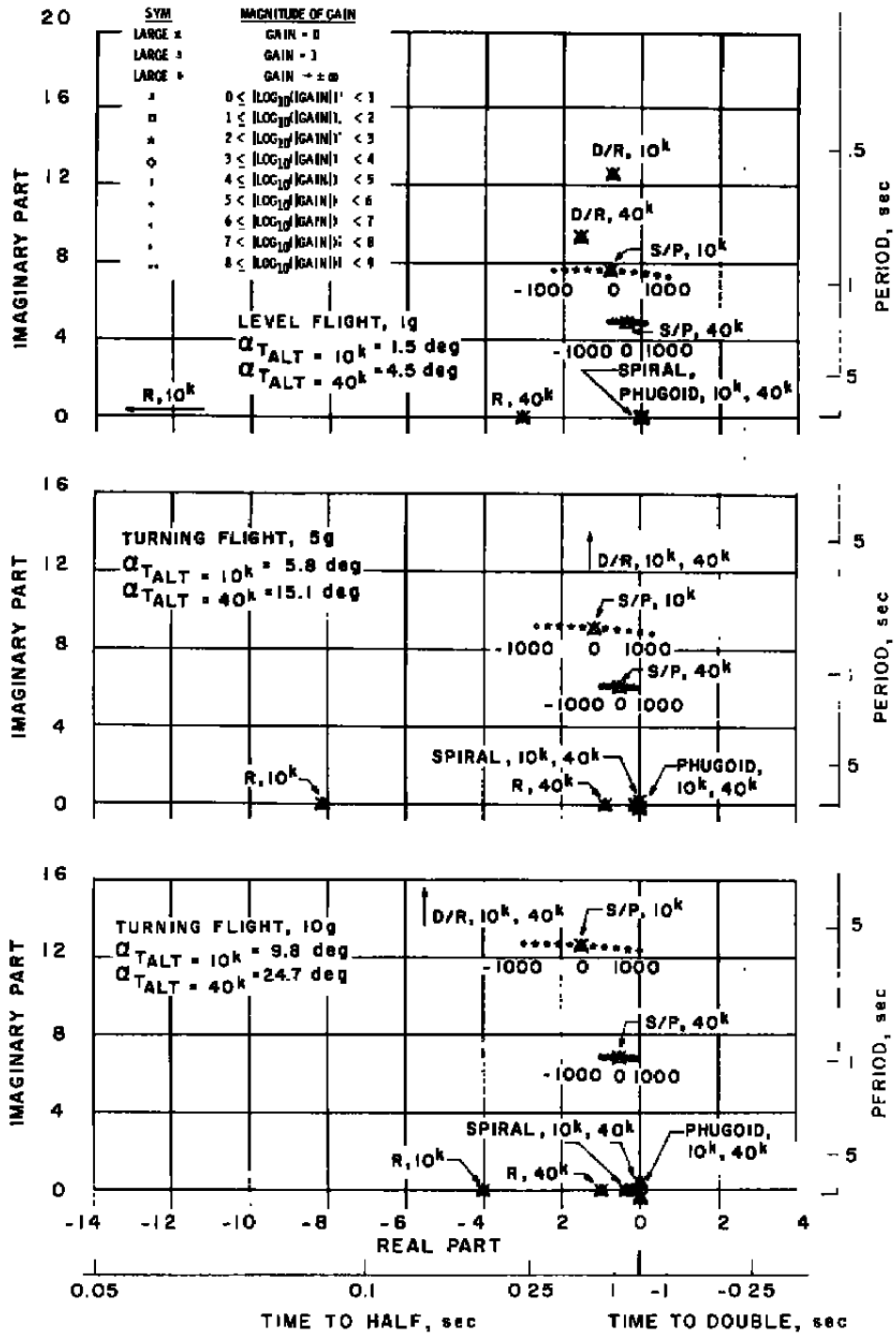

a. M = 0.8

Figure 6. Bank-to-turn configuration - locus of roots with C_{m_q} variation.

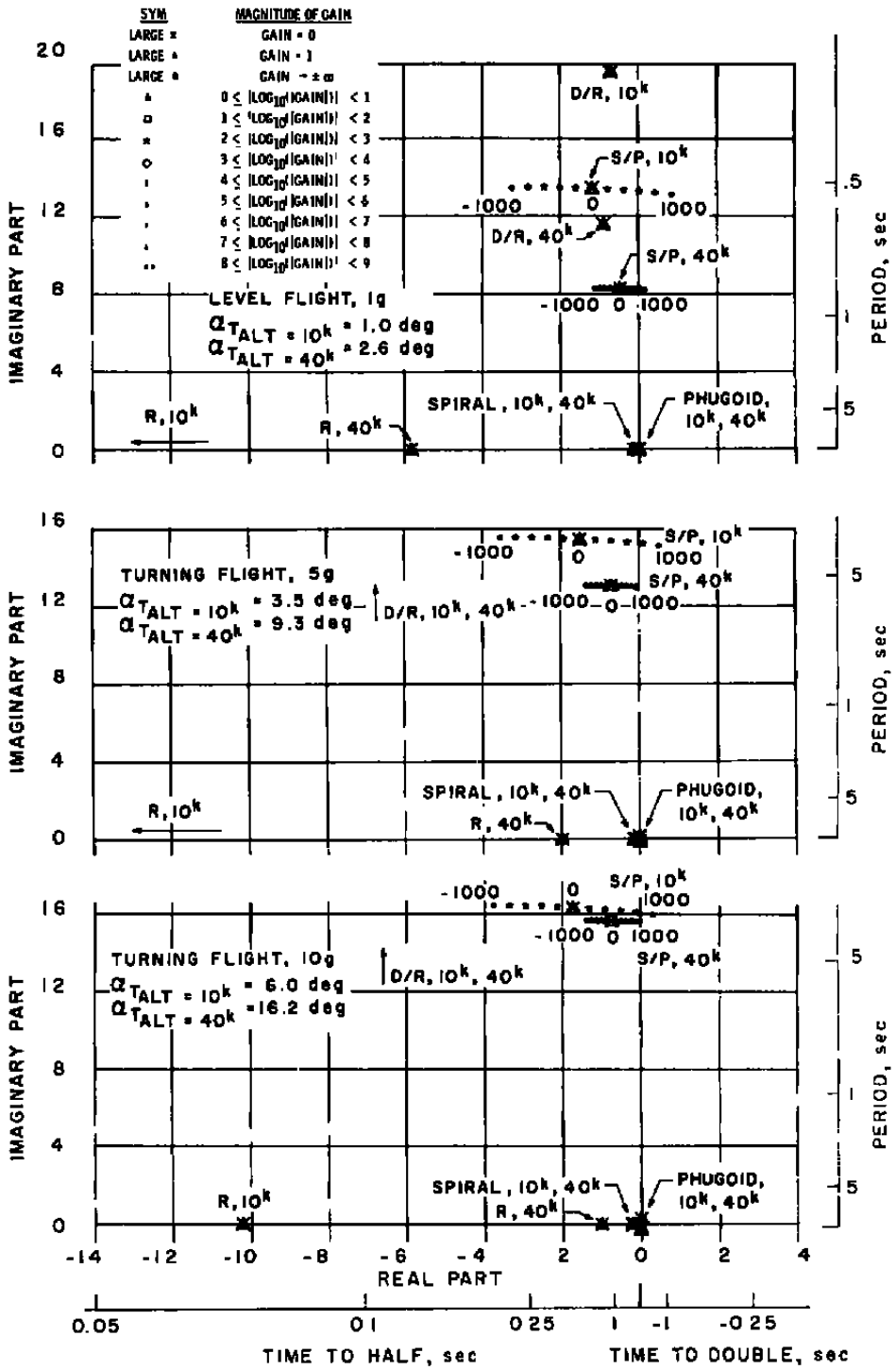

b. M = 1.1

Figure 6. Continued.

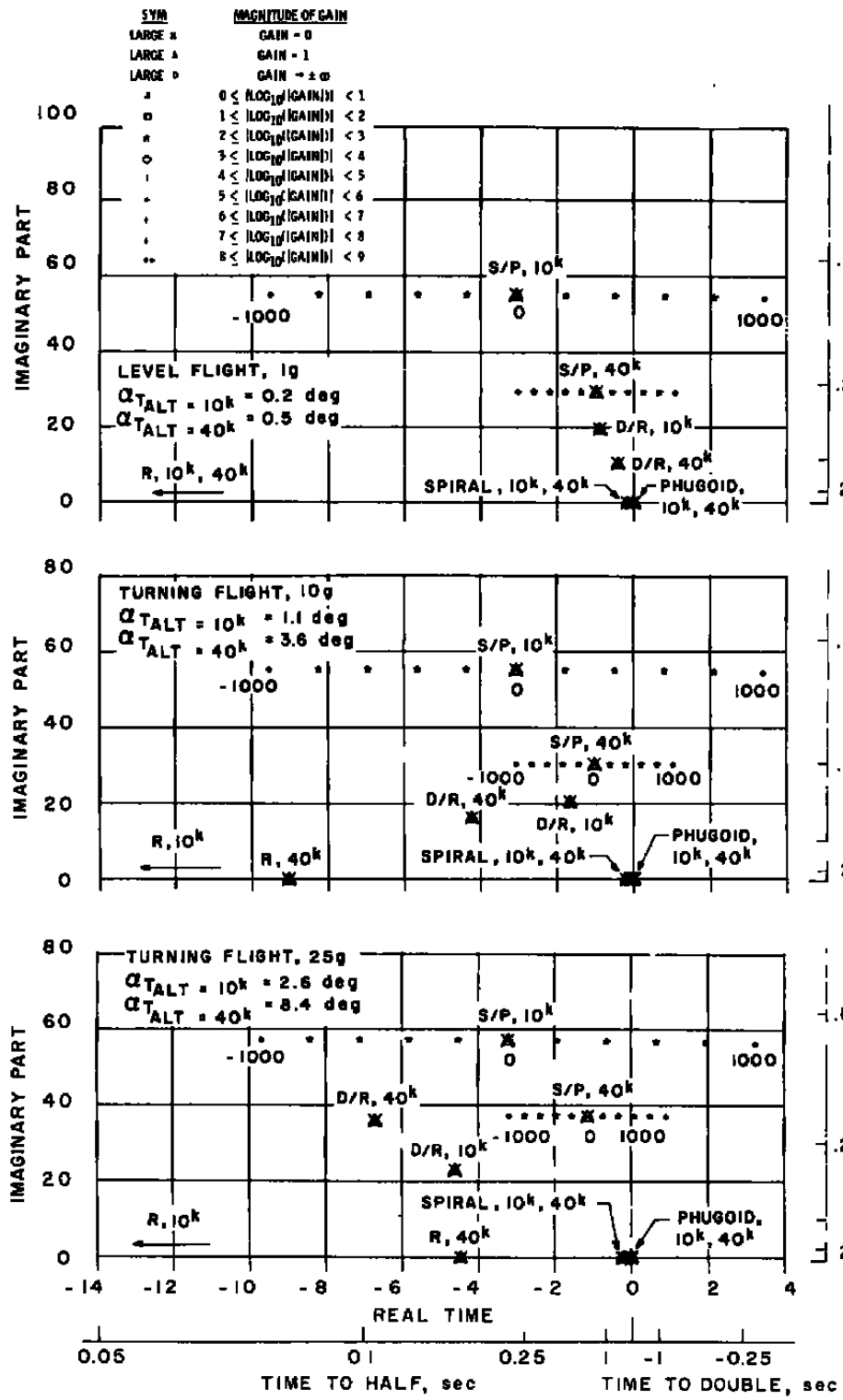

c. M = 3.5

Figure 6. Concluded.

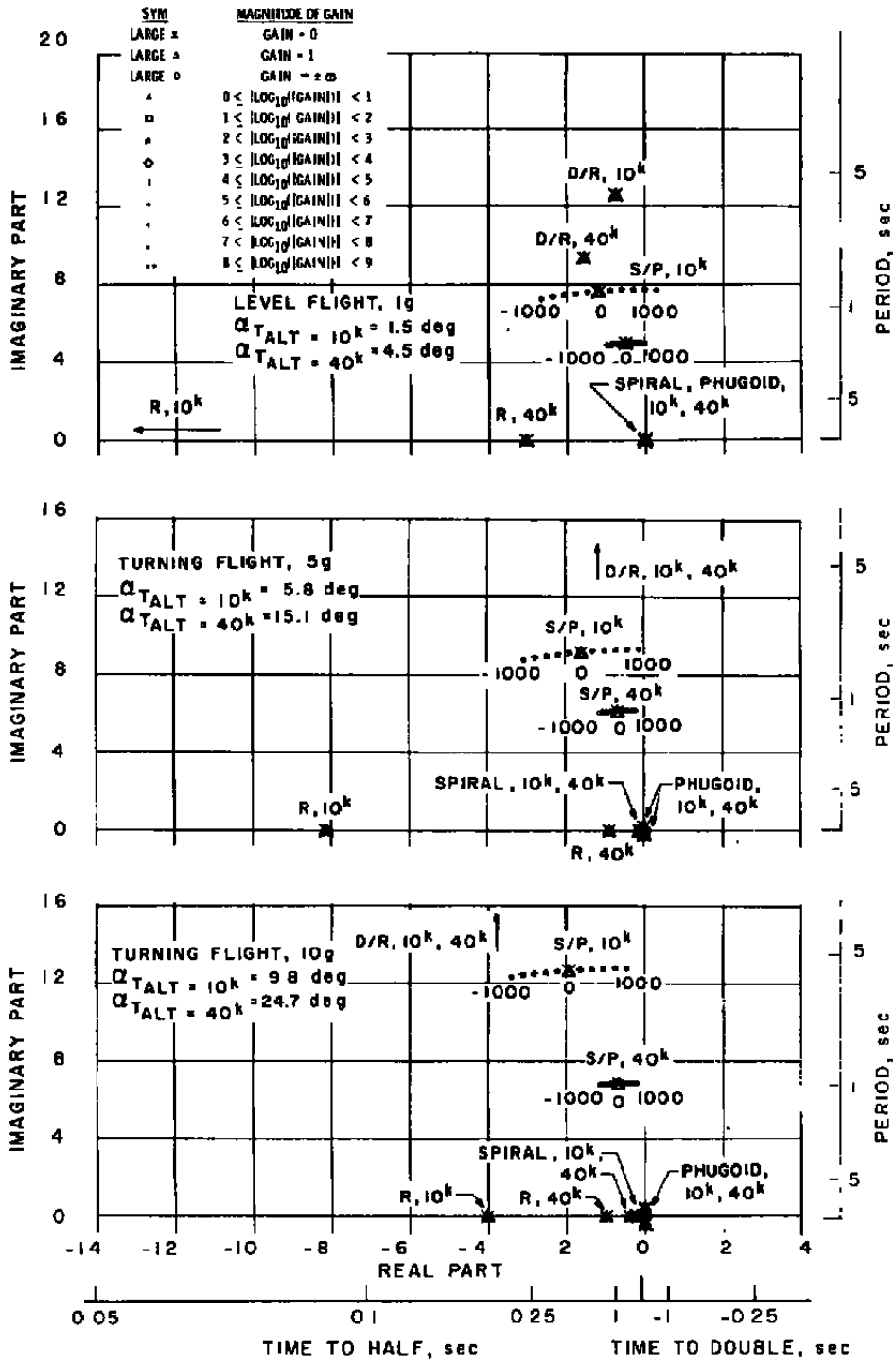

a. M = 0.8

Figure 7. Bank-to-turn configuration - locus of roots with $C_{m_{\dot{\alpha}}}$ variation.

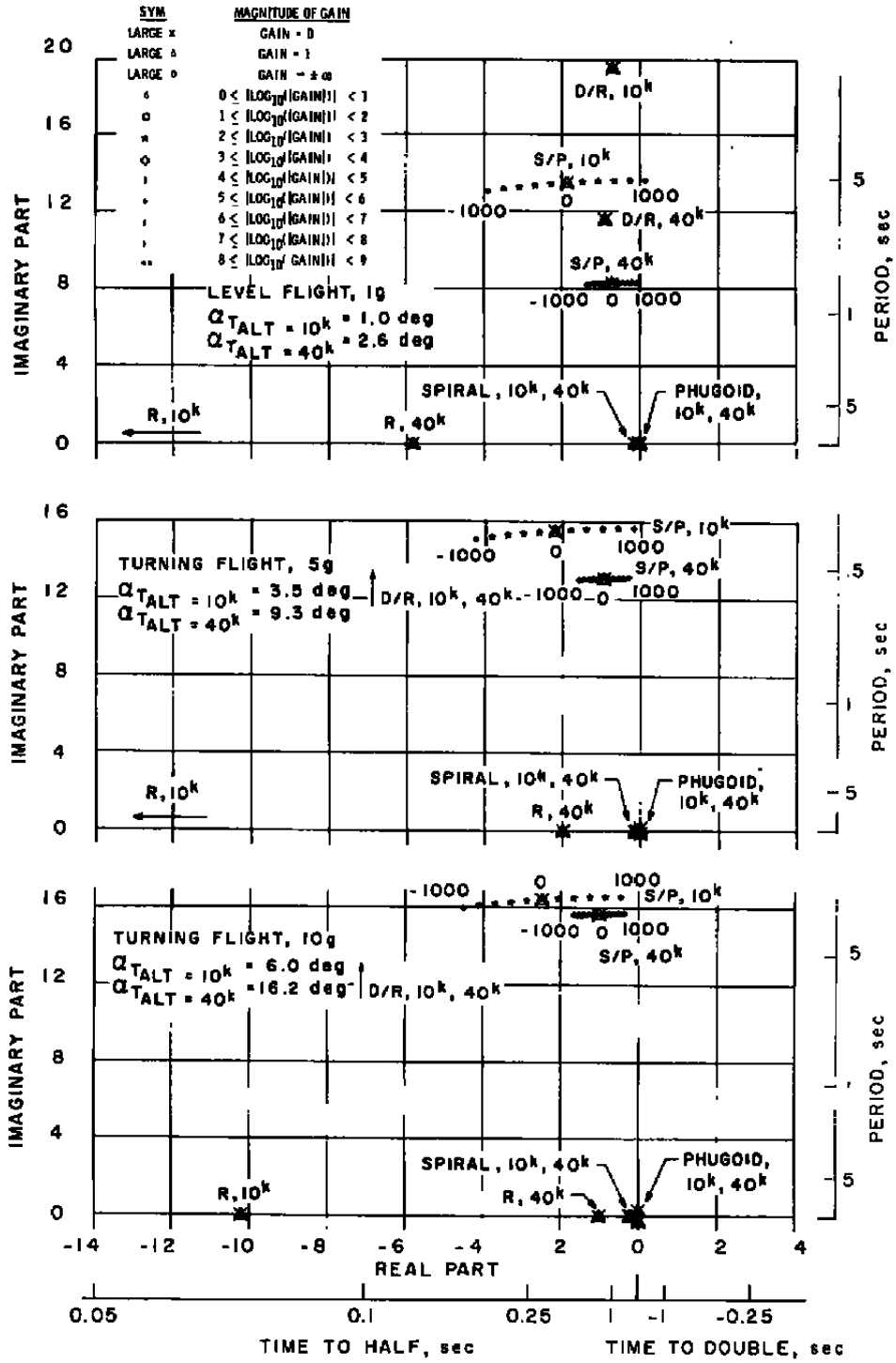

b. M = 1.1

Figure 7. Continued.

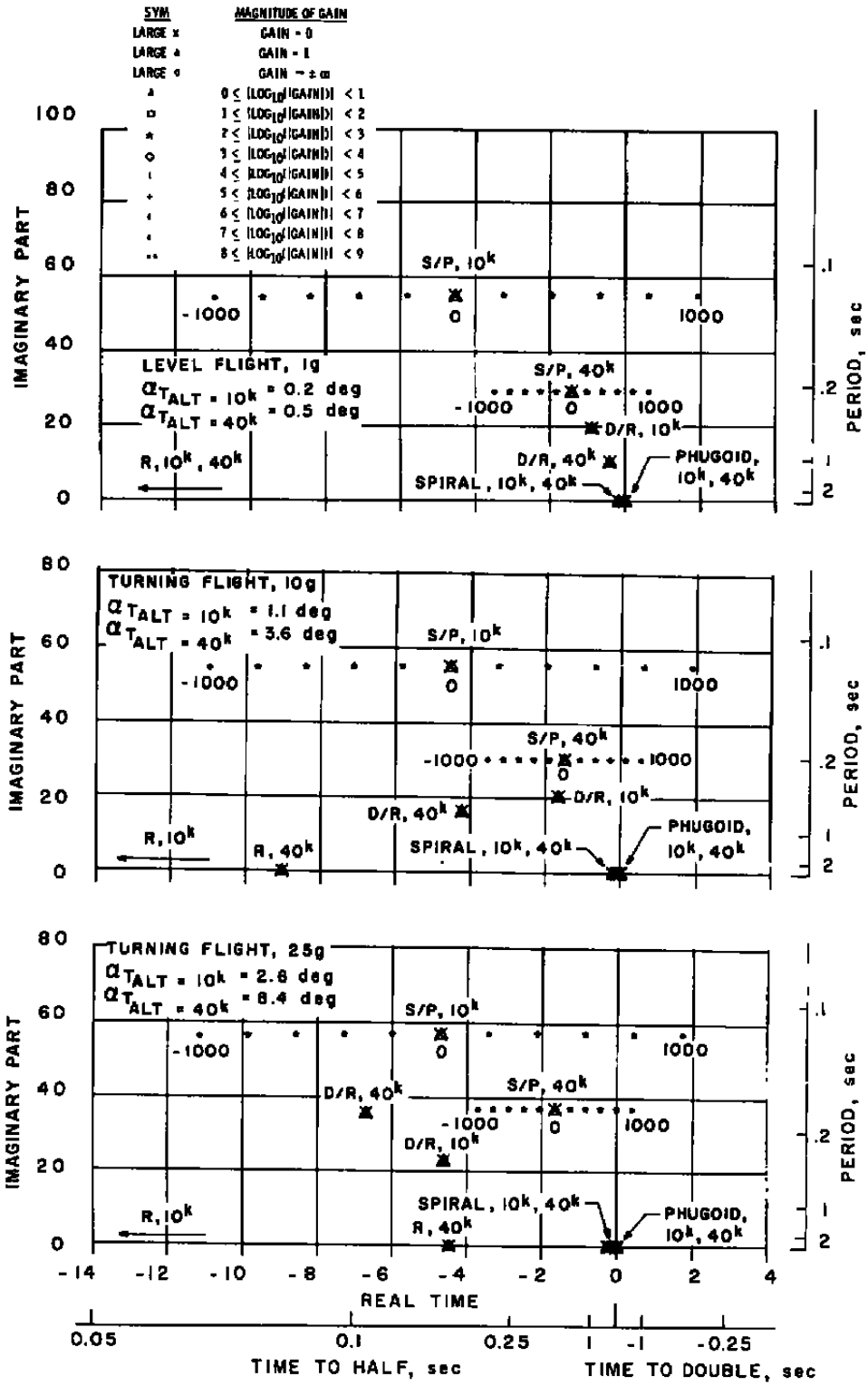

c. M = 3.5

Figure 7. Concluded.

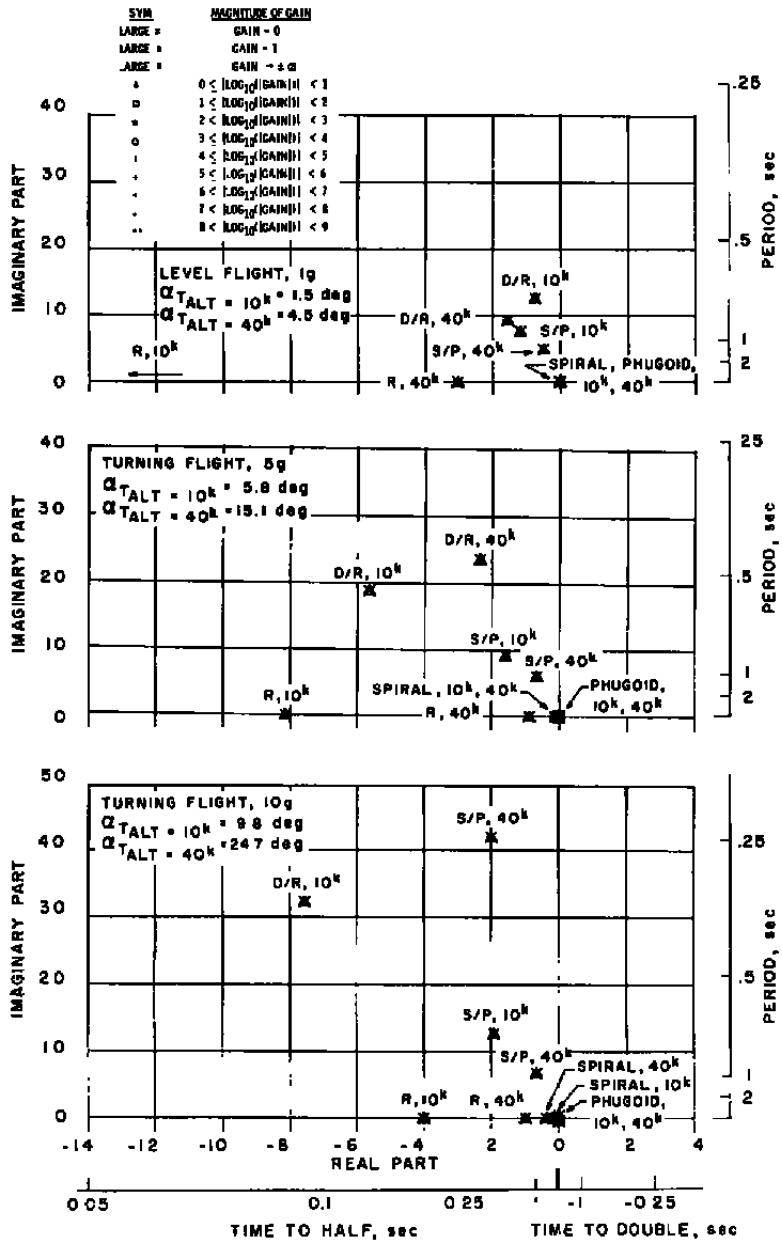

a. M = 0.8

Figure 8. Bank-to-turn configuration - locus of roots with C_{L_q}, $C_{L_{\dot{\alpha}}}$, C_{y_r}, C_{n_q} and C_{m_r} variation.

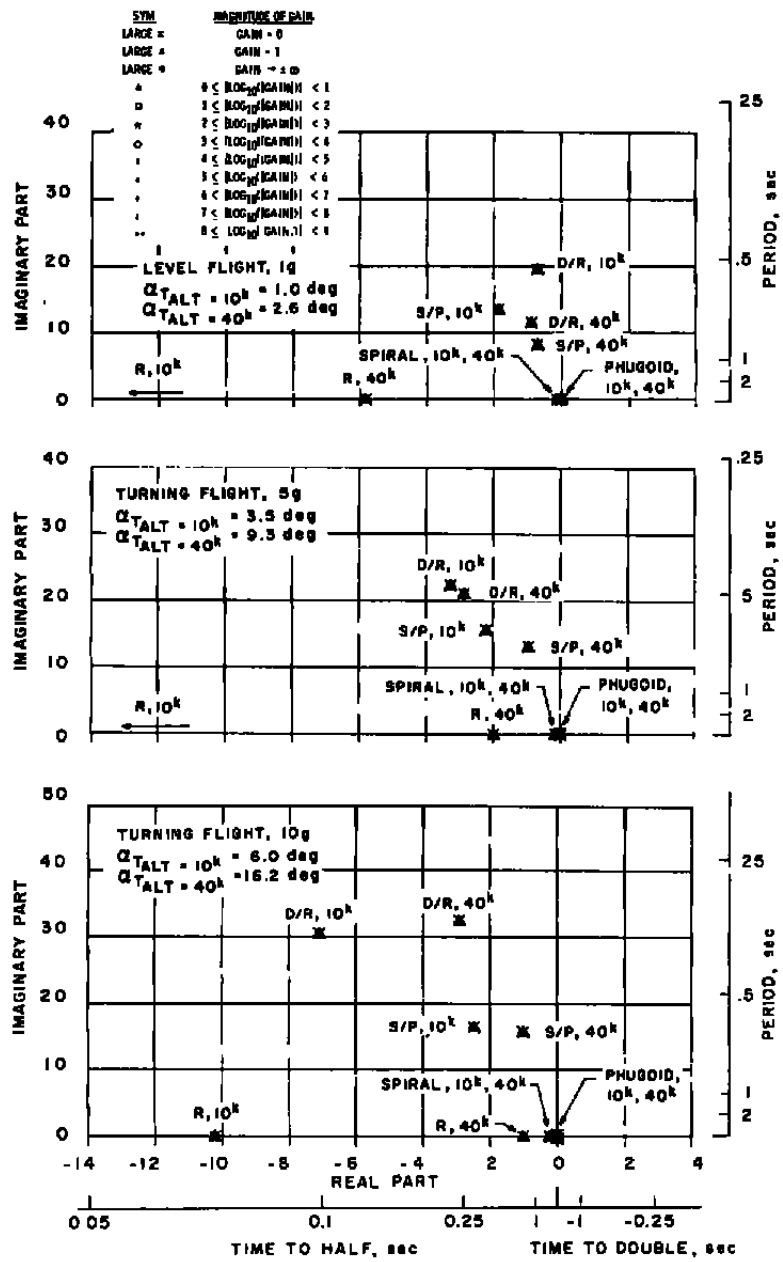

b. M = 1.1

Figure 8. Continued.

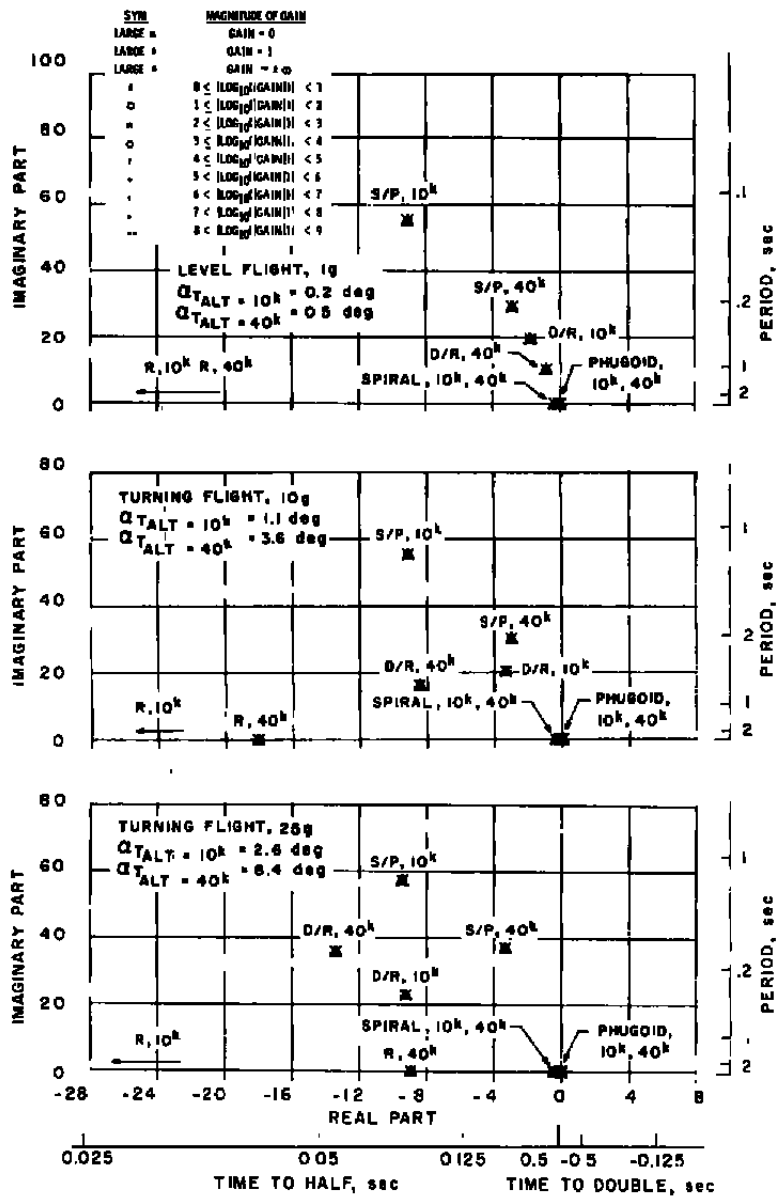

c. M = 3.5

Figure 8. Concluded.

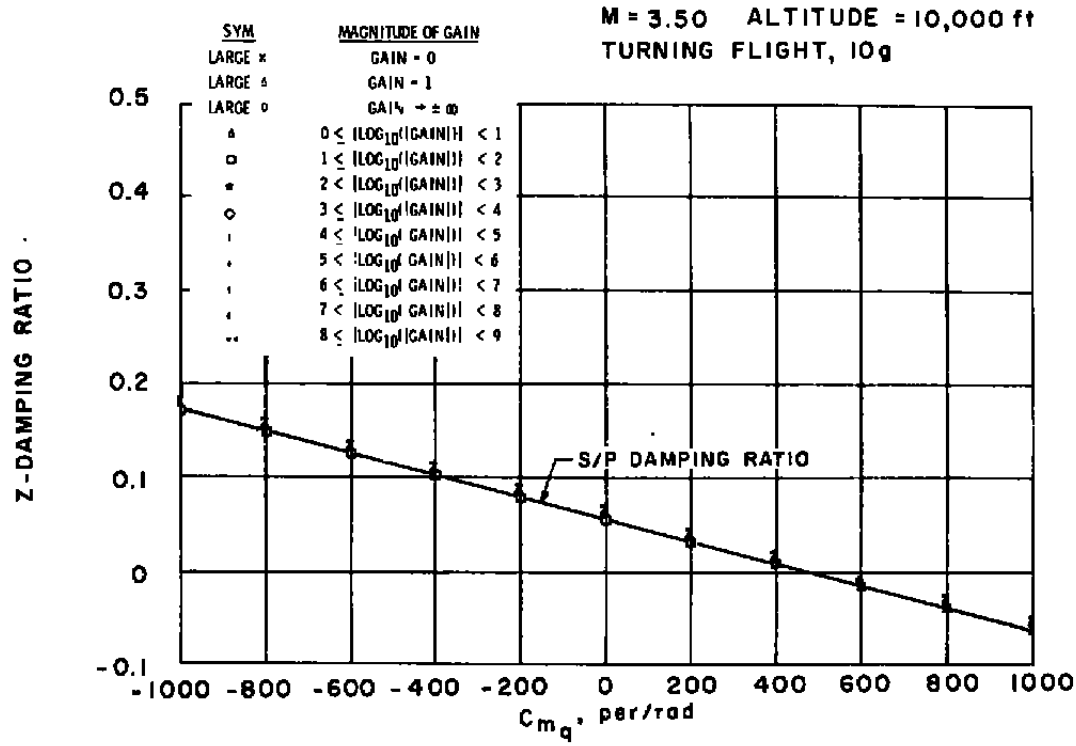

a. Damping ratio

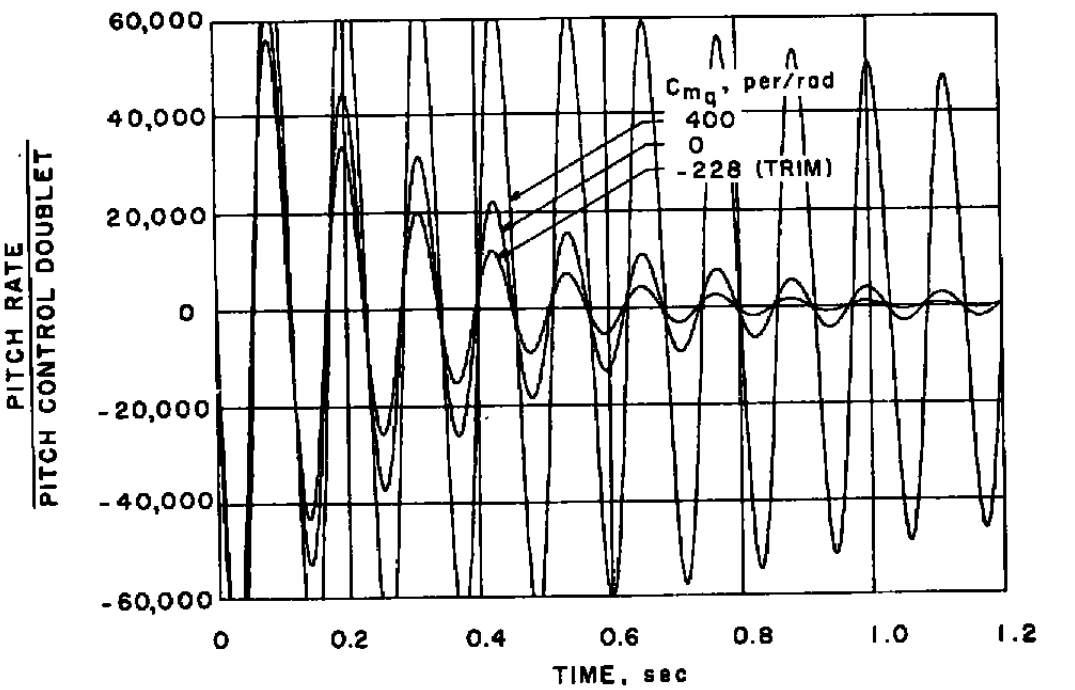

b. Time reponse

Figure 9. Bank-to-turn configuration - effect of C_{m_q} on damping ratio and time response.

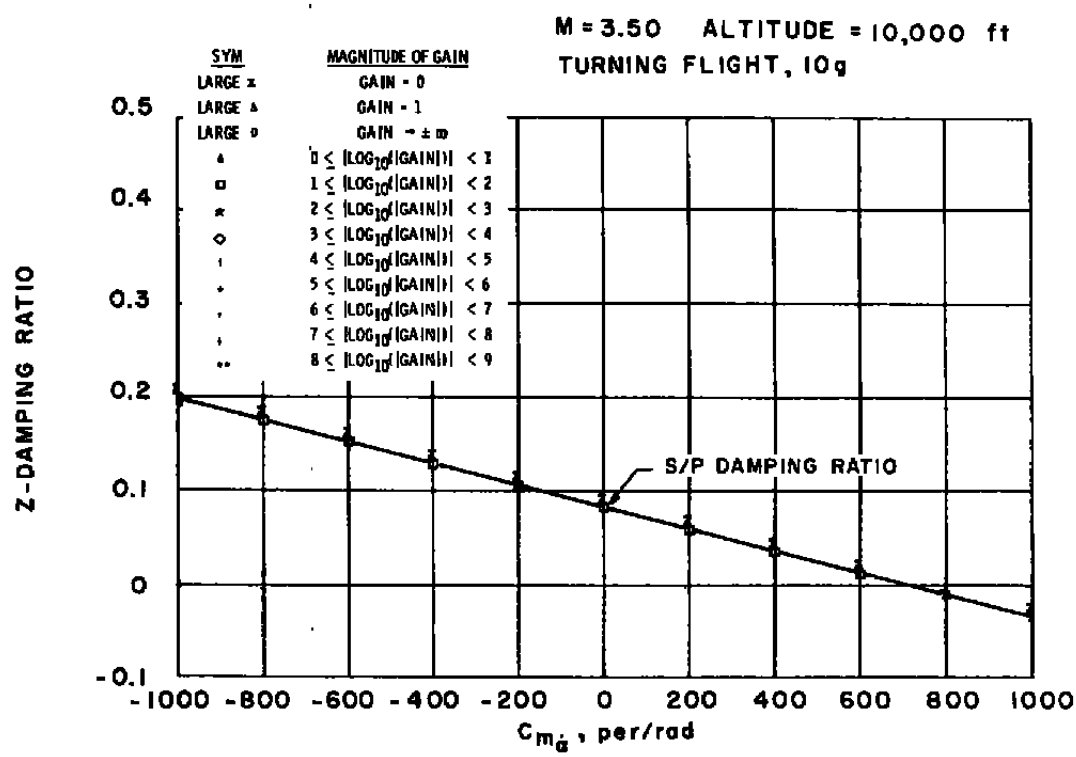

a. Damping ratio

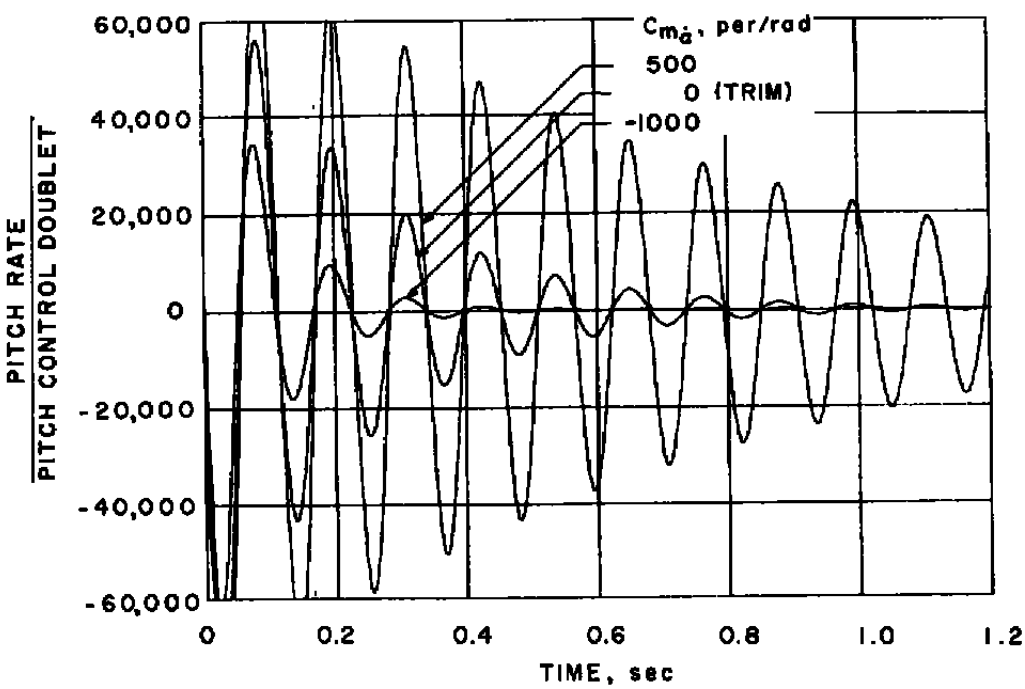

b. Time response

Figure 10. Bank-to-turn configuration - effect of $C_{m_{\dot{\alpha}}}$ on damping ratio and time response.

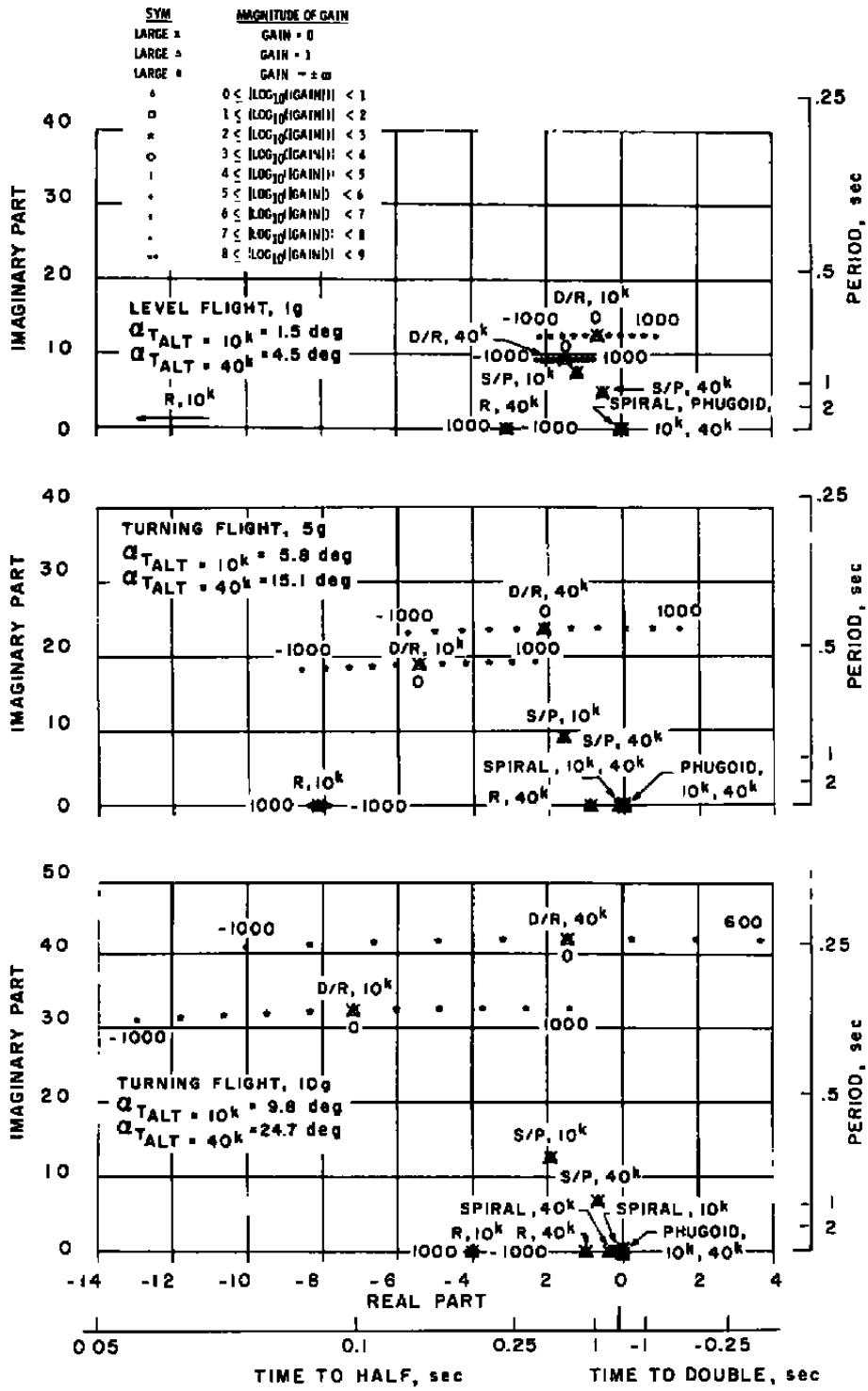

a. M = 0.8

Figure 11. Bank-to-turn configuration - locus of roots with C_{n_r} variation.

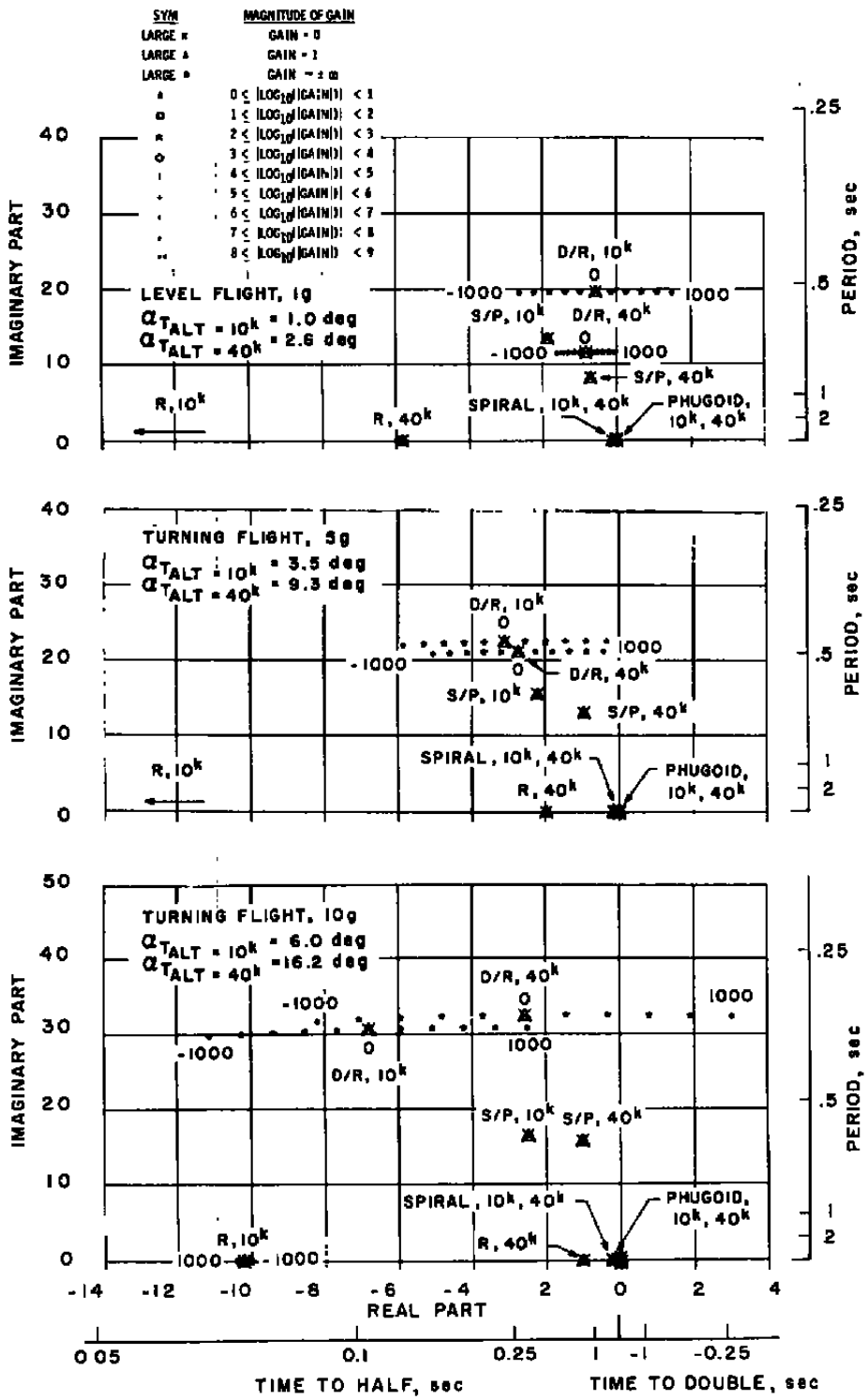

b. M = 1.1

Figure 11. Continued.

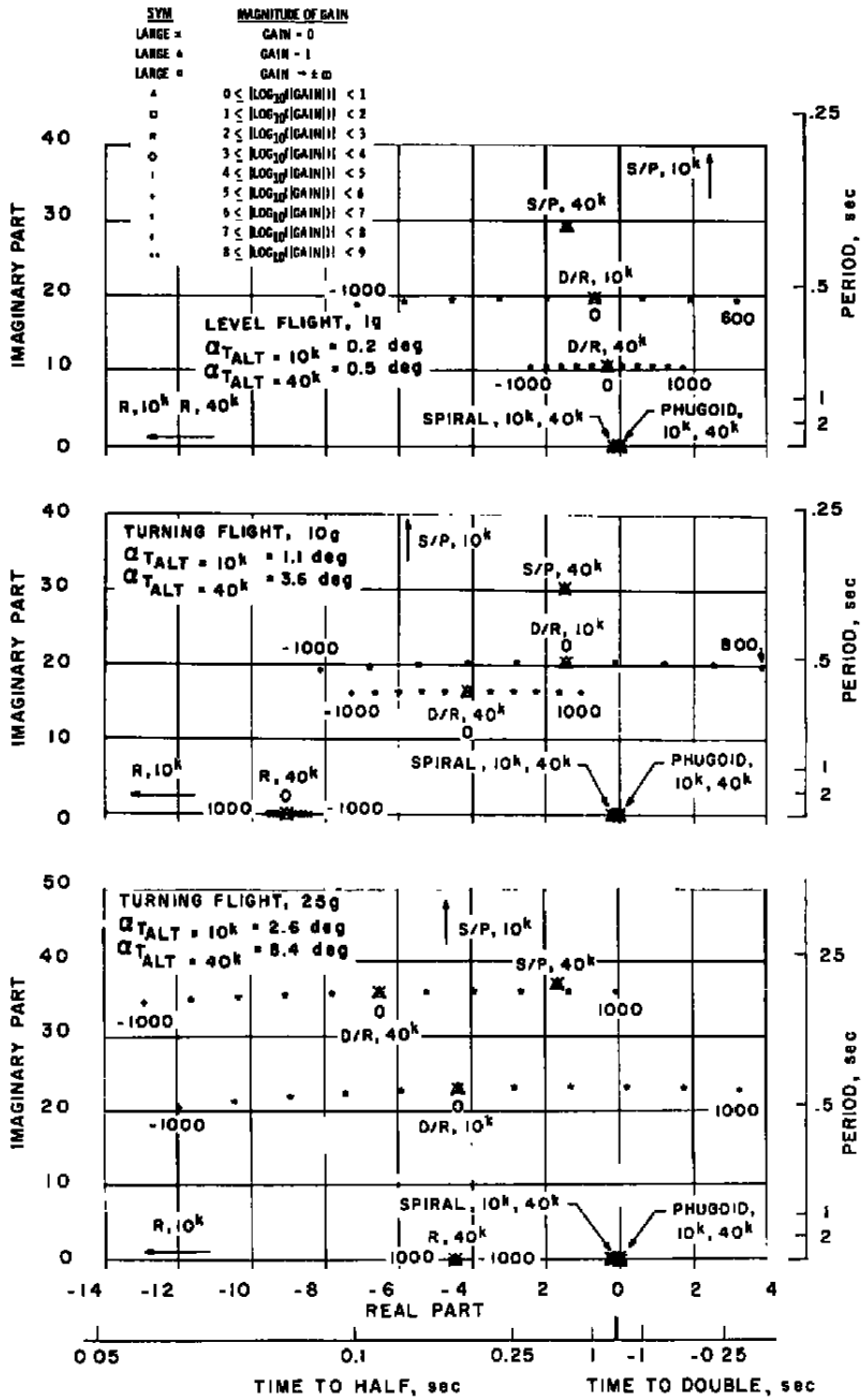

c. M = 3.5

Figure 11. Concluded.

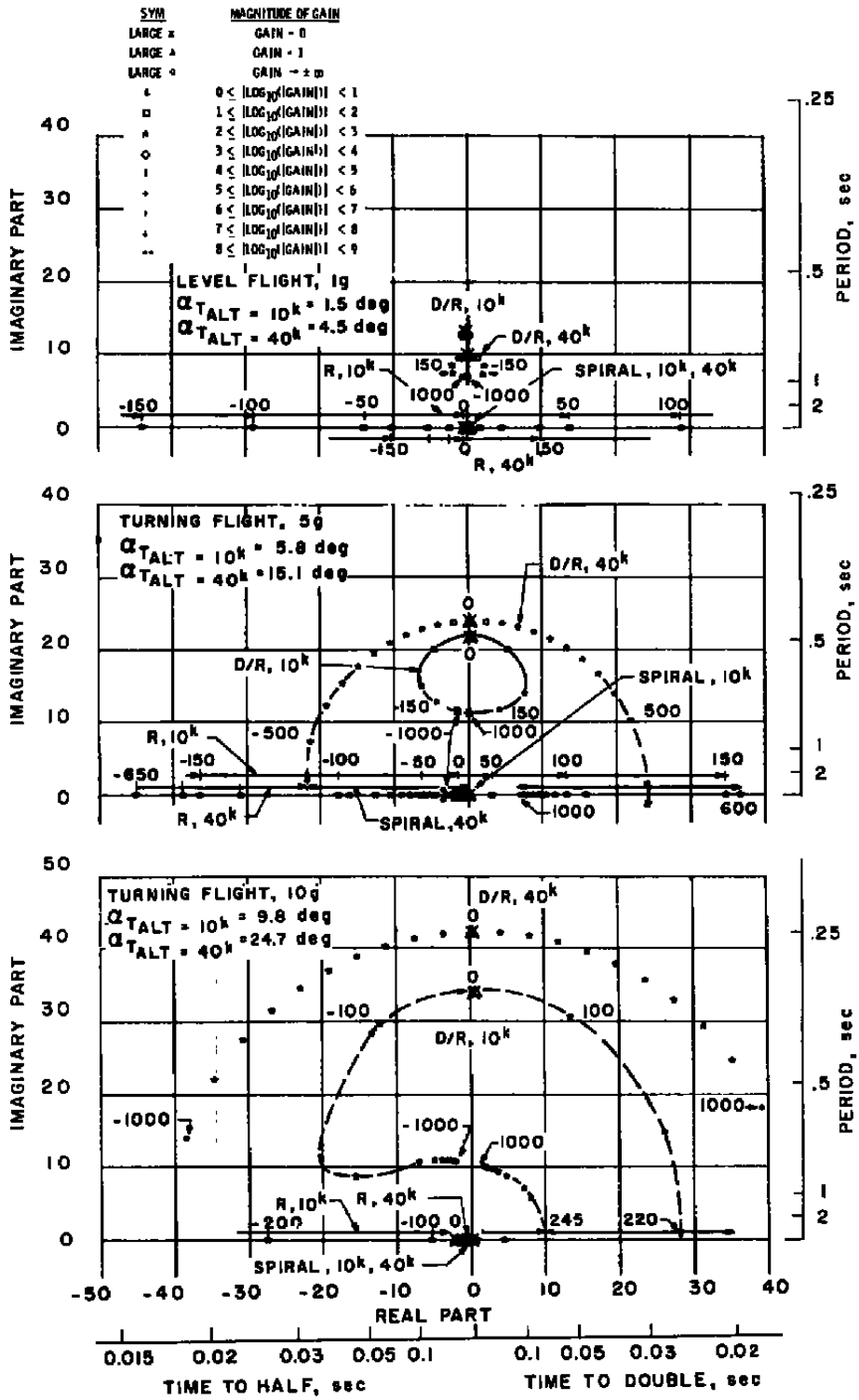

a. M = 0.8

Figure 12. Bank-to-turn configuration - locus of roots with $C\ell_p$ variation.

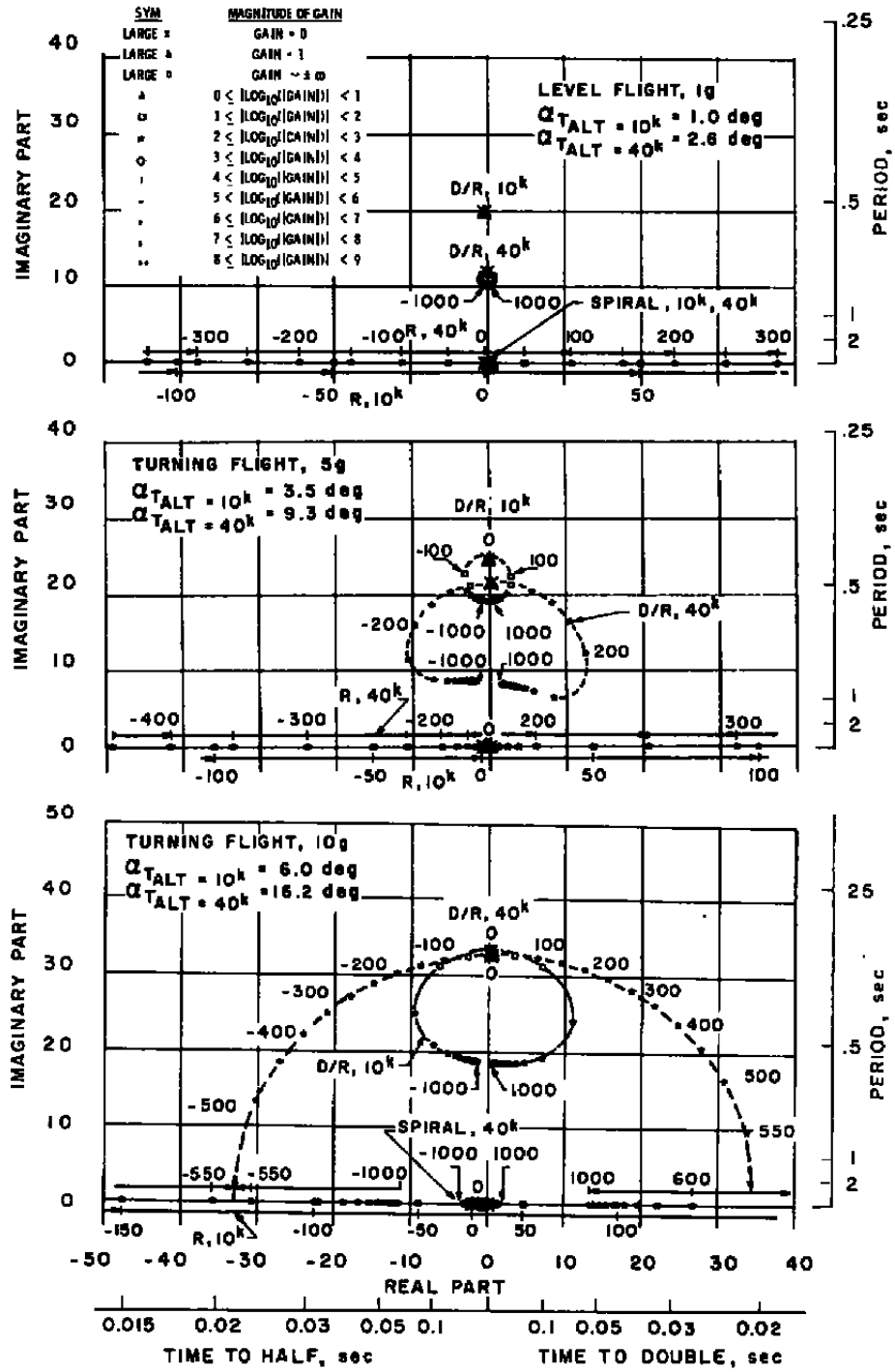

b. M = 1.1

Figure 12. Continued.

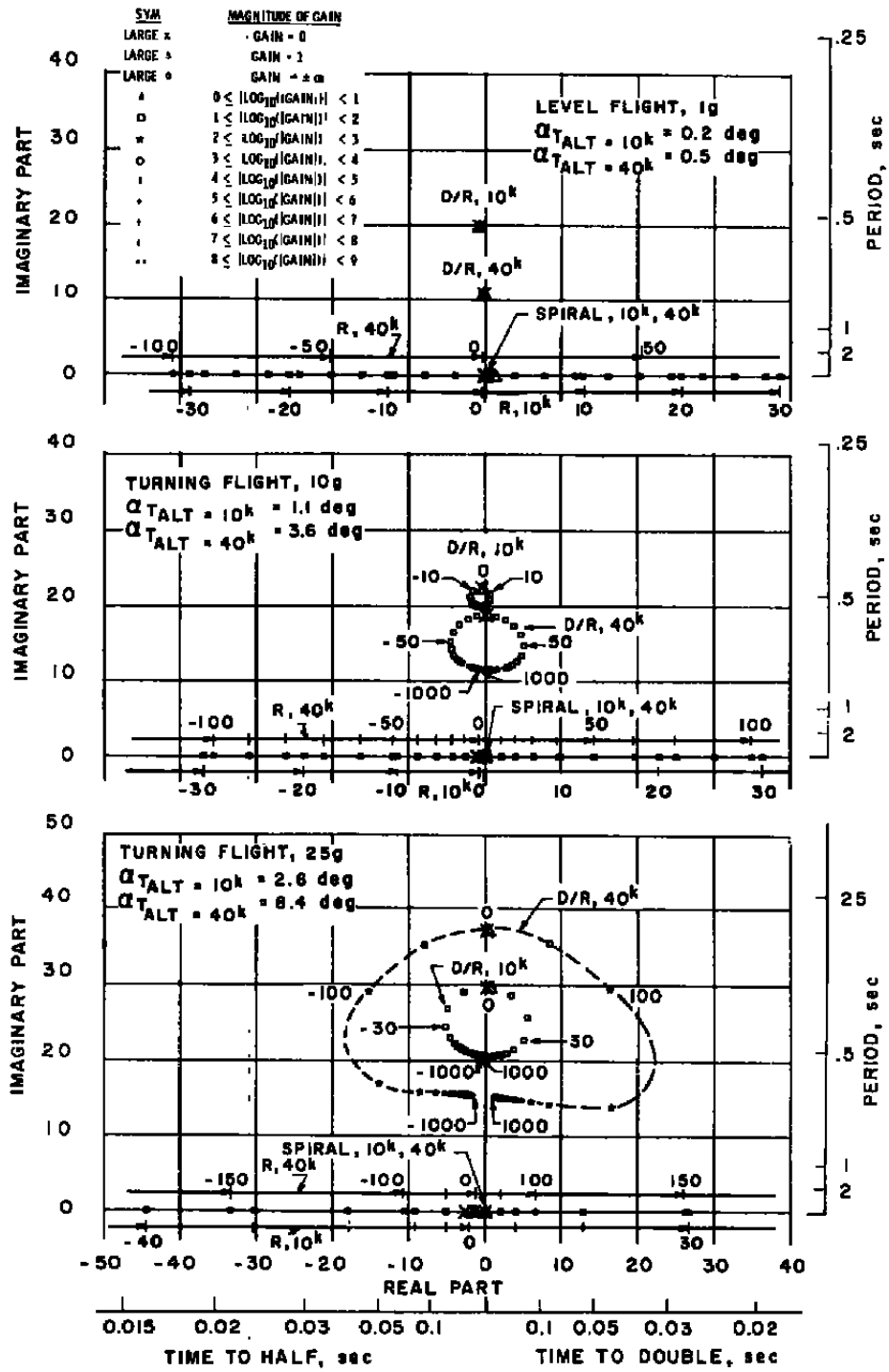

c. M = 3.5

Figure 12. Concluded.

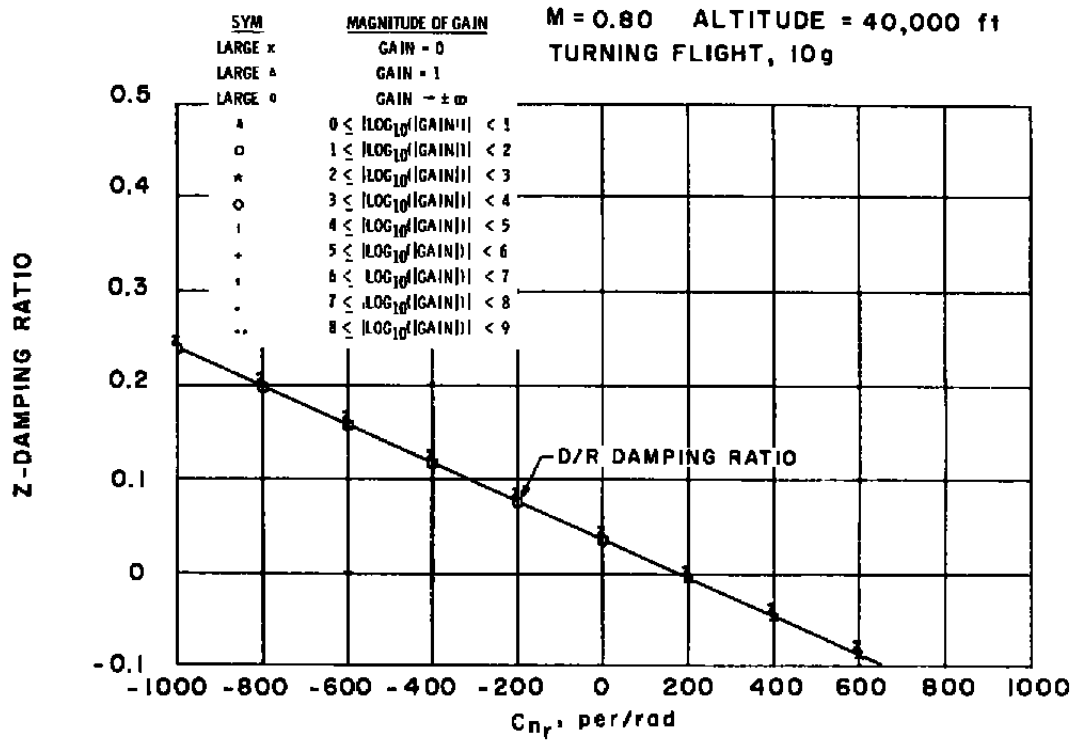

a. Damping ratio

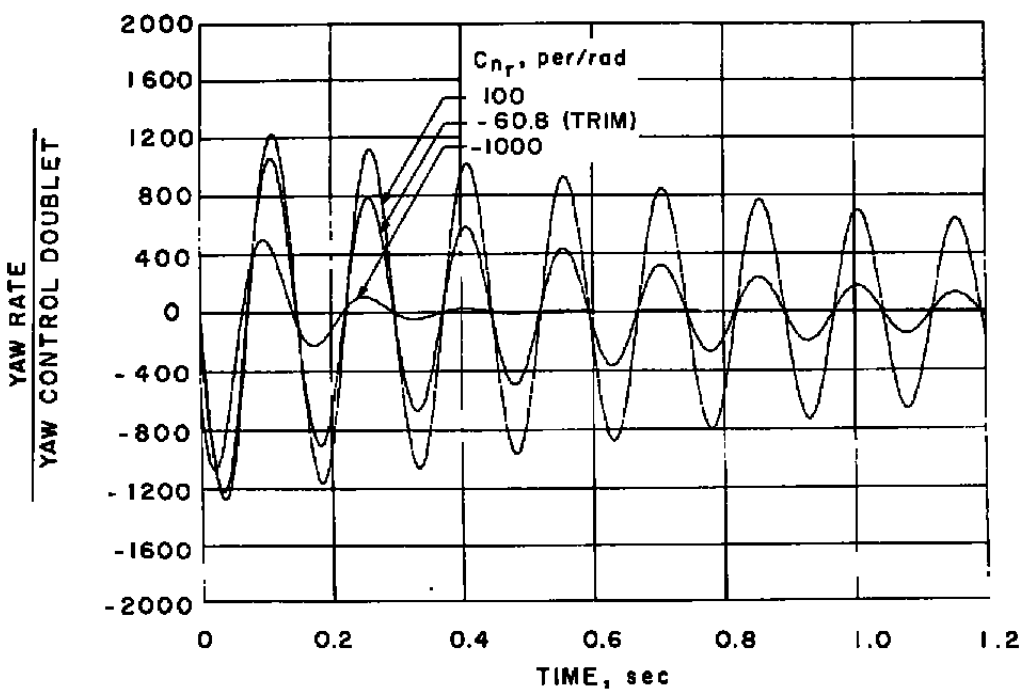

b. Time response

Figure 13. Bank-to-turn configuration - effect of C_{n_r} on damping ratio and time response.

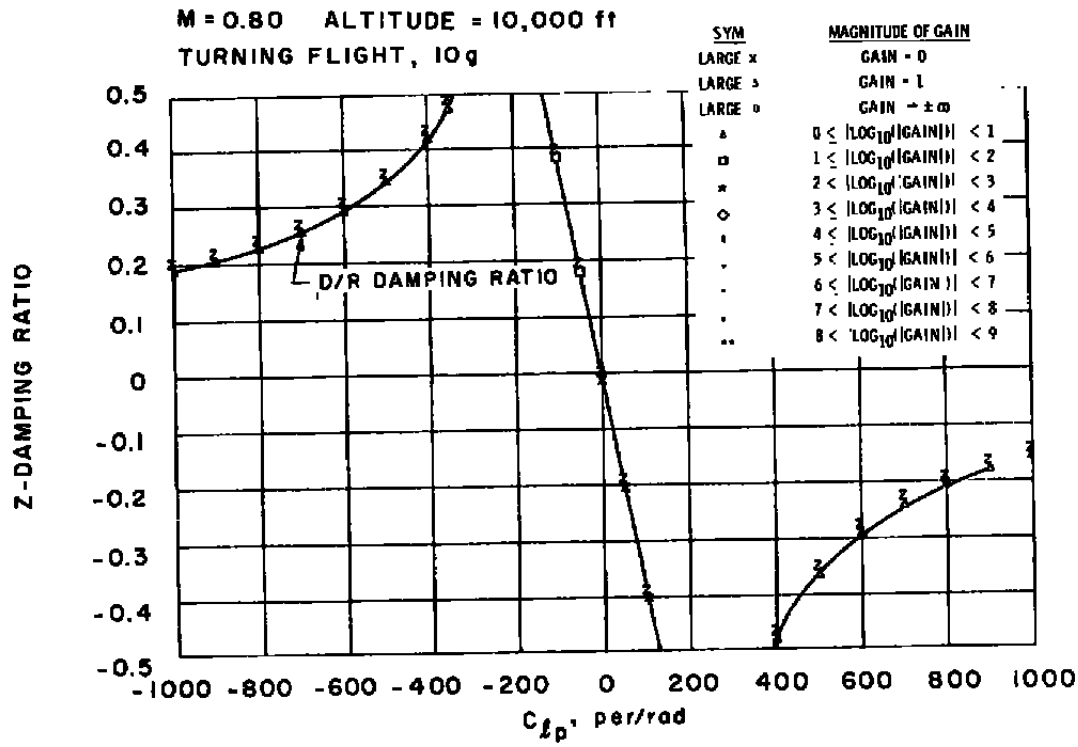

a. Damping ratio

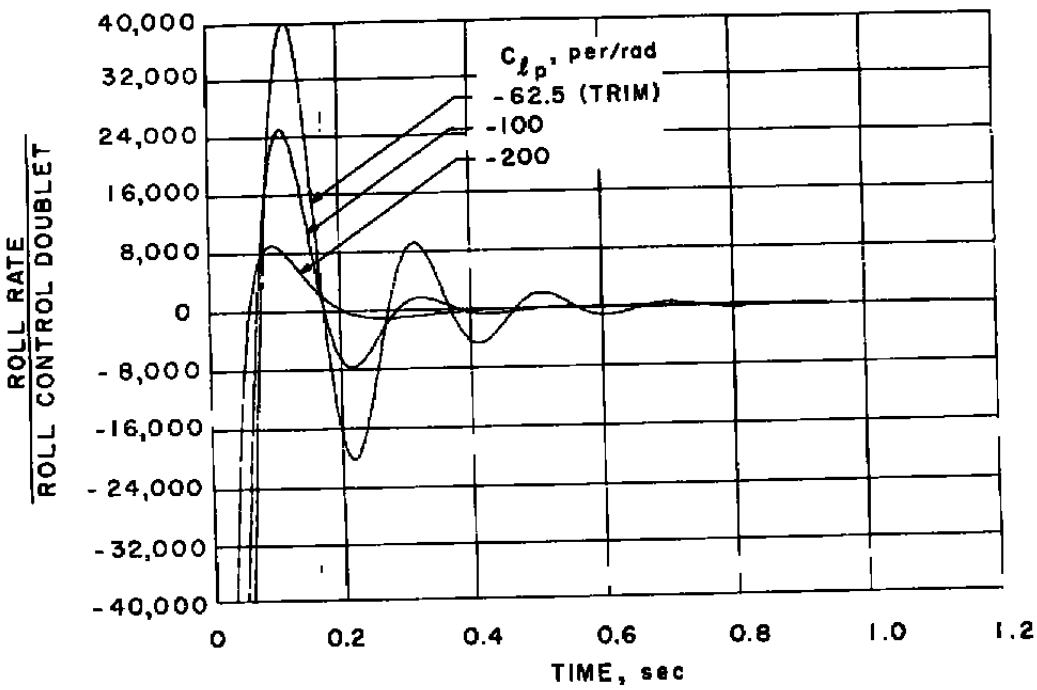

b. Time response

Figure 14. Bank-to-turn configuration - effect of $C\ell_p$ on damping ratio and time response.

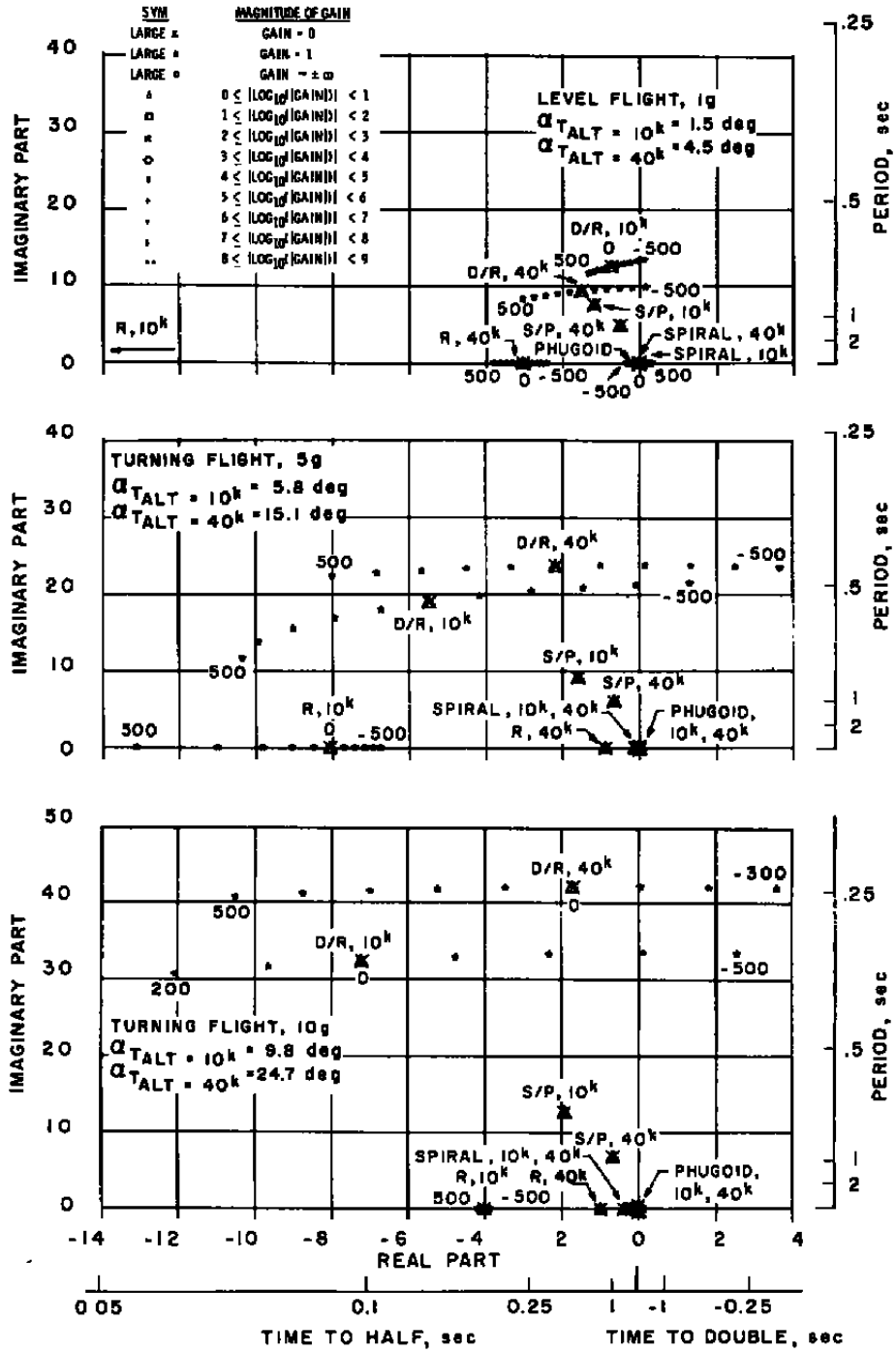

a. M = 0.8

Figure 15. Bank-to-turn configuration - locus of roots with $C\ell_r$ variation.

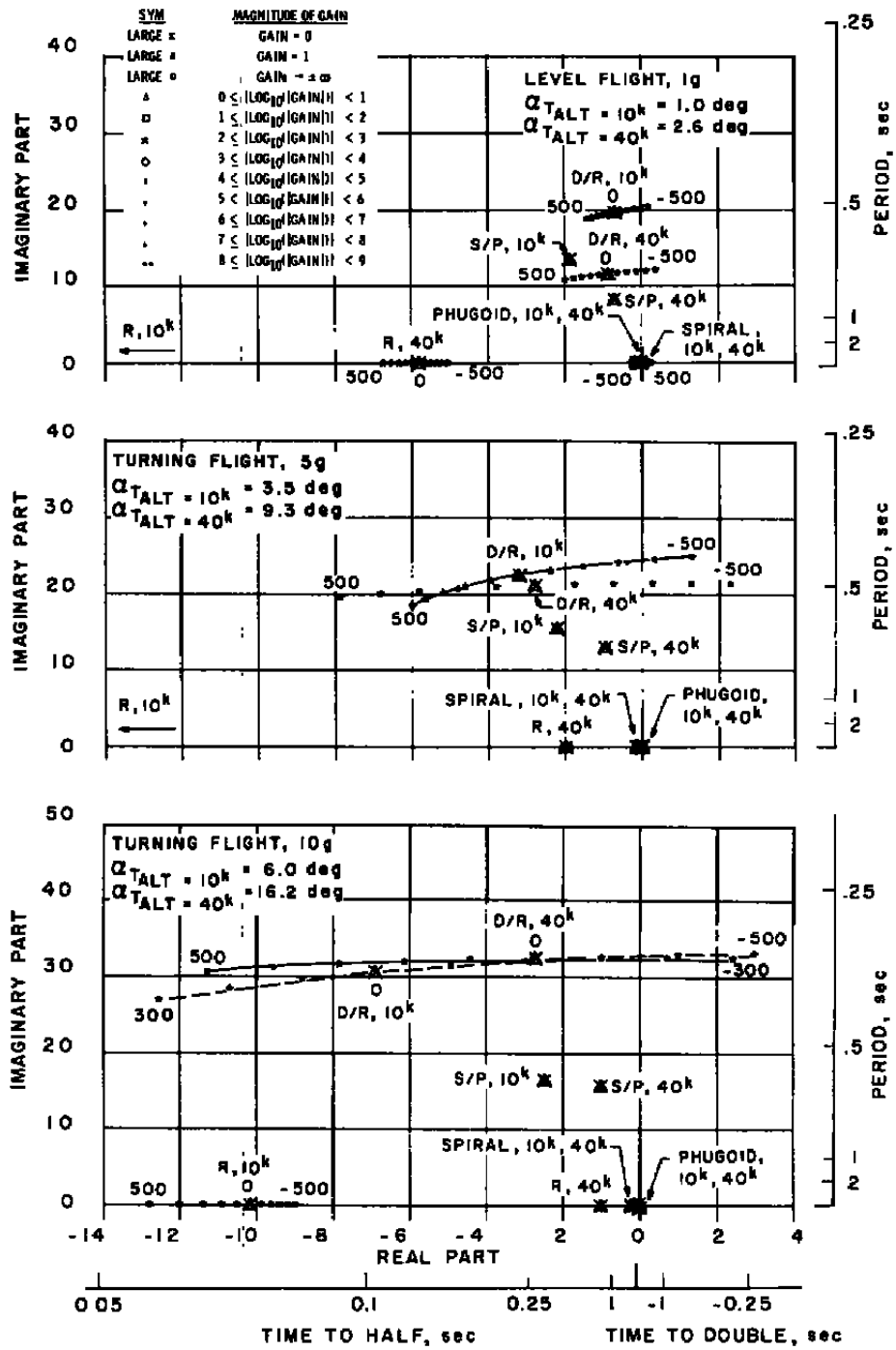

b. M = 1.1

Figure 15. Continued.

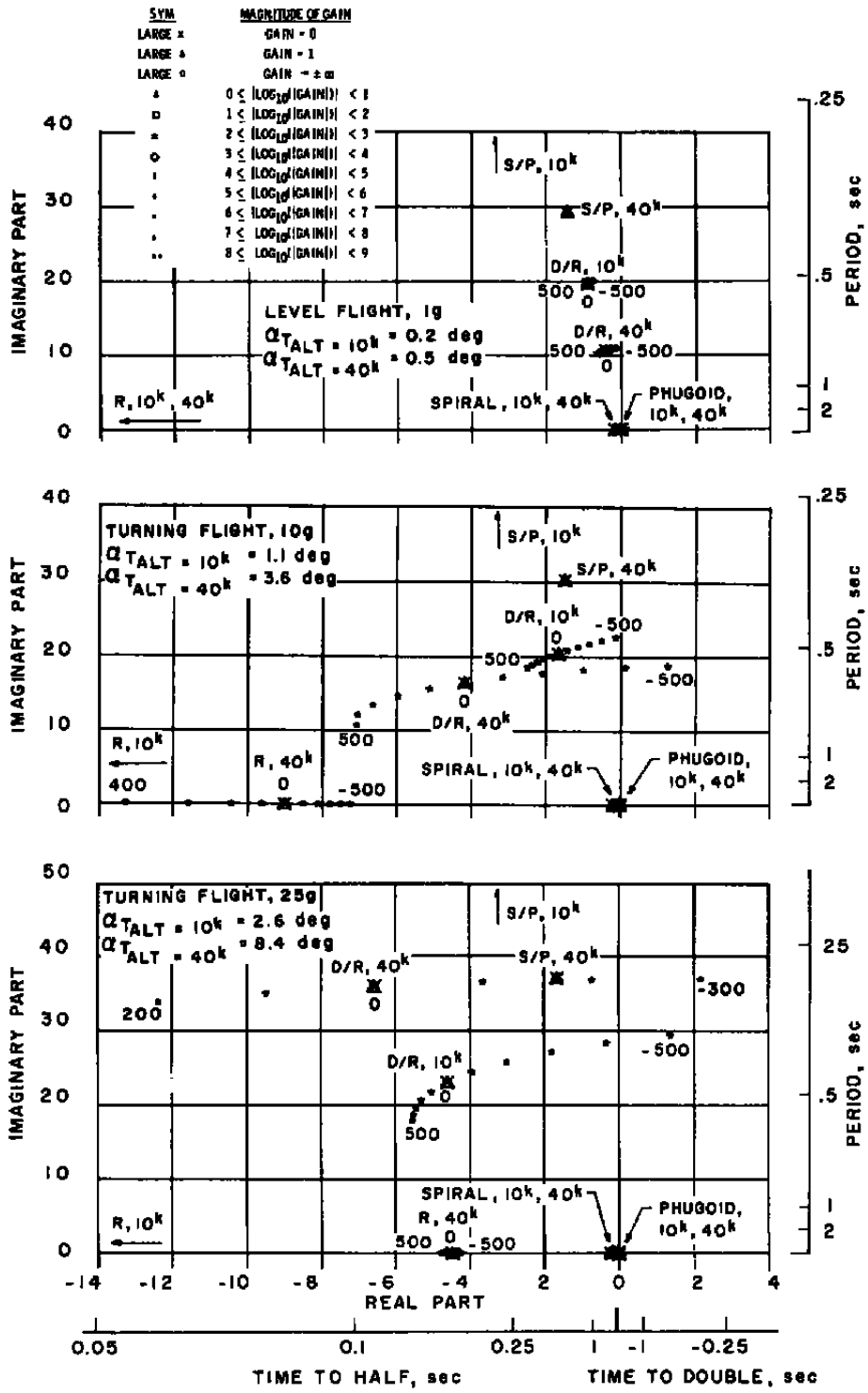

c. M = 3.5

Figure 15. Concluded.

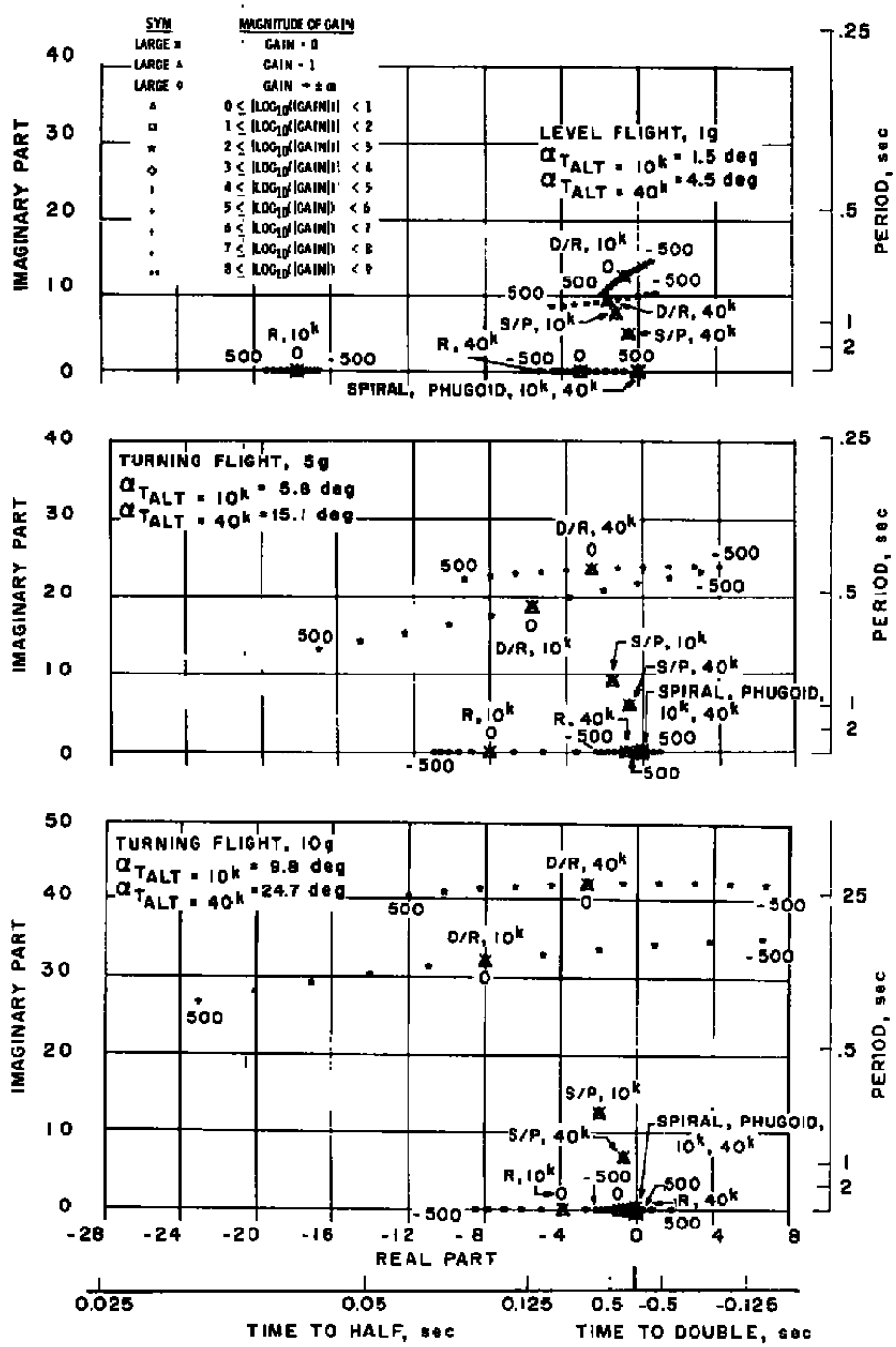

a. M = 0.8

Figure 16. Bank-to-turn configuration - locus of roots with C_{n_p} variation.

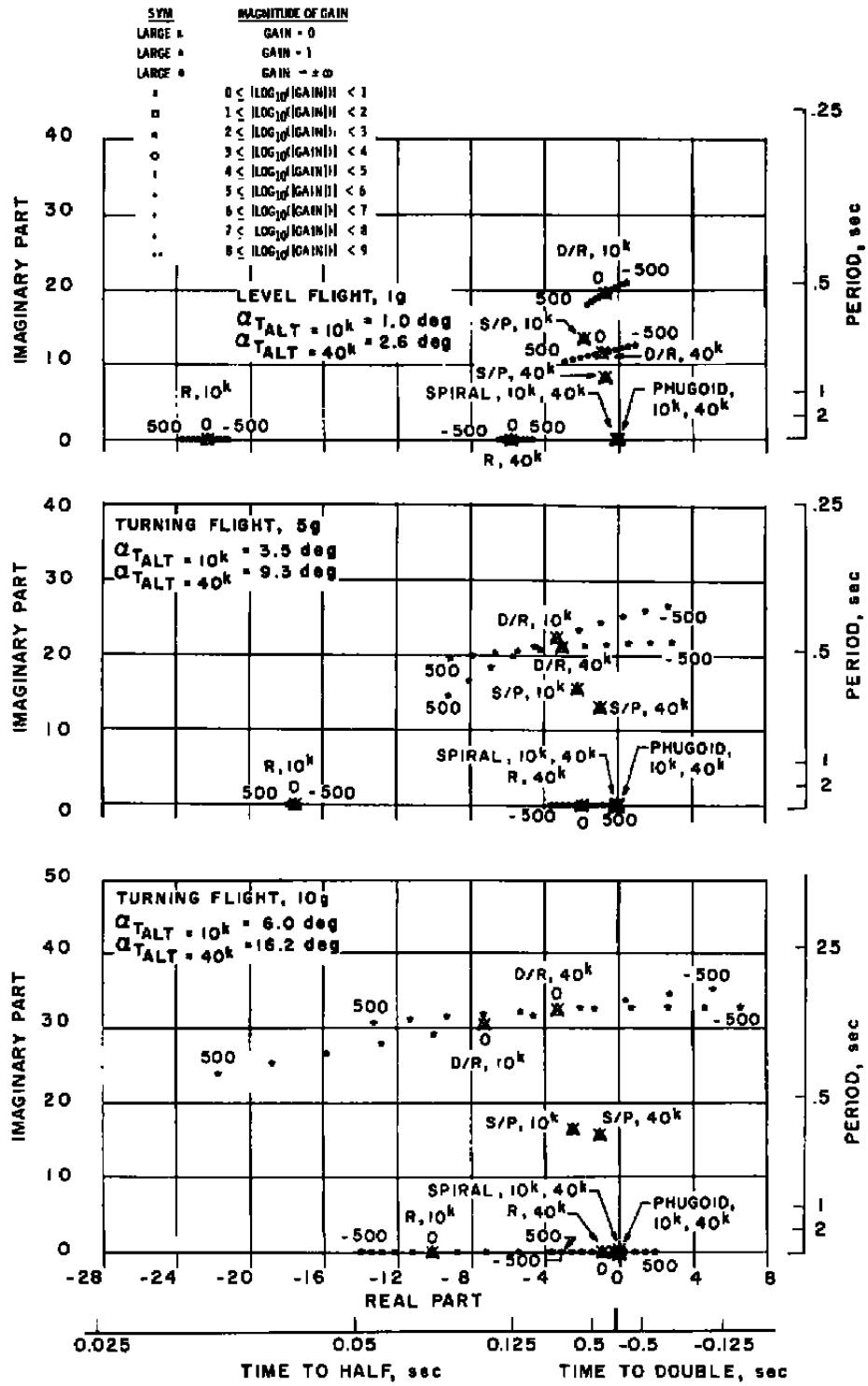

b. M = 1.1

Figure 16. Continued.

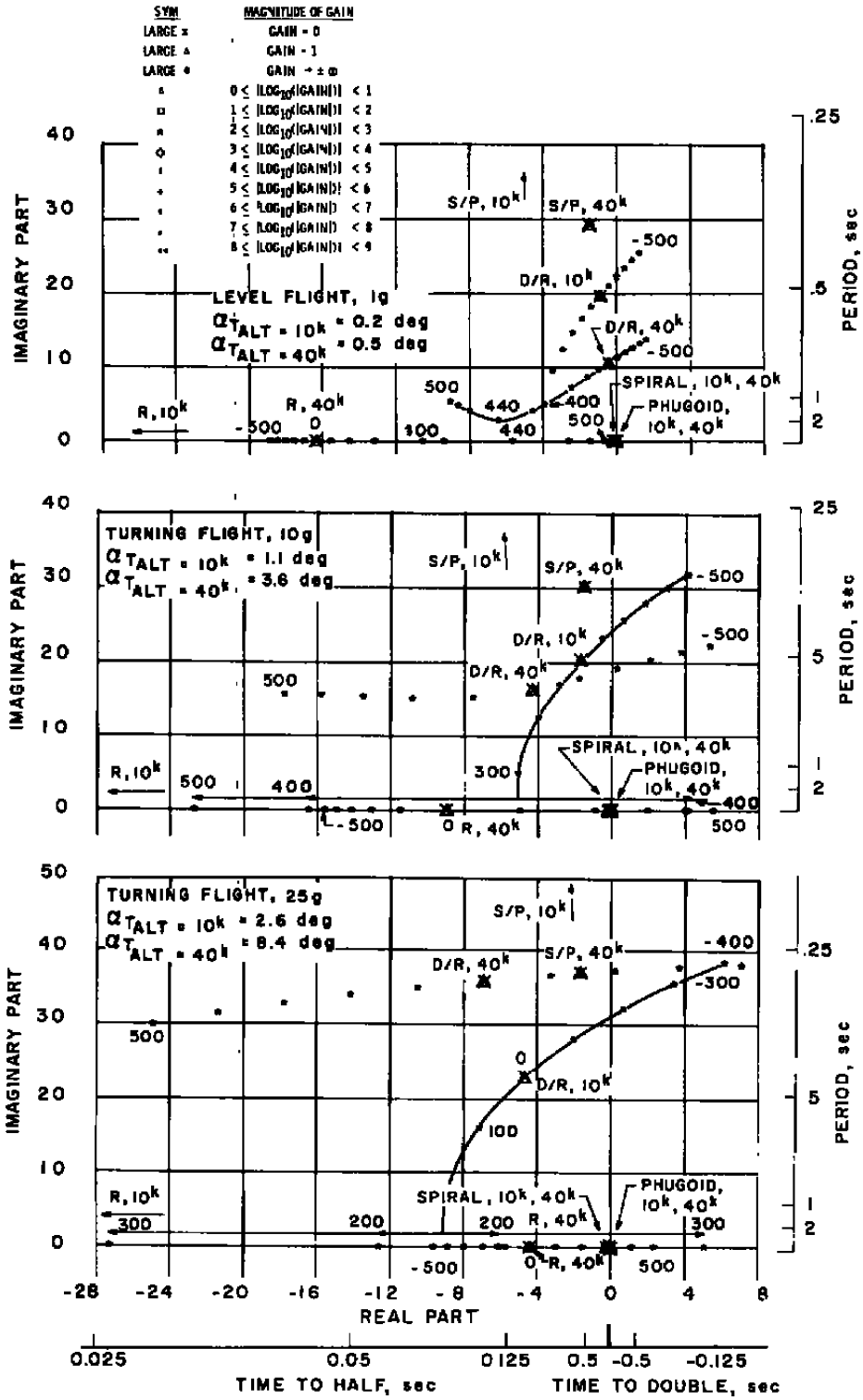

c. M = 3.5

Figure 16. Concluded.

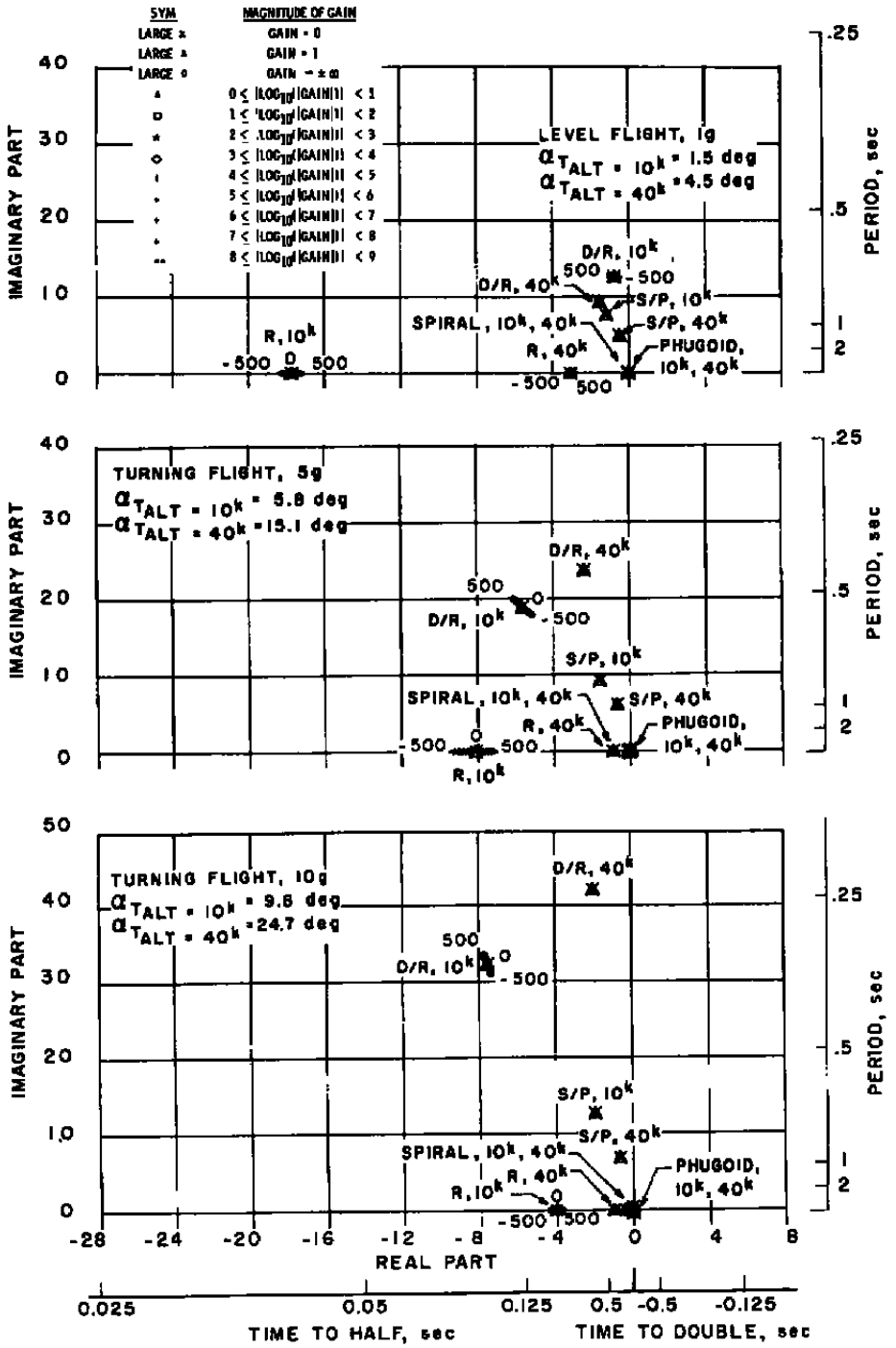

a. M = 0.8

Figure 17. Bank-to-turn configuration - locus of roots with C_{Y_p} variation.

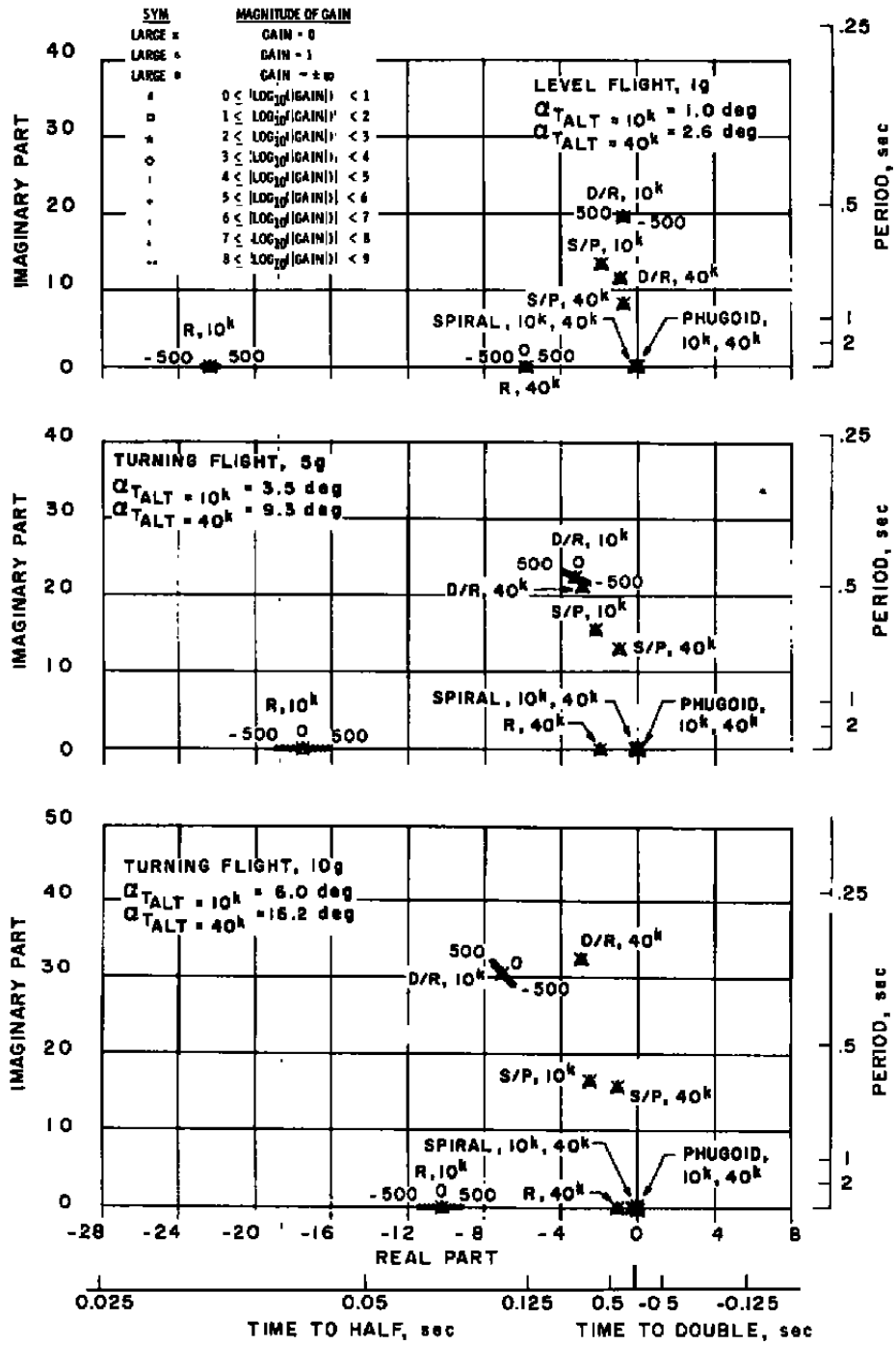

b. M = 1.1

Figure 17. Continued.

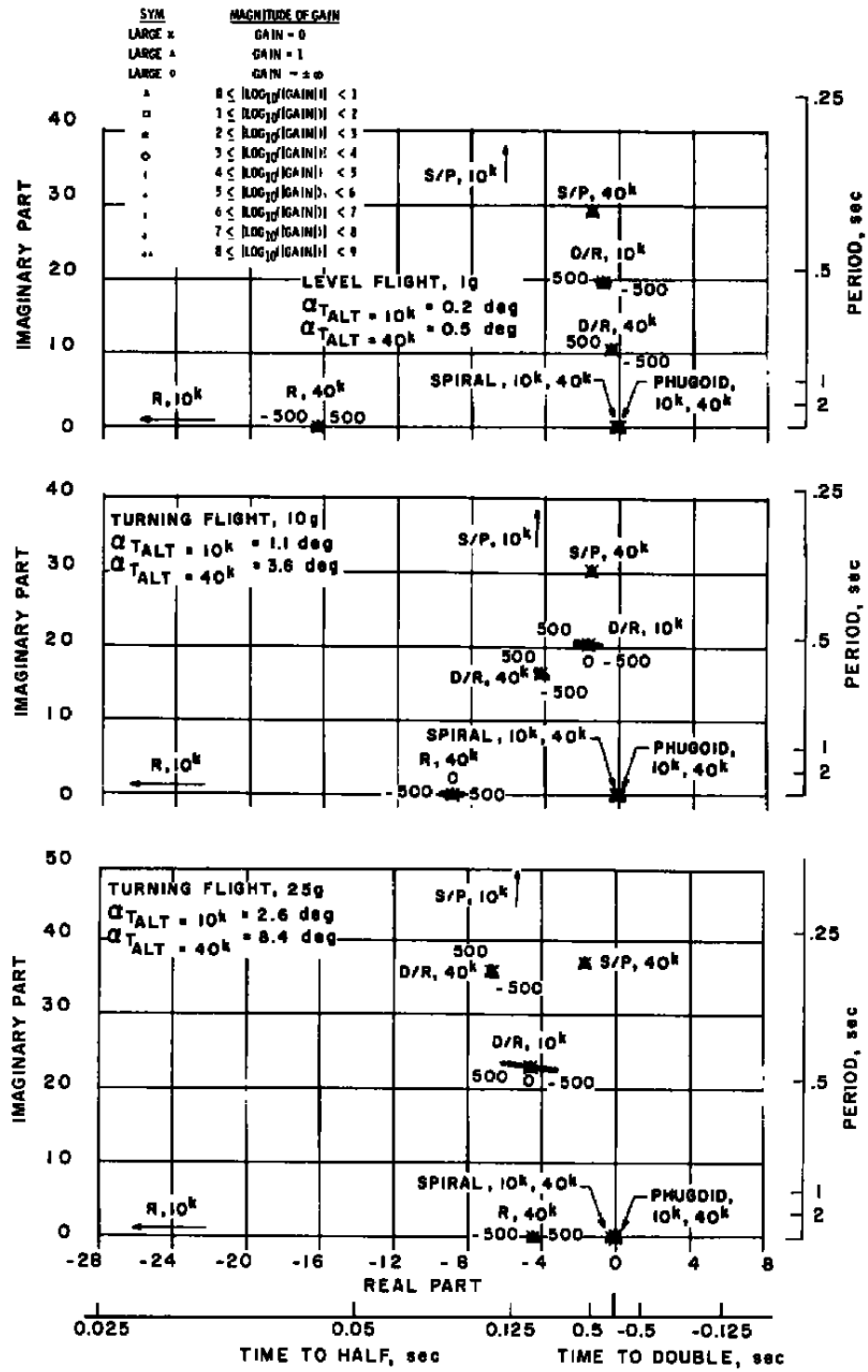

c. M = 3.5

Figure 17. Concluded.

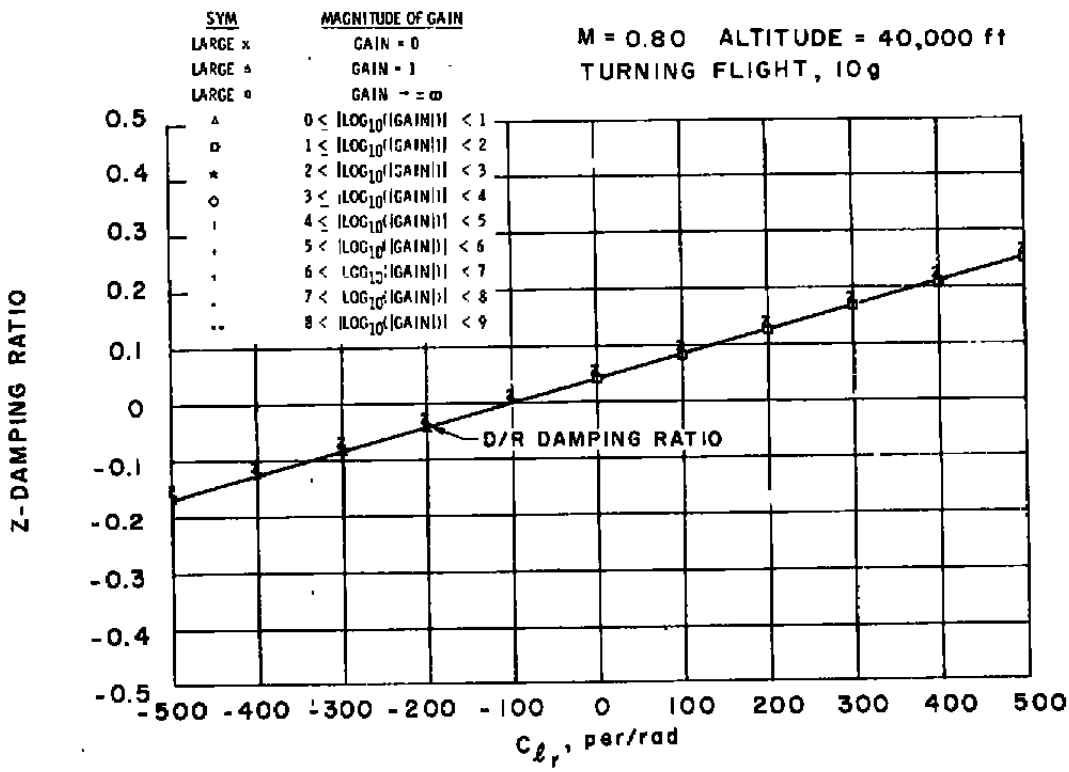

a. Damping ratio

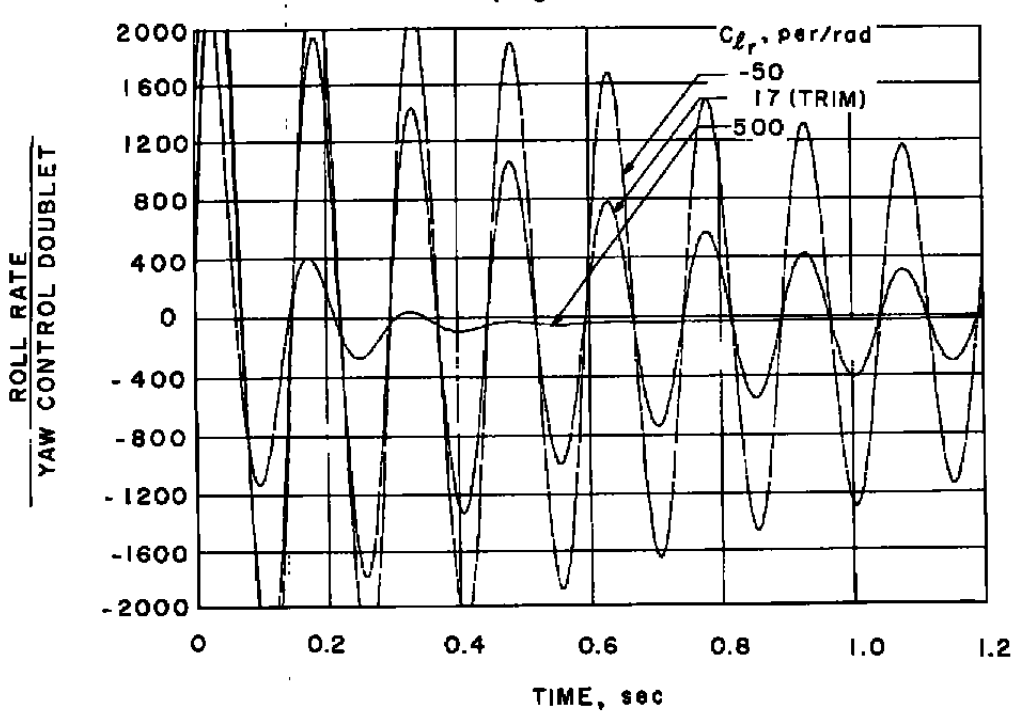

b. Time response

Figure 18. Bank-to-turn configuration - effect of $C\ell_r$ on damping ratio and time response.

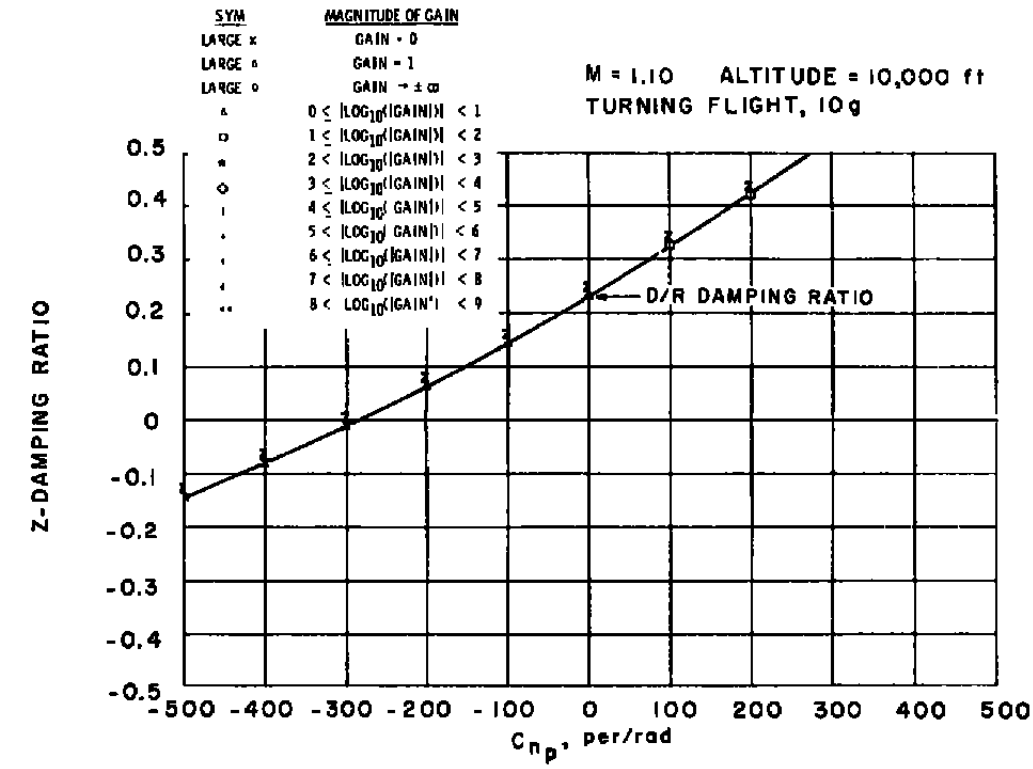

a. Damping ratio

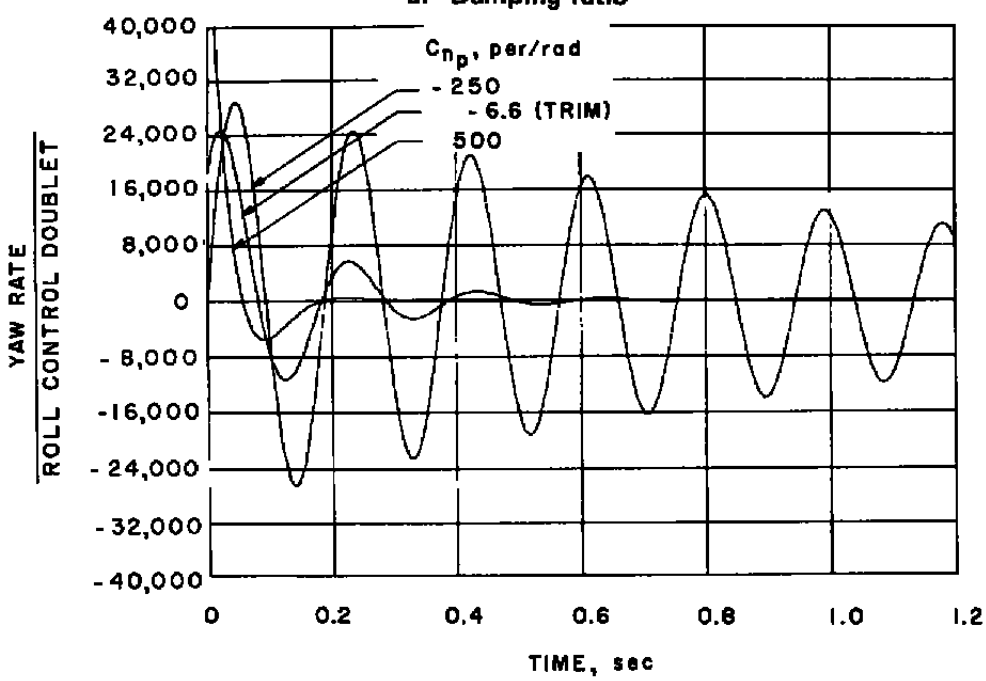

b. Time response

Figure 19. Bank-to-turn configuration - effect of C_{n_p} on damping ratio and time response.

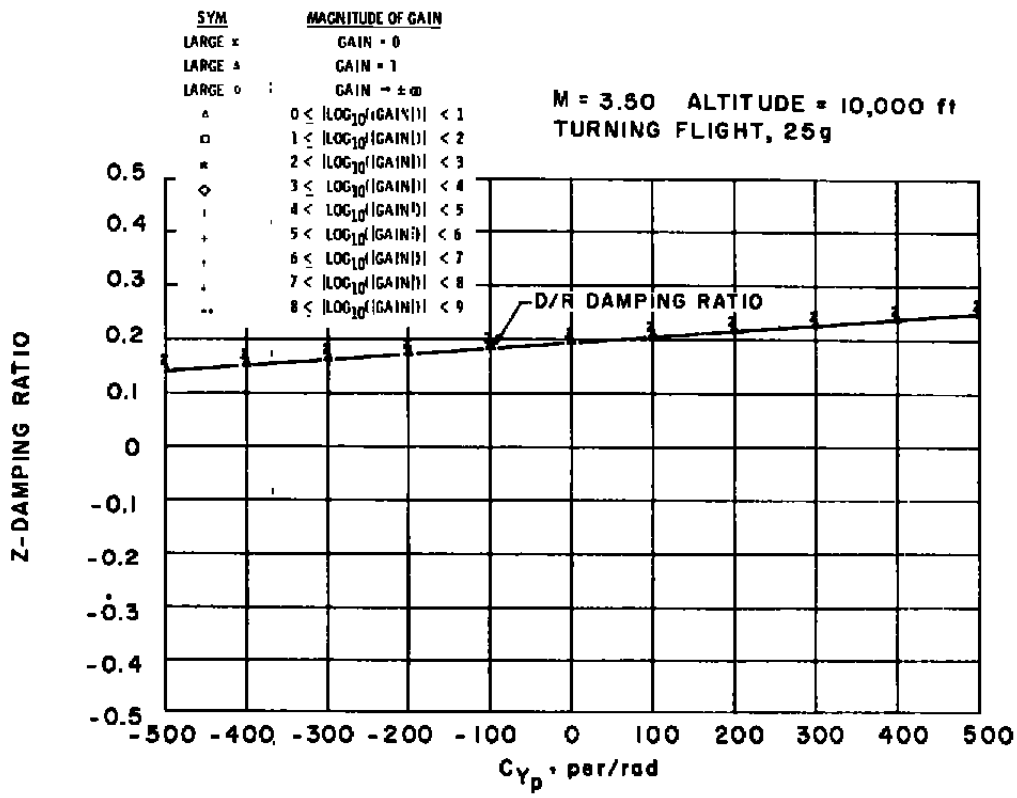

a. Damping ratio

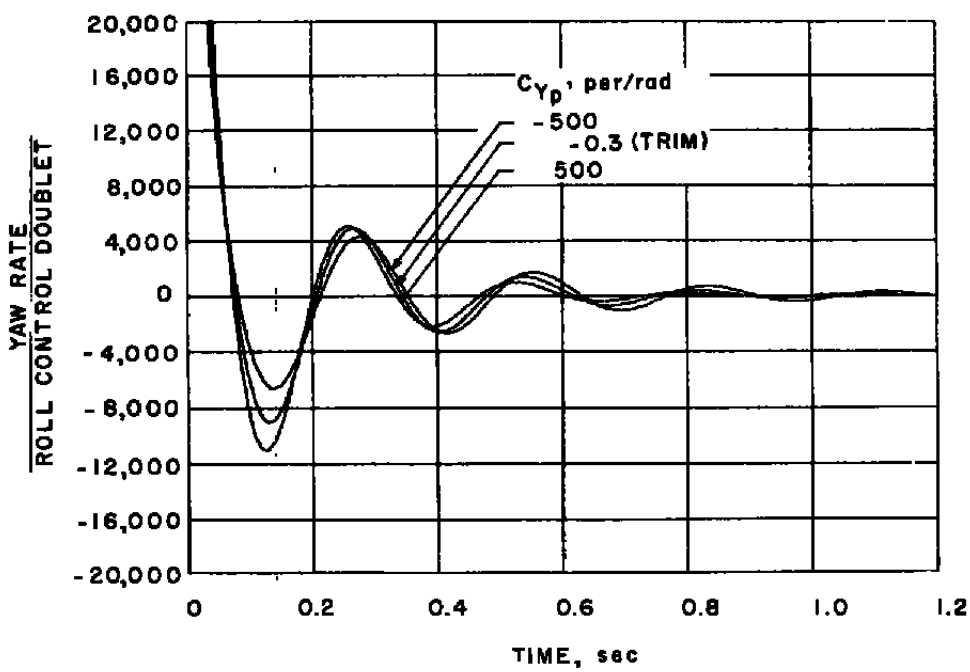

b. Time response

Figure 20. Bank-to-turn configuration - effect of C_{Y_p} on damping ratio and time response.

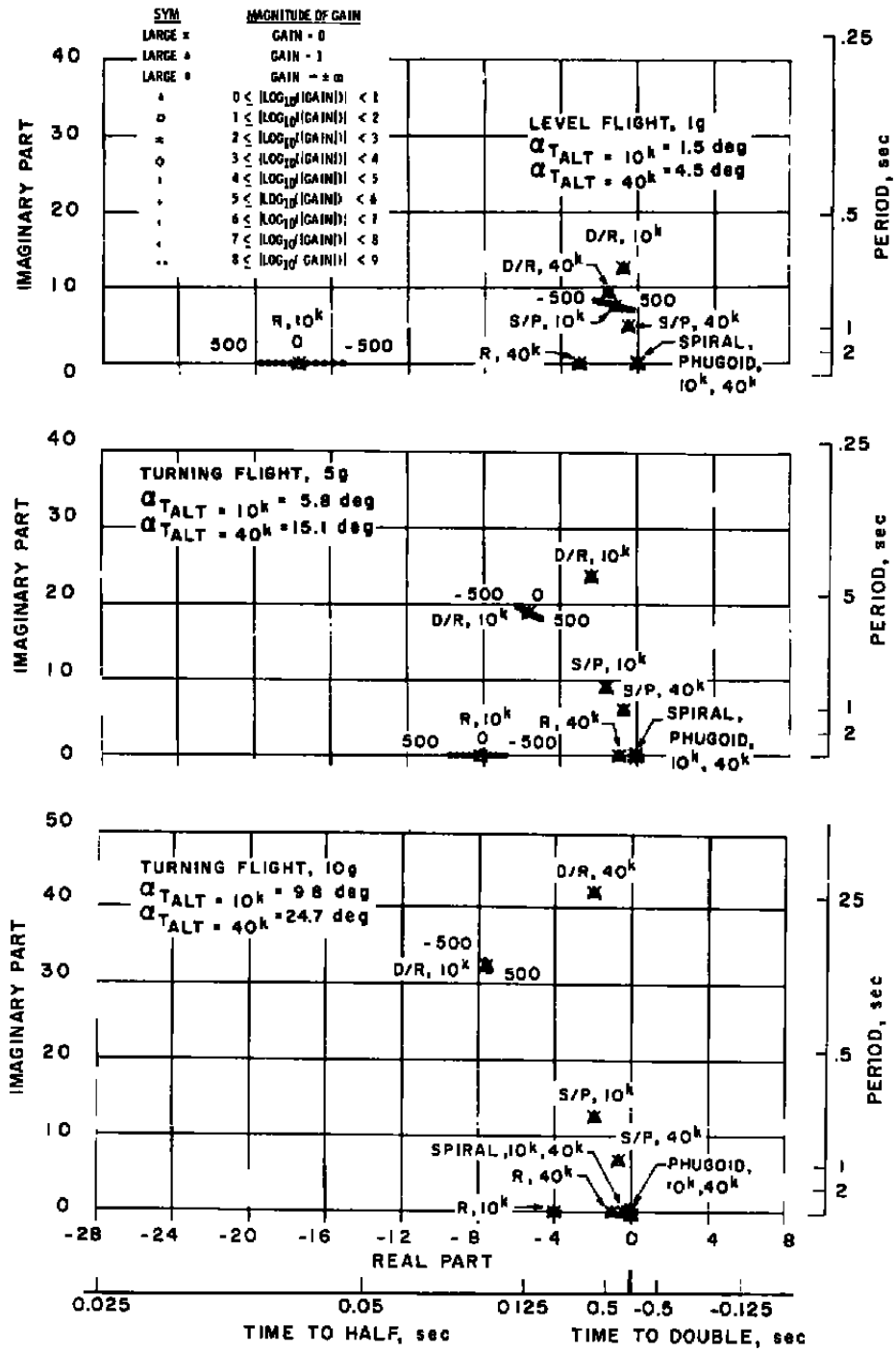

a. M = 0.8

Figure 21. Bank-to-turn configuration - locus of roots with $C\ell_q$ variation.

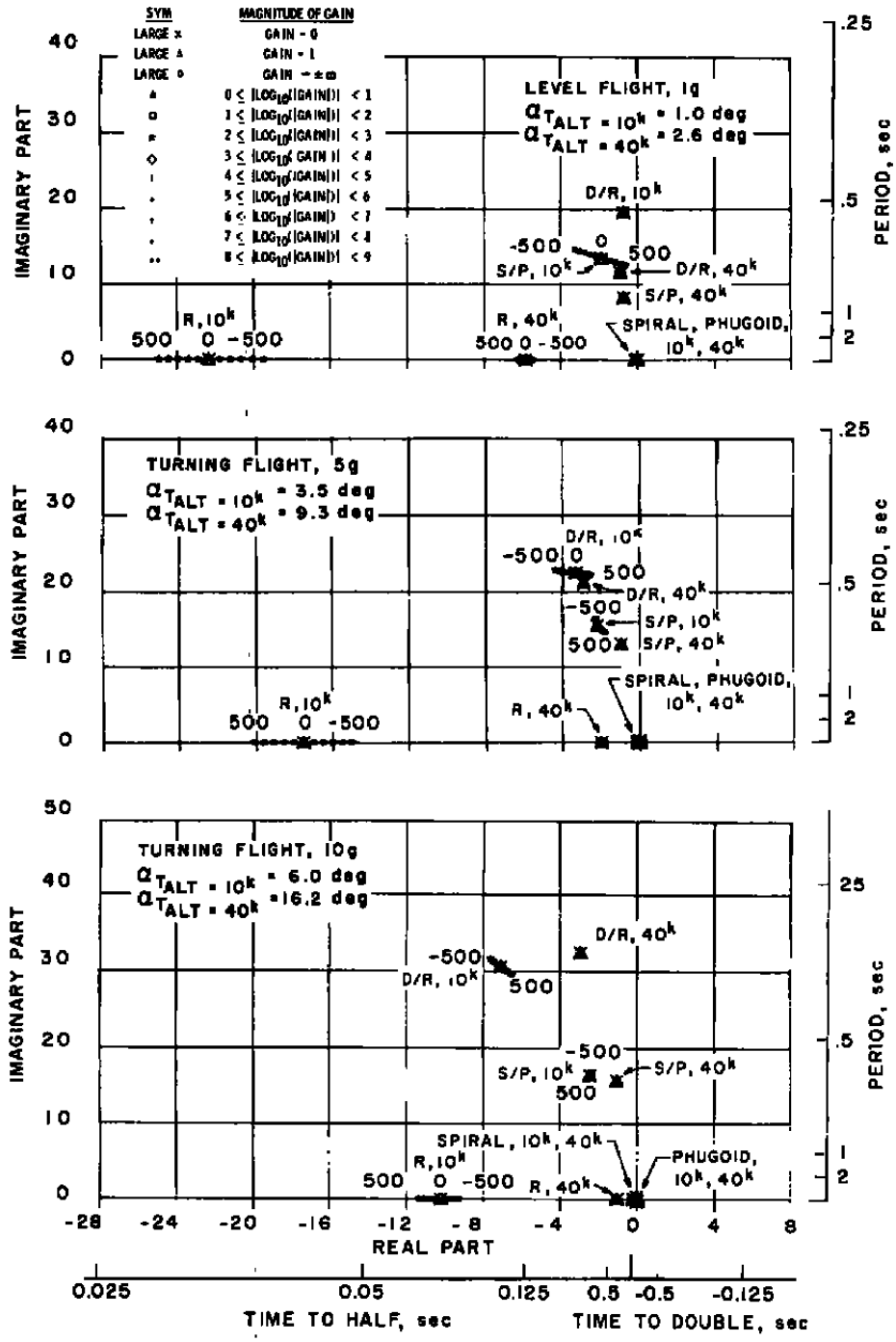

b. M = 1.1

Figure 21. Continued.

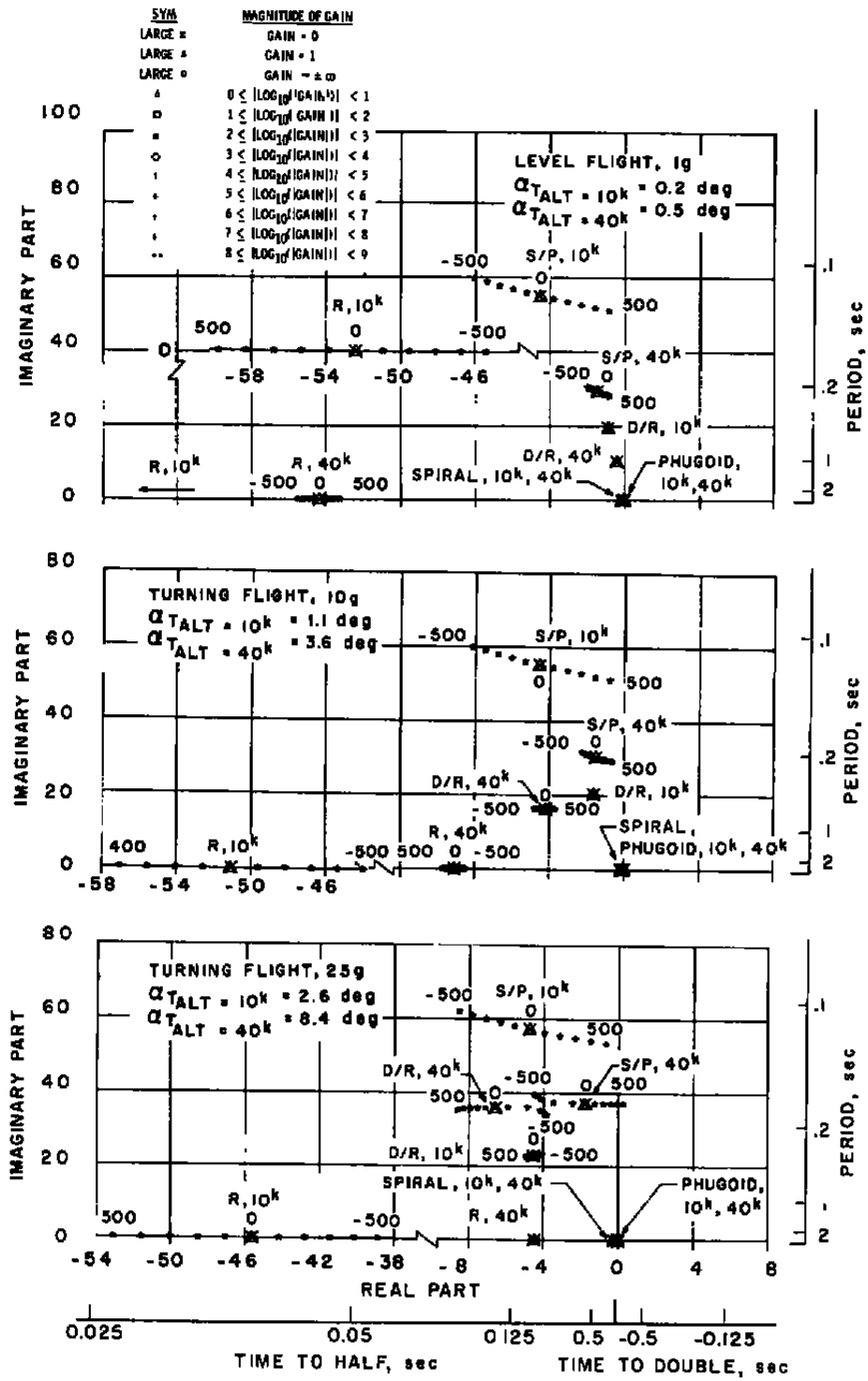

c. M = 3.5

Figure 21. Concluded.

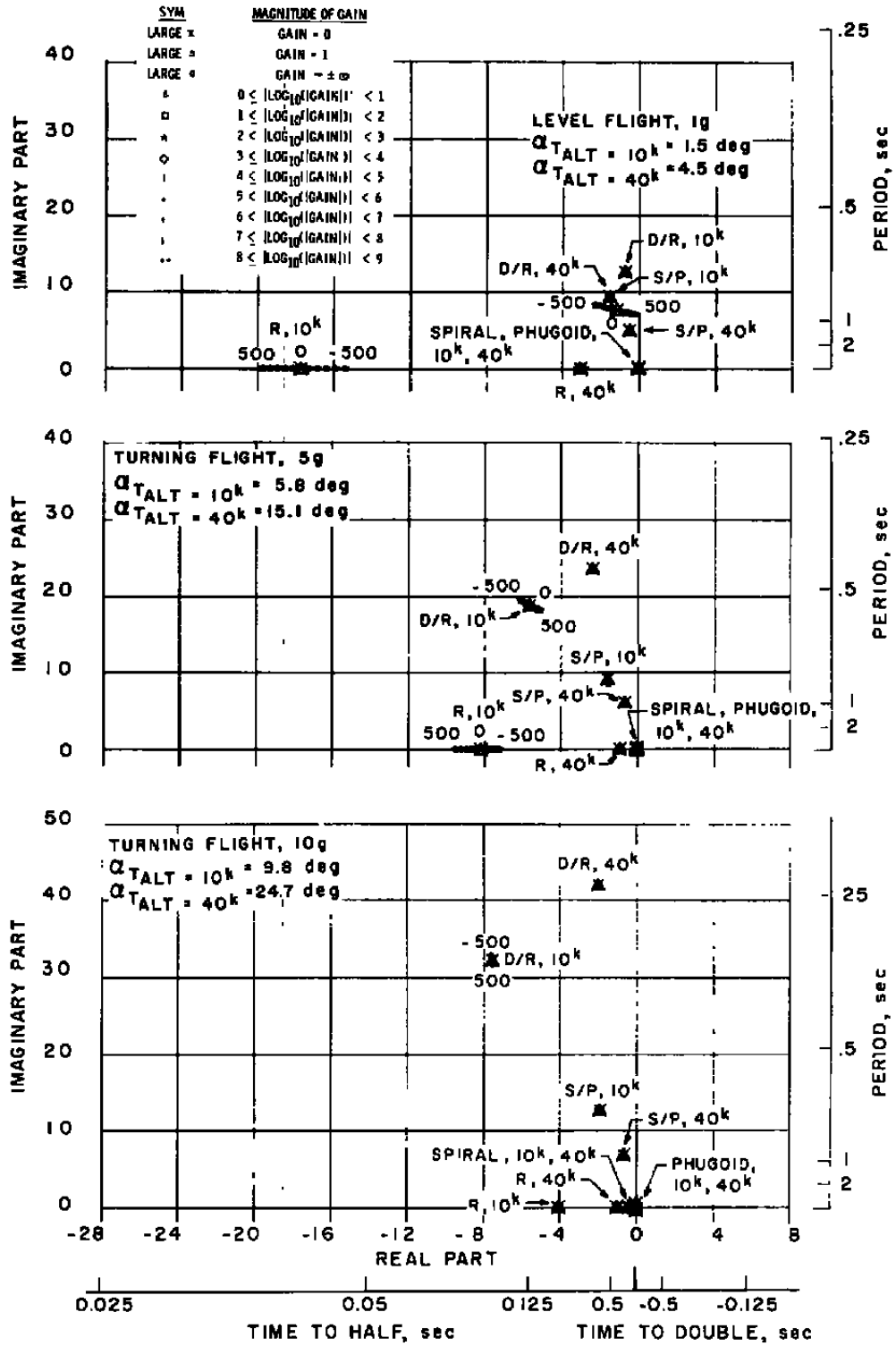

a. M = 0.8

Figure 22. Bank-to-turn configuration - locus of roots with C_{m_p} variation.

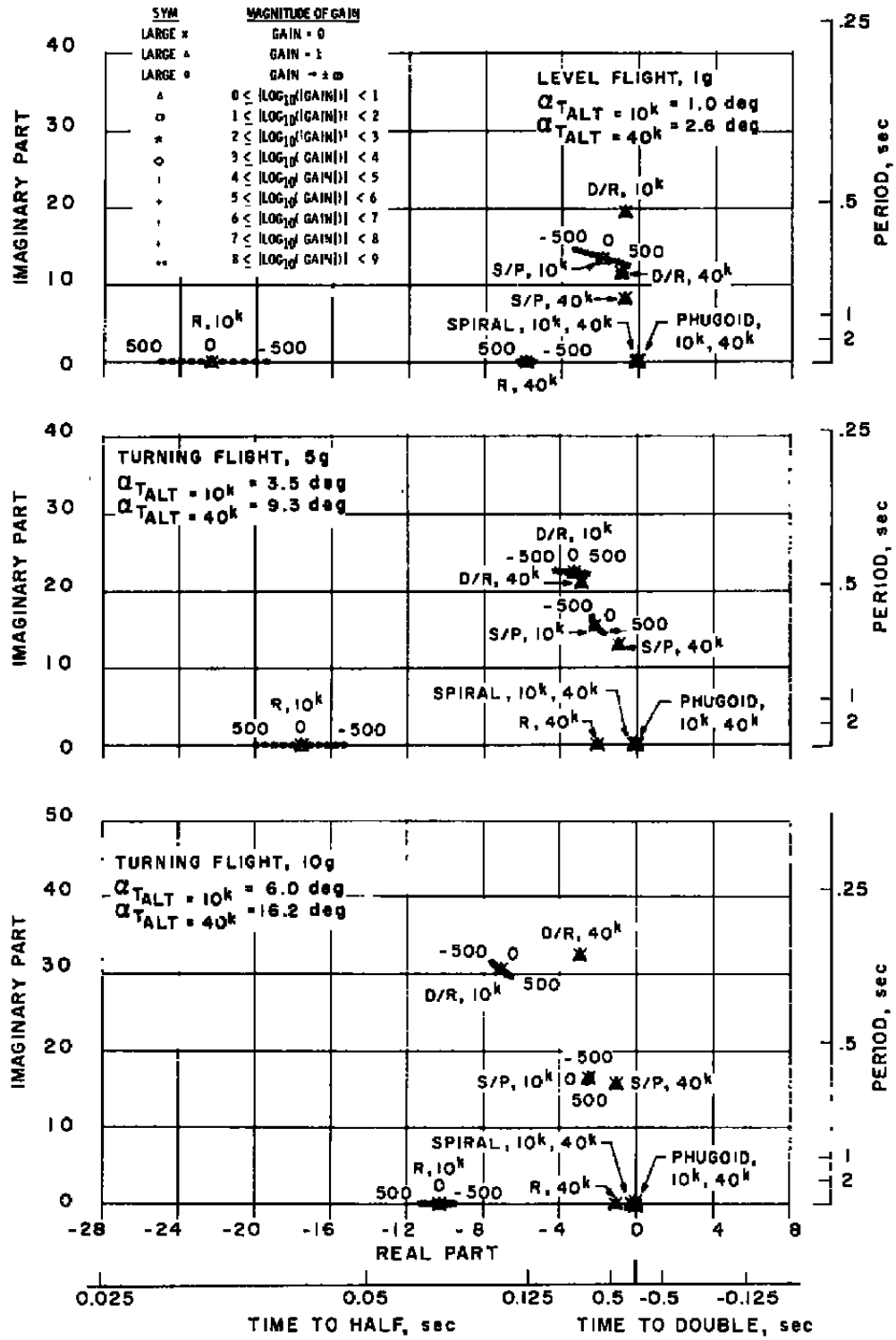

b. M = 1.1

Figure 22. Continued.

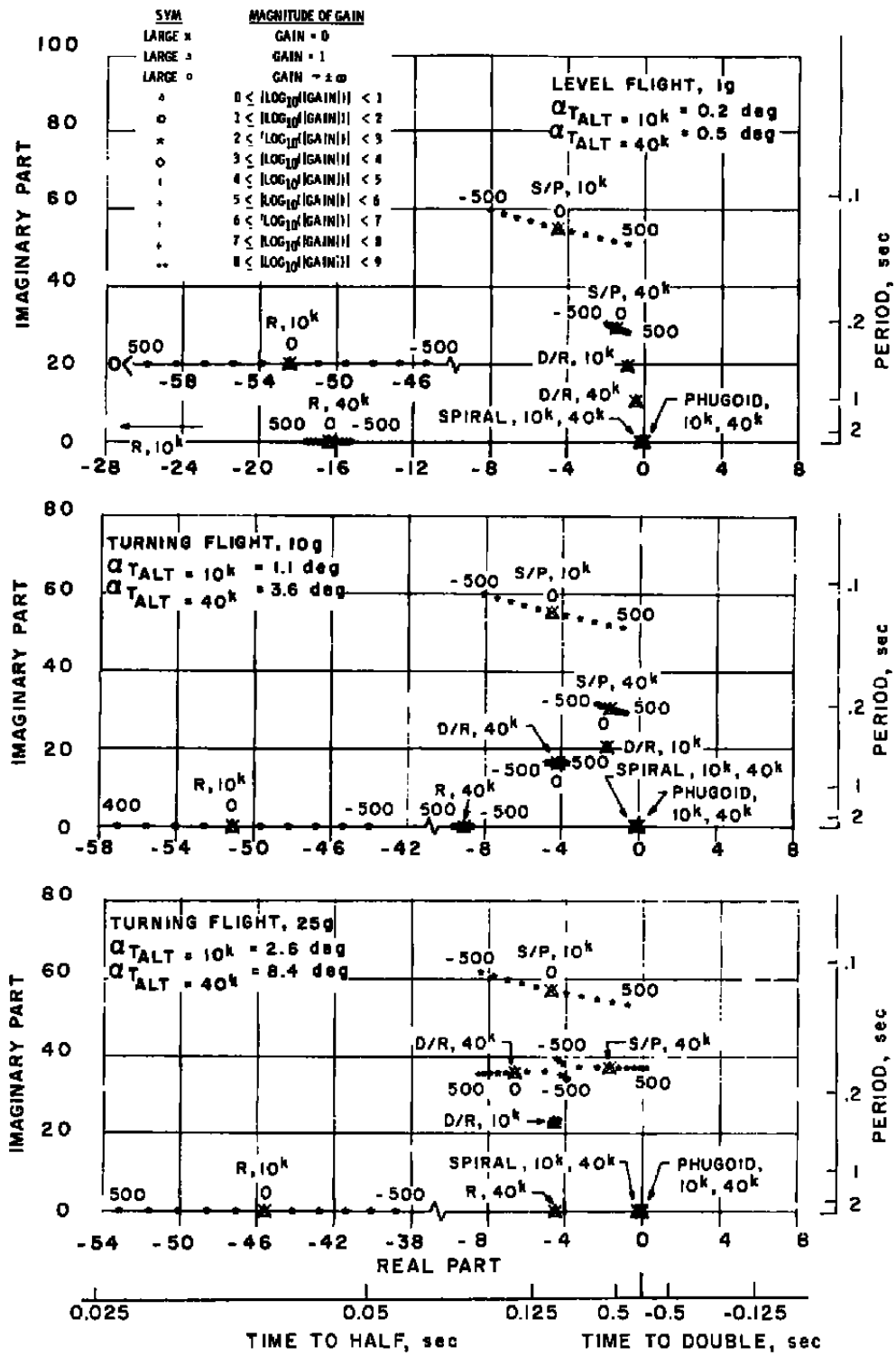

c. M = 3.5

Figure 22. Concluded.

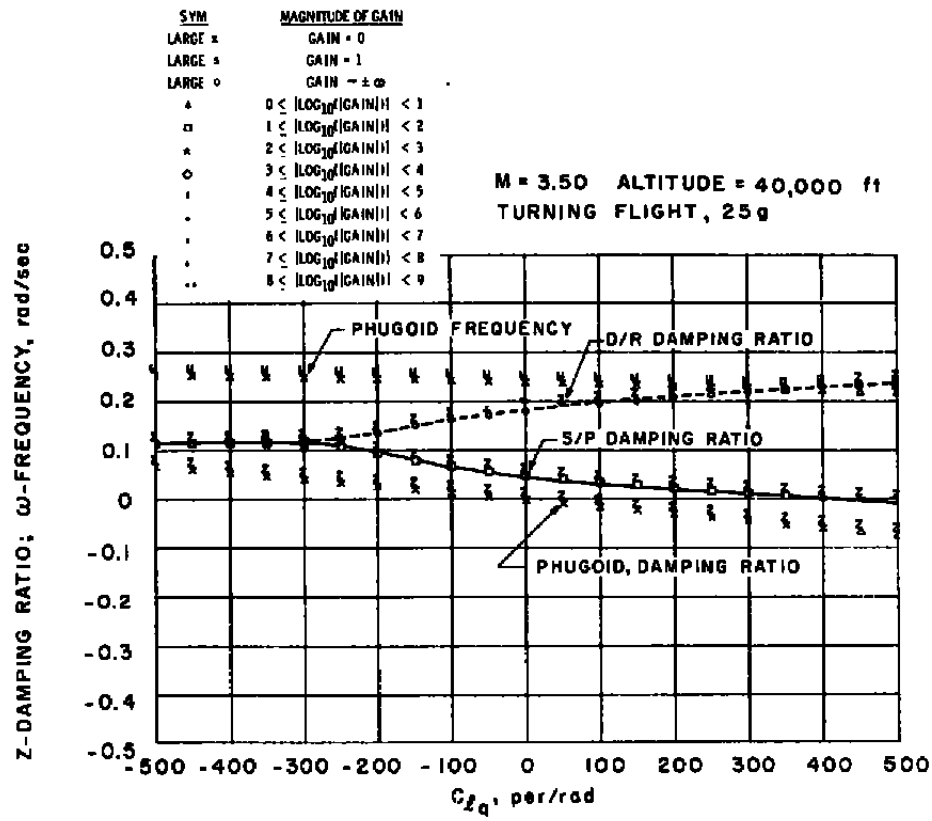

a. Damping ratio

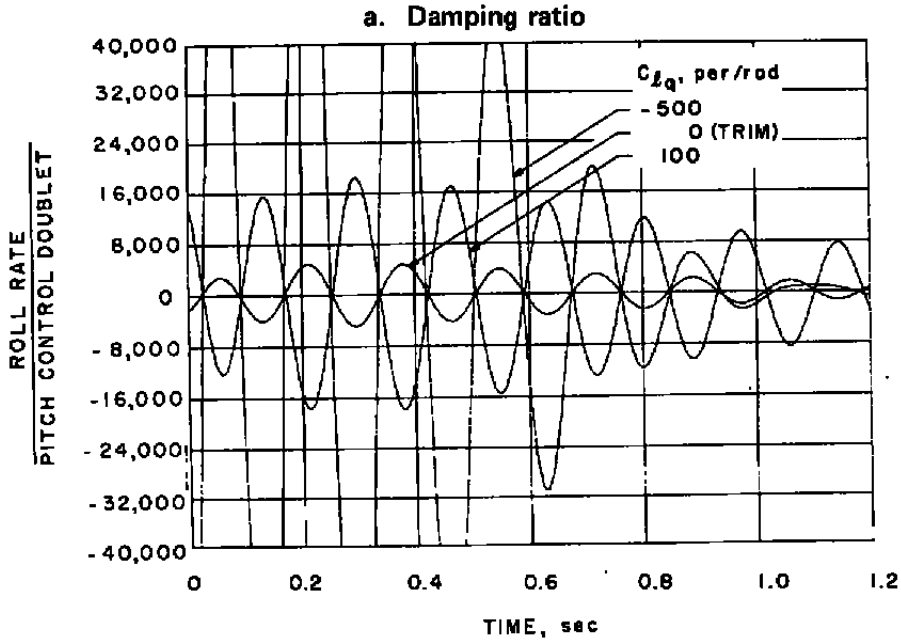

b. Time response

Figure 23. Bank-to-turn configuration - effect of C_{ℓ_q} on damping ratio and time response.

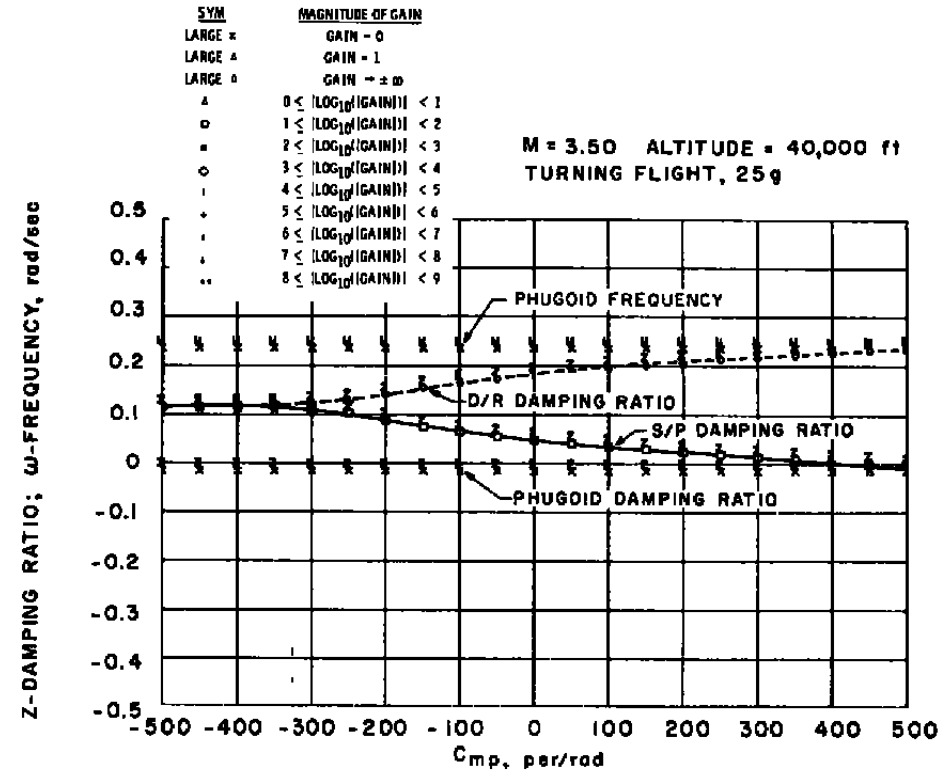

a. Damping ratio

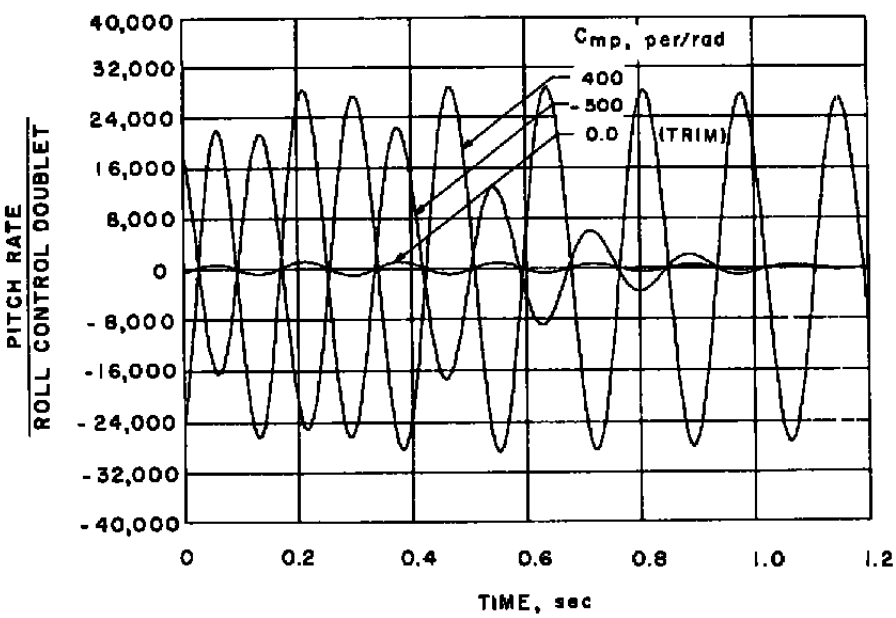

b. Time response

Figure 24. Bank-to-turn configuration - effect of C_{m_p} on damping ratio and time response.

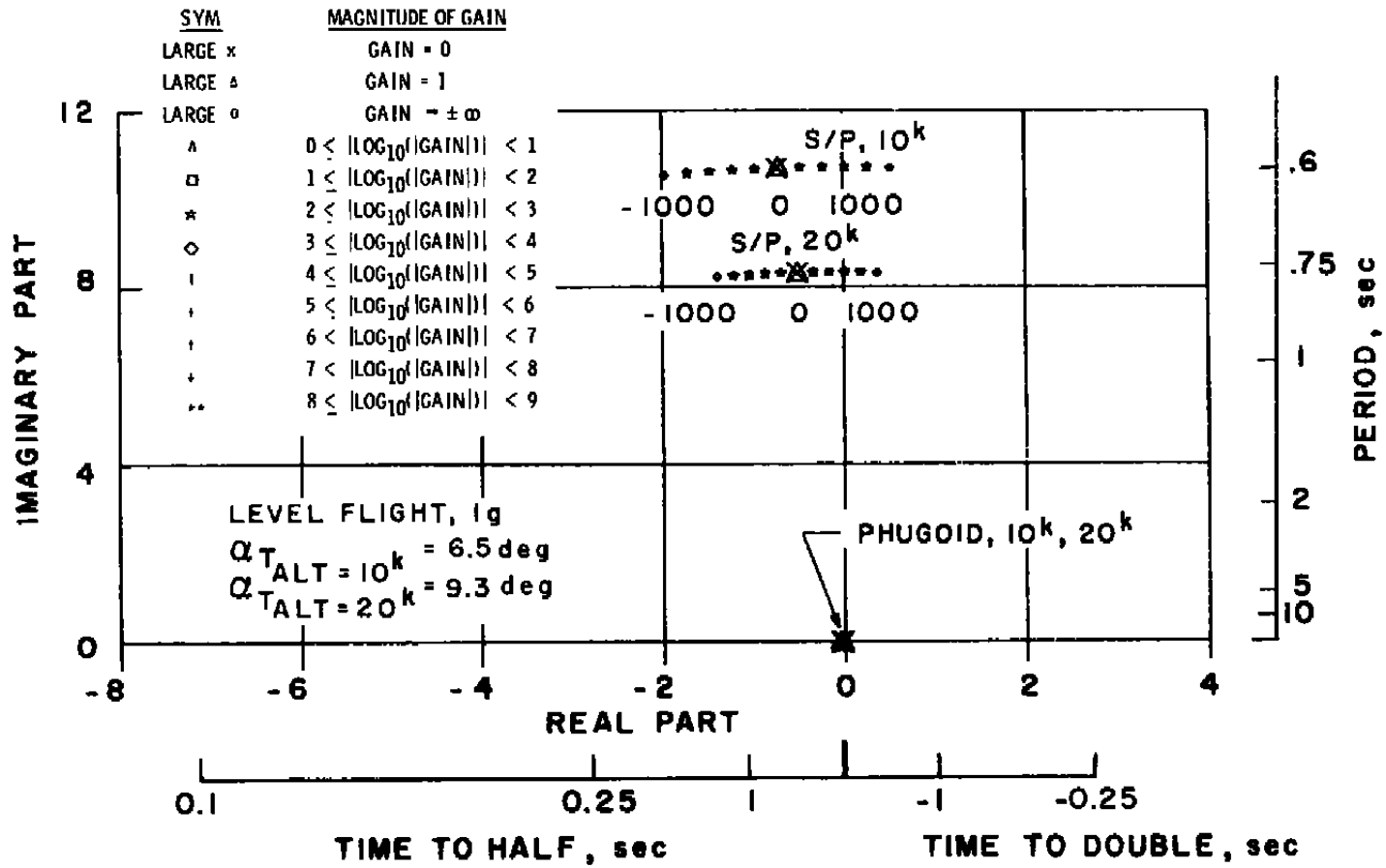

a. M = 1.3

Figure 25. Yaw-to-turn configuration - locus of roots with C_{m_q} variation.

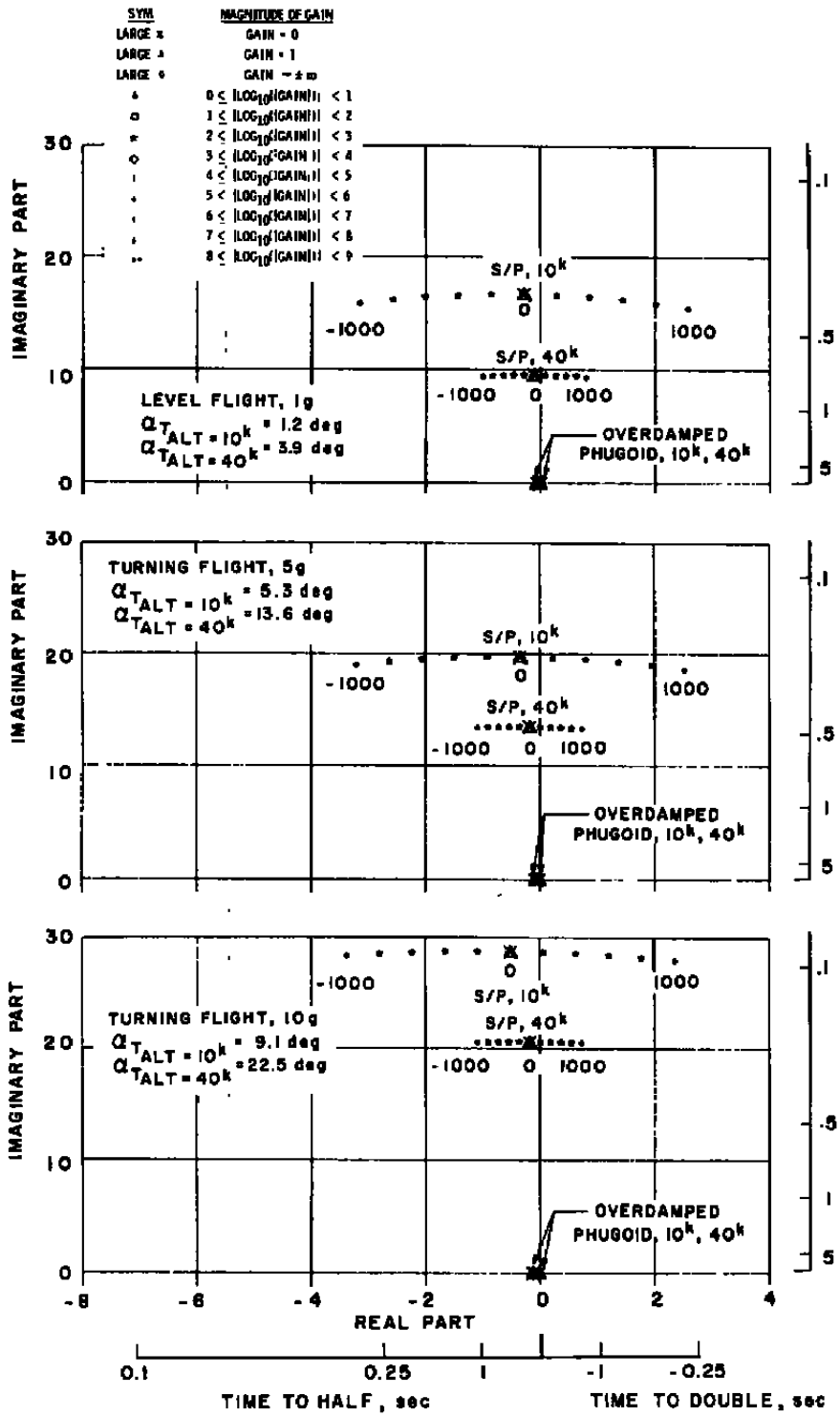

b. M = 3.0

Figure 25. Concluded.

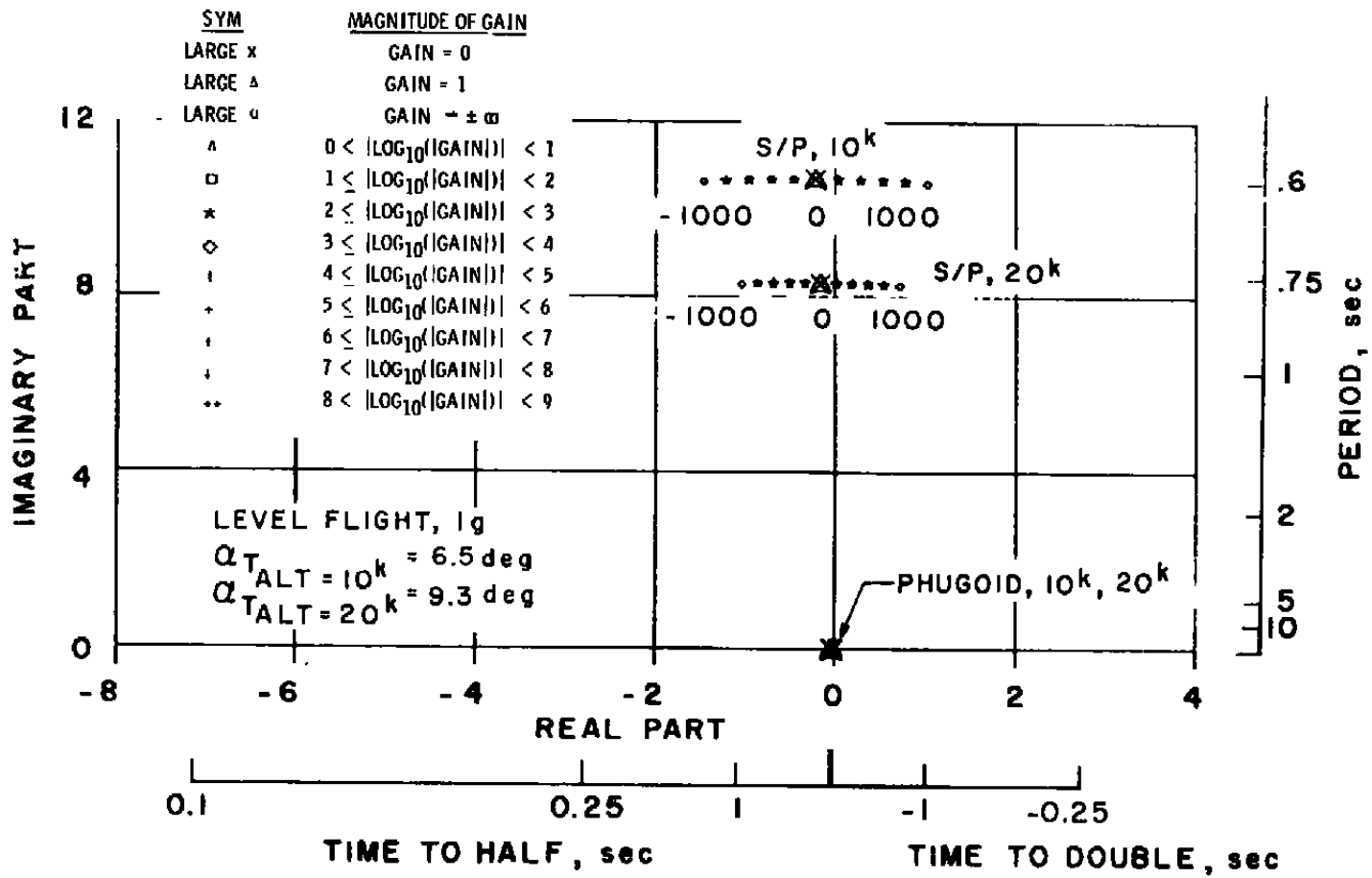

a. M = 1.3

Figure 26. Yaw-to-turn configuration - locus of roots with C_{m_d} variation.

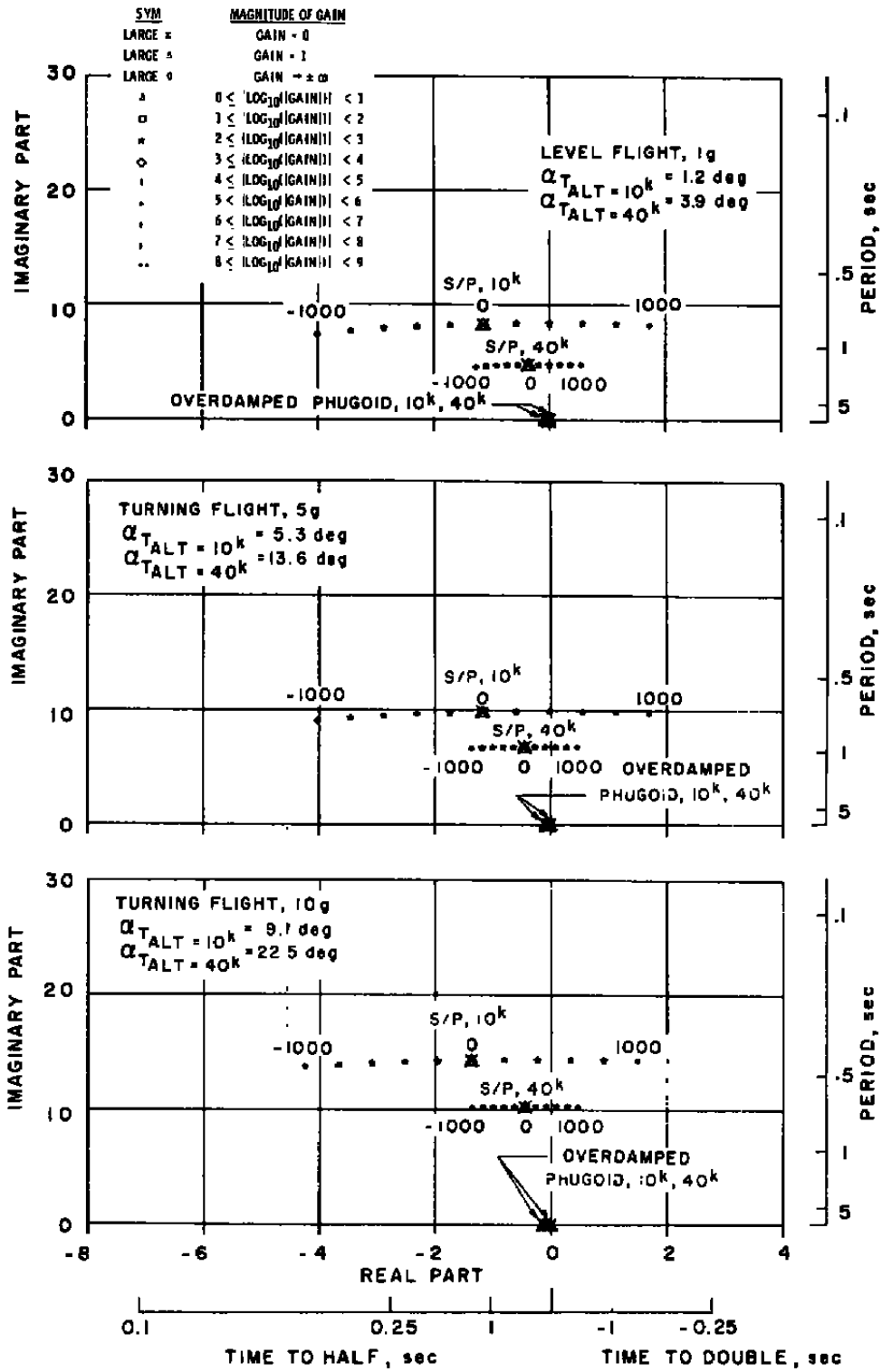

b. M = 3.0

Figure 26. Concluded.

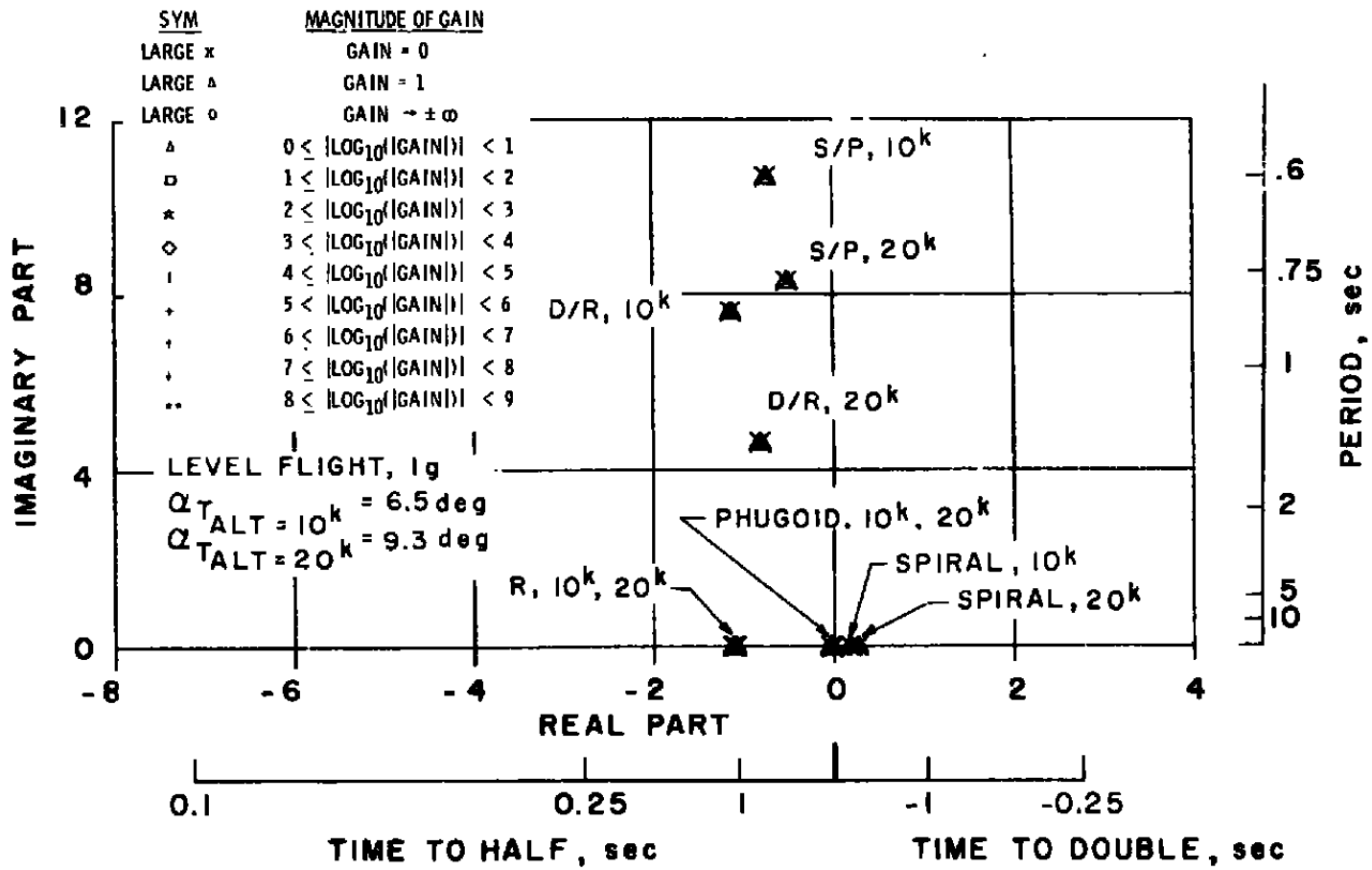

a. M = 1.3

Figure 27. Yaw-to-turn configuration - locus of roots with C_{L_q}, $C_{L_{\dot{\alpha}}}$, C_{y_r}, C_{y_p}, and C_{m_r} variation.

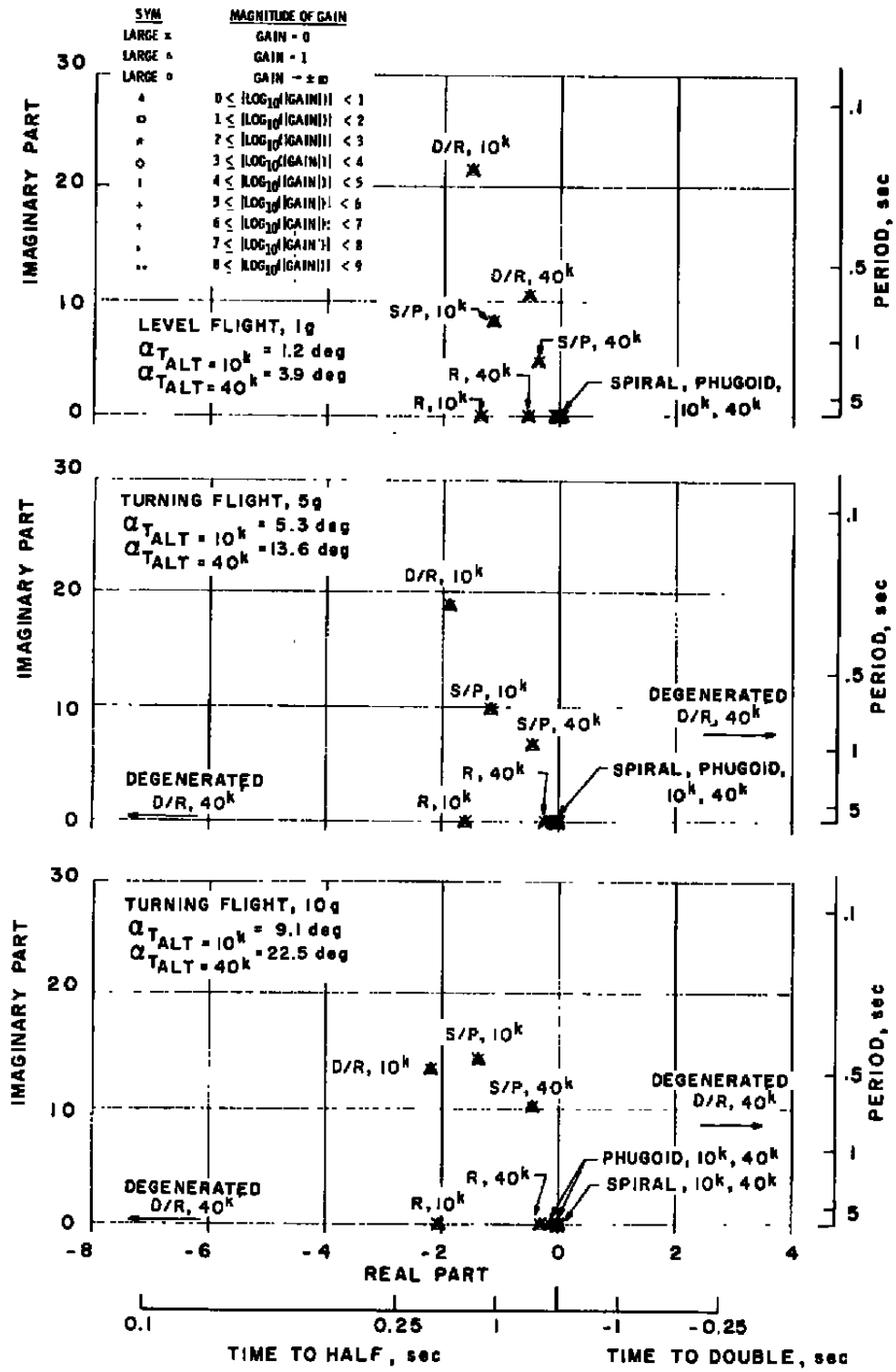

b. M = 3.0

Figure 27. Concluded.

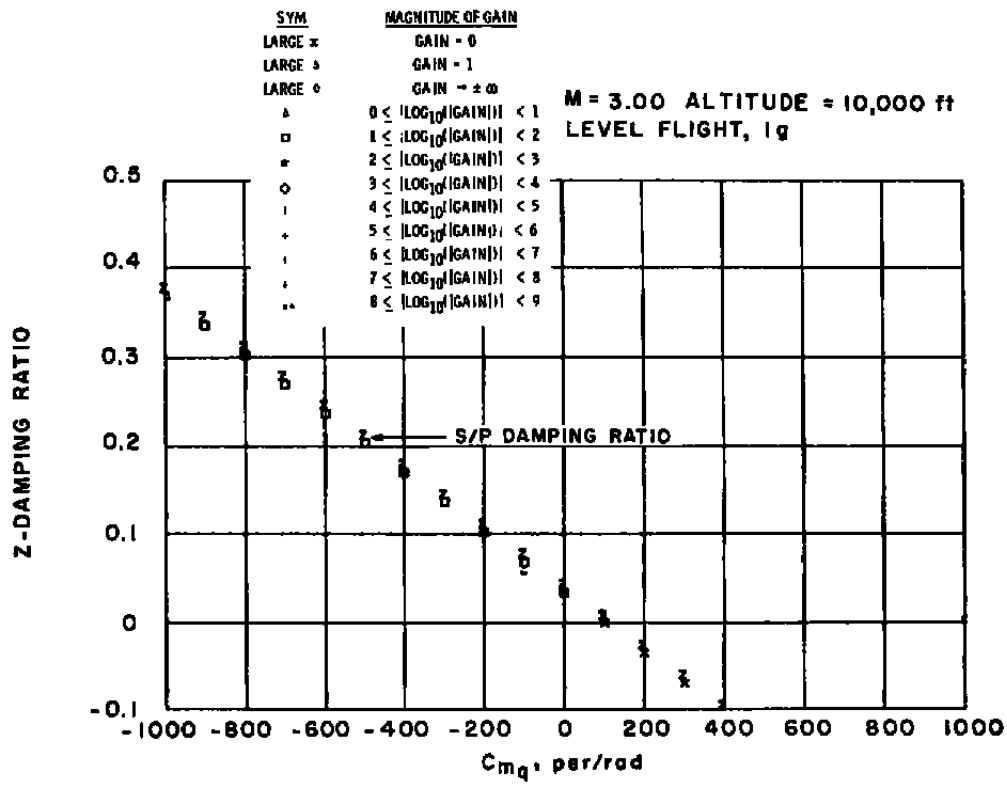

a. Damping ratio

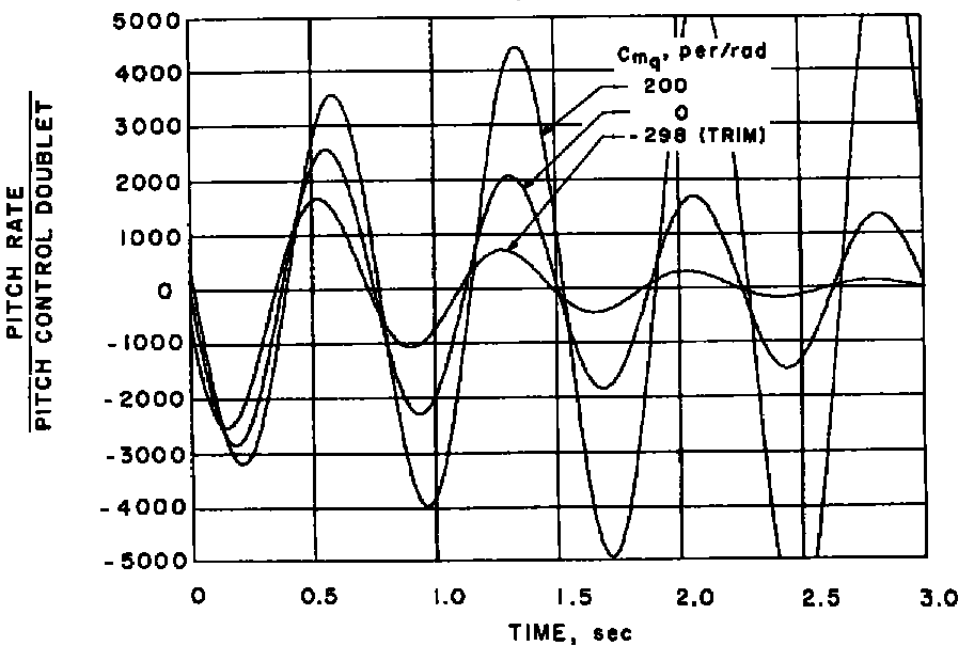

b. Time response

Figure 28. Yaw-to-turn configuration - effect of C_{m_q} on damping ratio and time response.

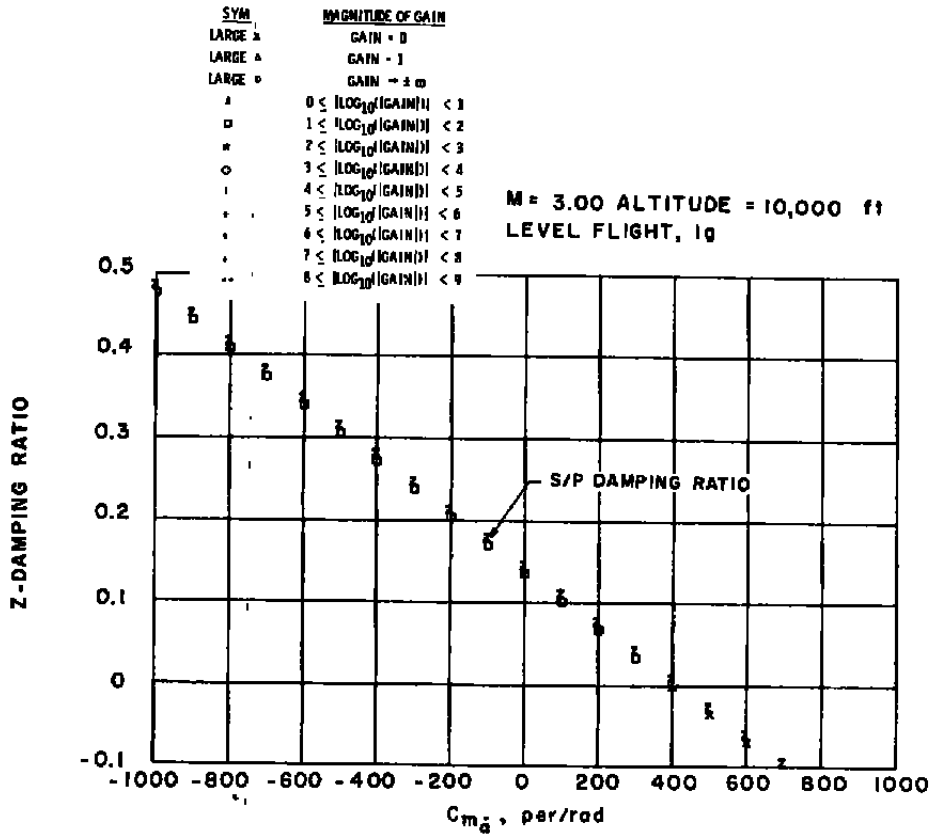

a. Damping ratio

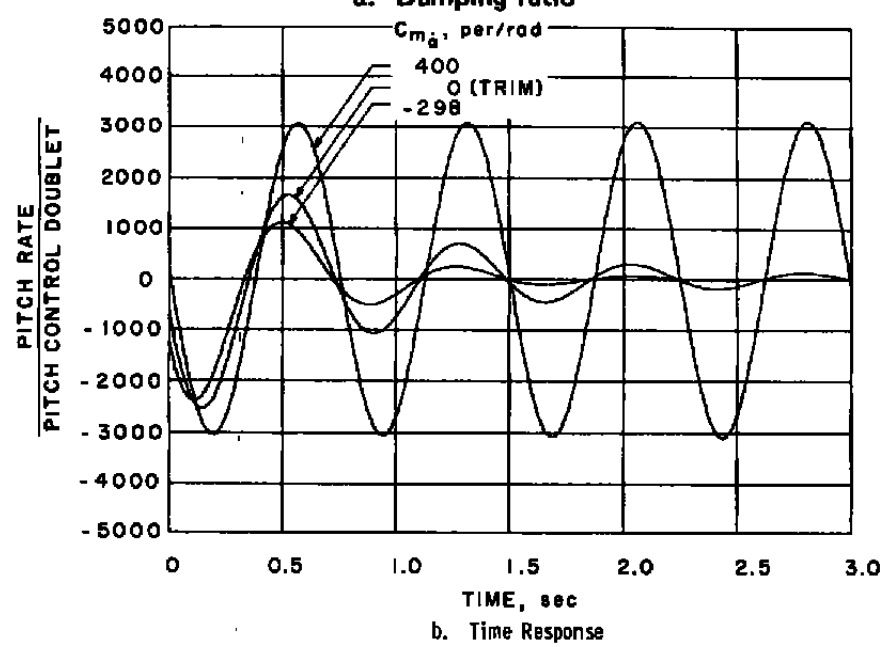

b. Time Response

b. Time response

Figure 29. Yaw-to-turn configuration - effect of $C_{m_{\dot{\alpha}}}$ on damping ratio and time response.

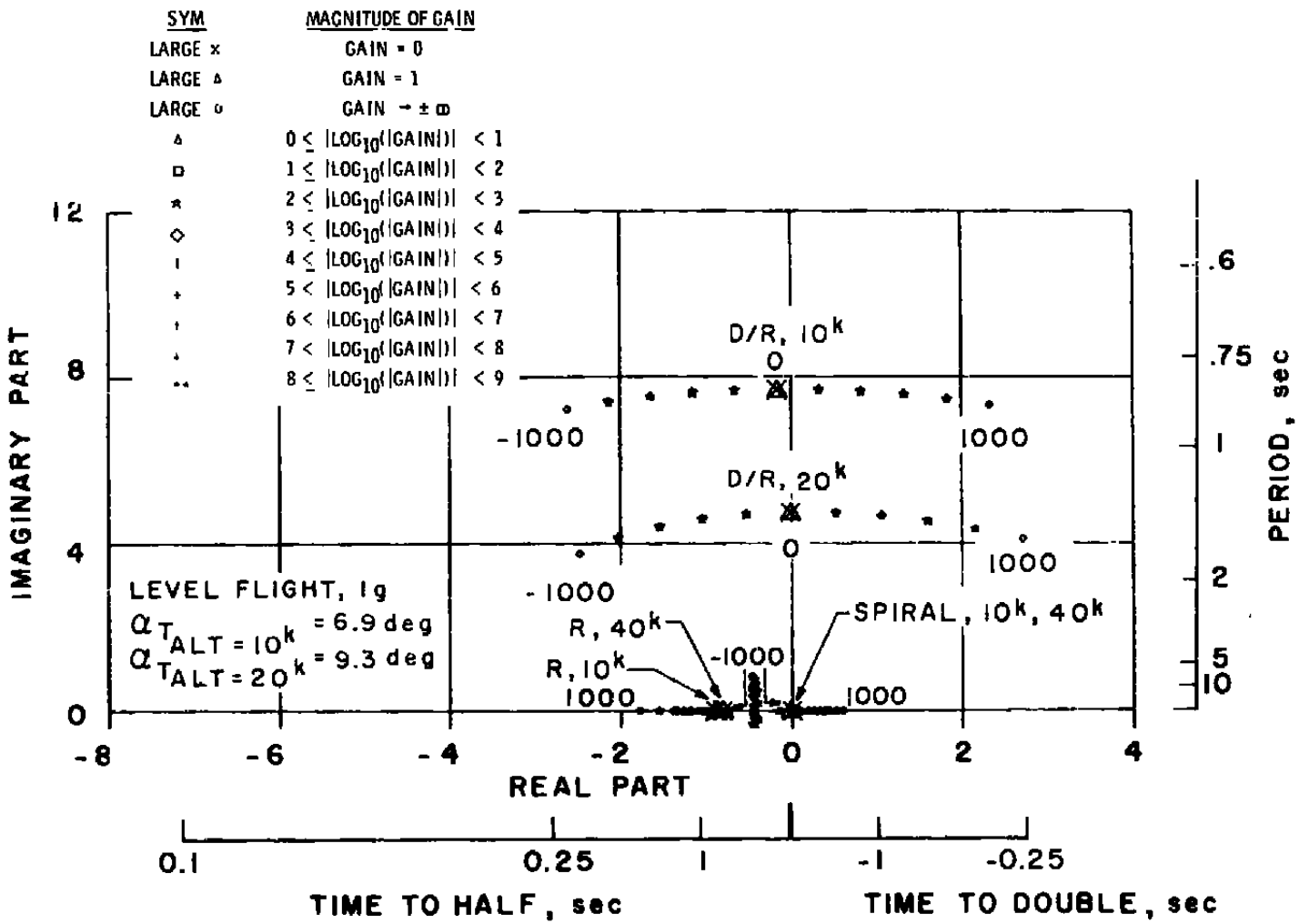

a. M = 1.3

Figure 30. Yaw-to-turn configuration - locus of roots with C_{n_r} variation.

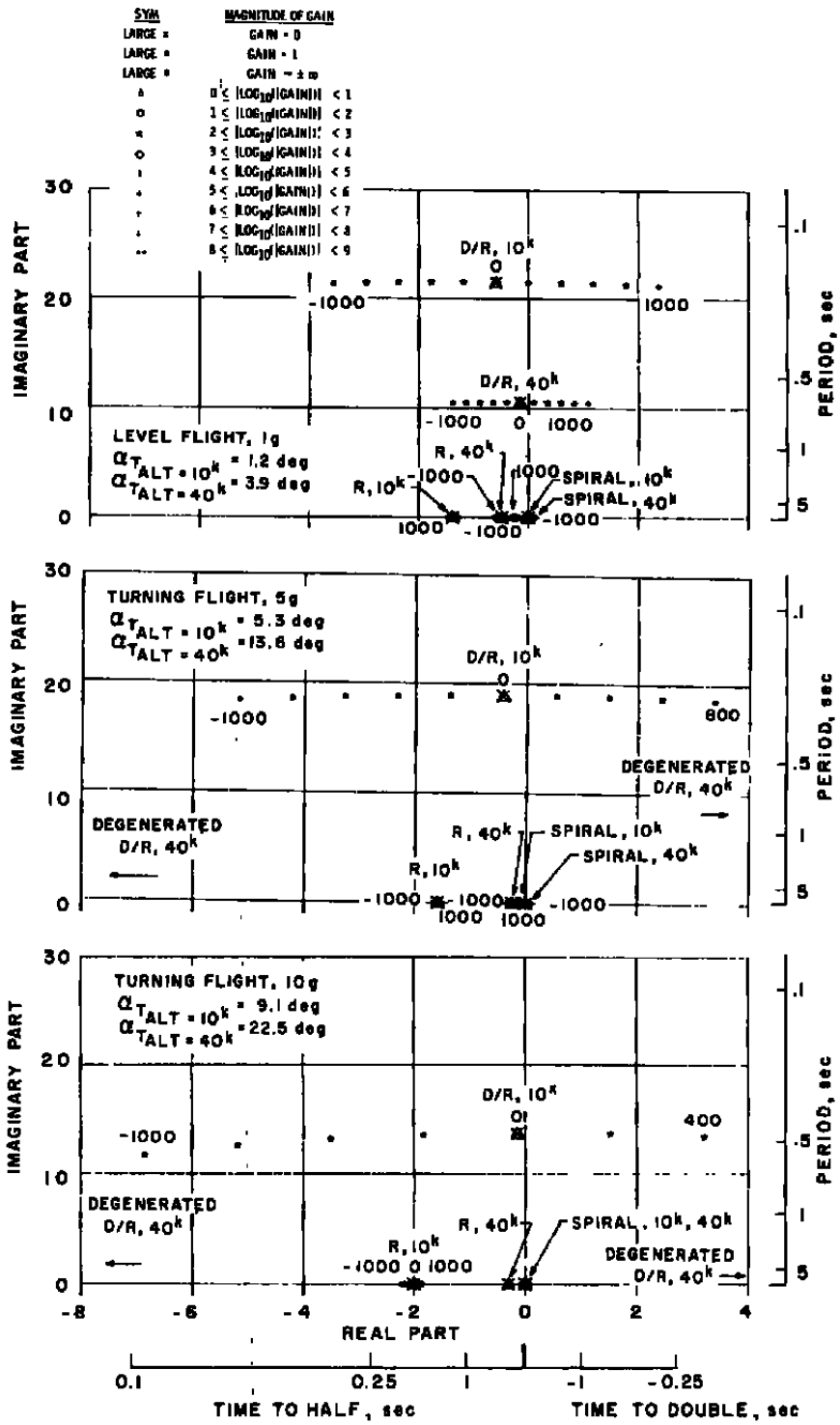

b. M = 3.0

Figure 30. Concluded.

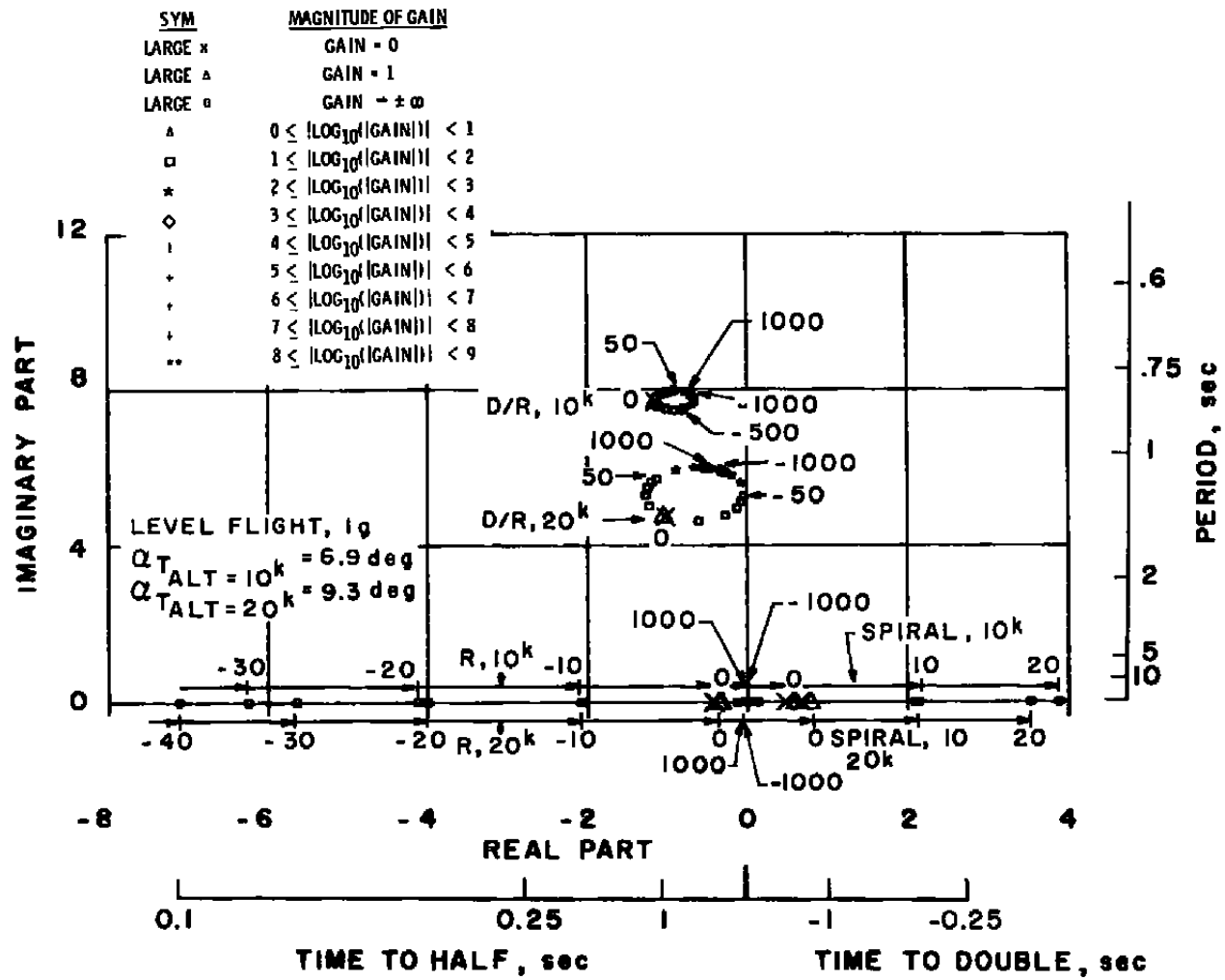

a. M = 1.3

Figure 31. Yaw-to-turn configuration - locus of roots with $C\ell_p$ variation.

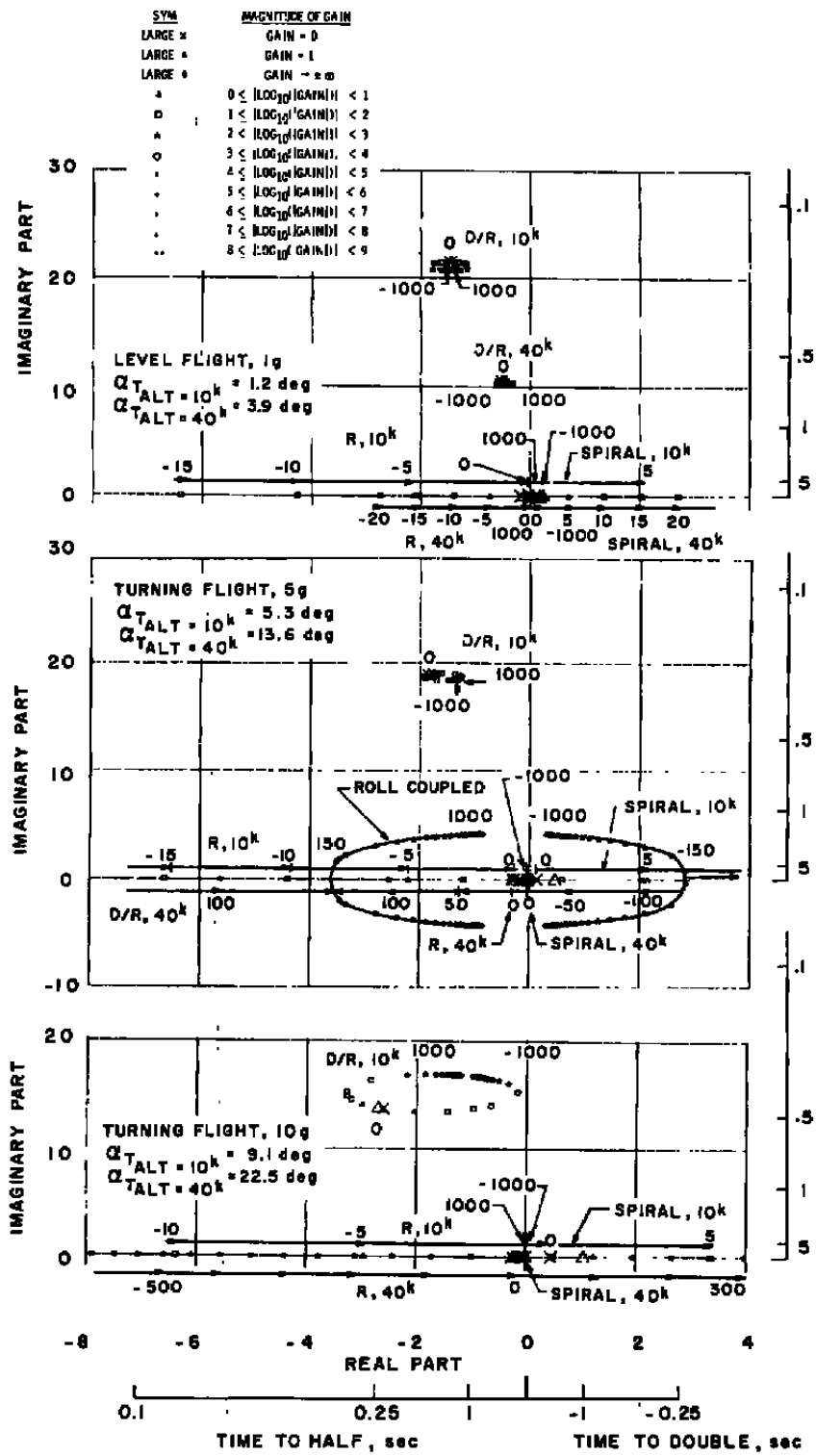

b. M = 3.0

Figure 31. Concluded.

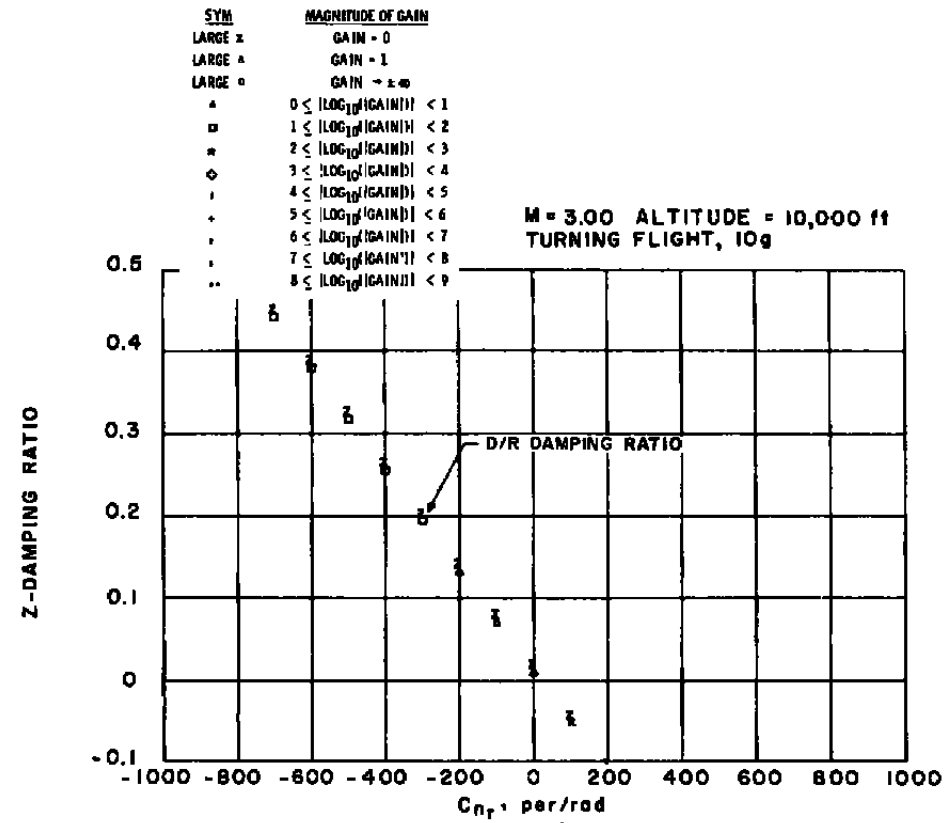

a. Damping ratio

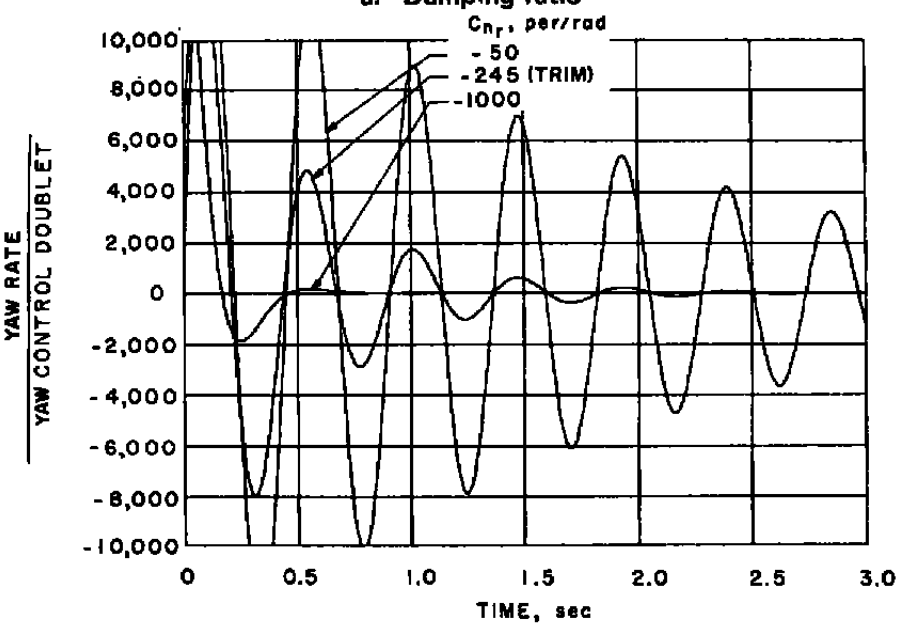

b. Time response

Figure 32. Yaw-to-turn configuration - effect of C_{n_r} on damping ratio and time response.

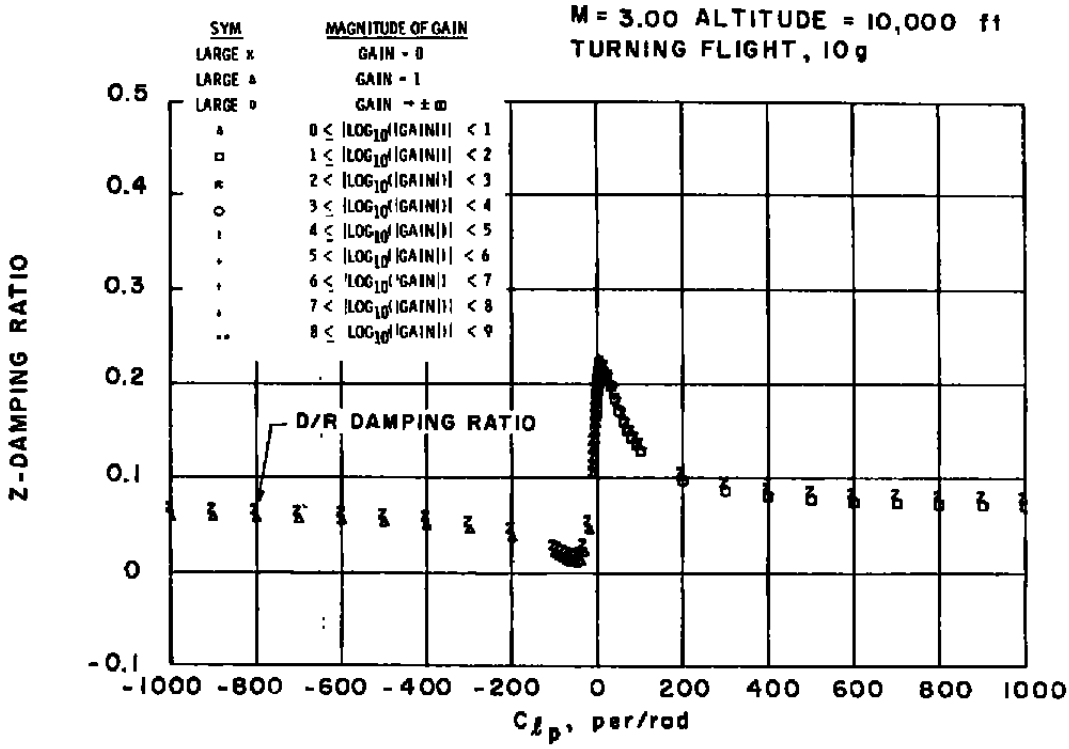

a. Damping ratio

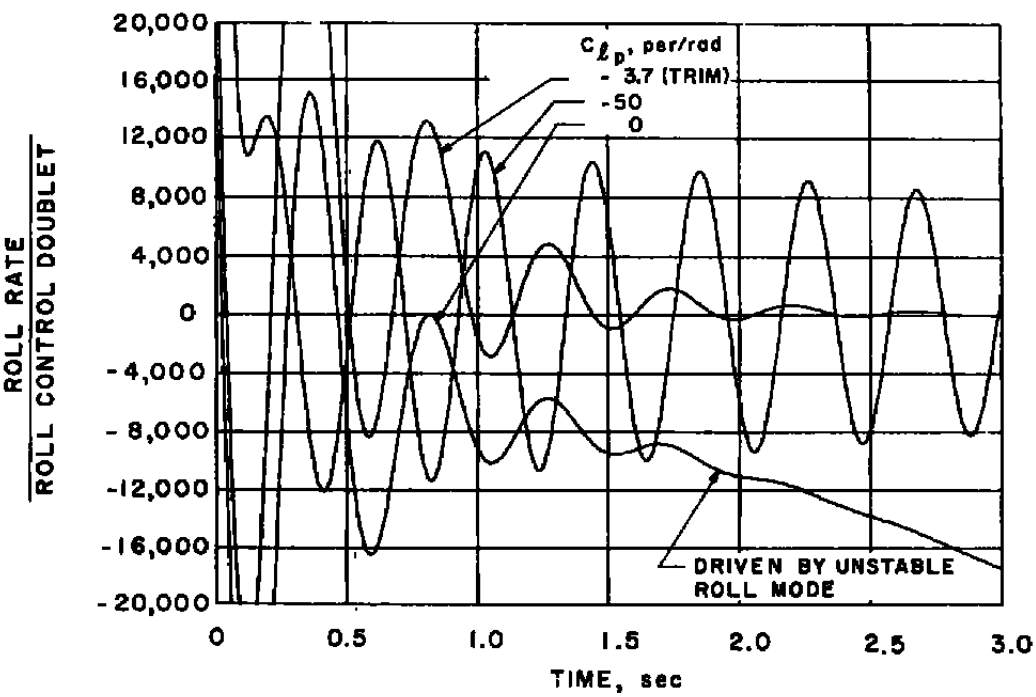

b. Time response

Figure 33. Yaw-to-turn configuration - effect of C_{ℓ_p} on damping ratio and time response.

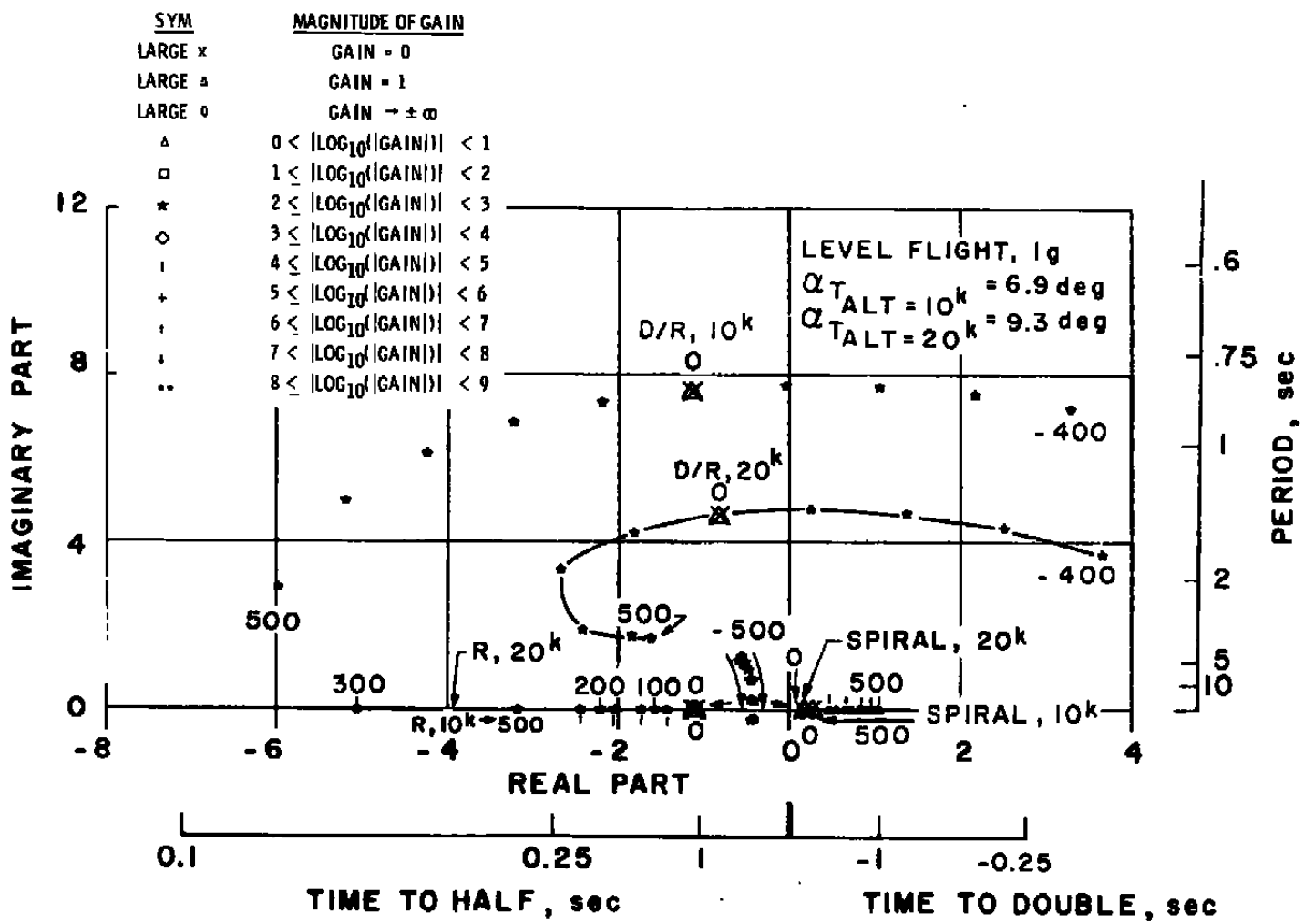

a. M = 1.3

Figure 34. Yaw-to-turn configuration - locus of roots with C_{ℓ_r} variation.

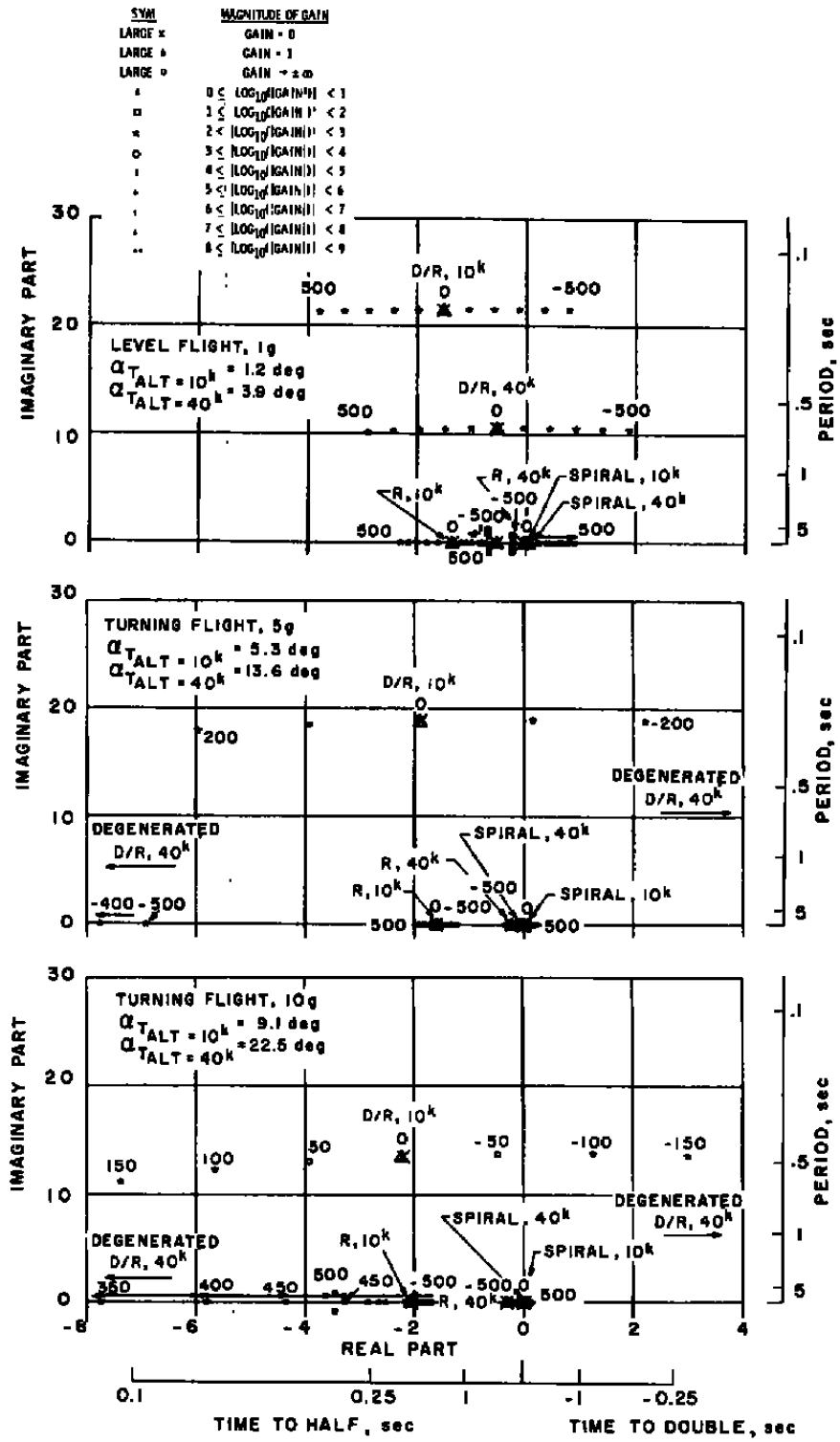

b. M = 3.0

Figure 34. Concluded.

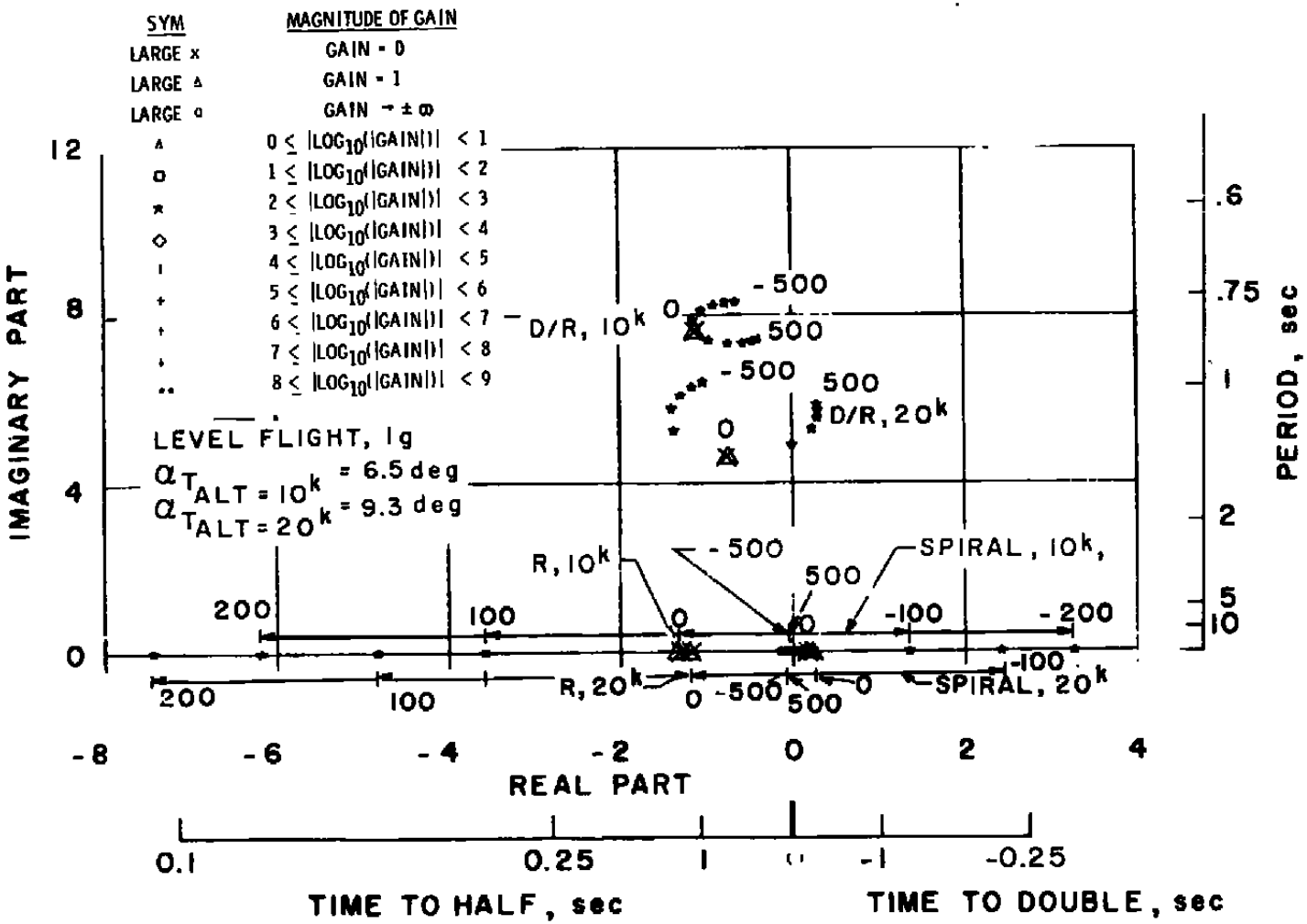

a. M = 1.3

Figure 35. Yaw-to-turn configuration - locus of roots with C_{n_p} variation.

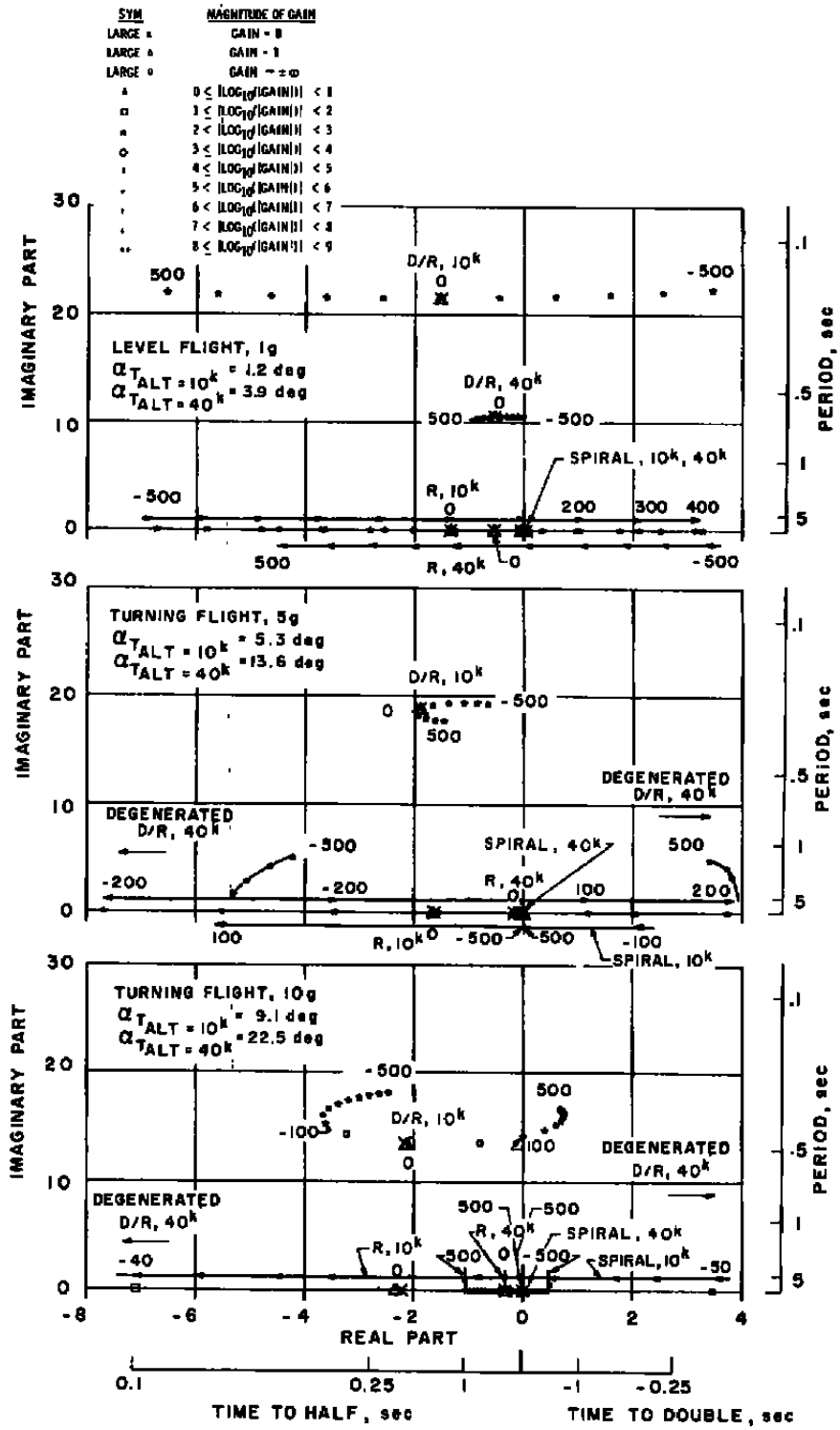

b. M = 3.0

Figure 35. Concluded.

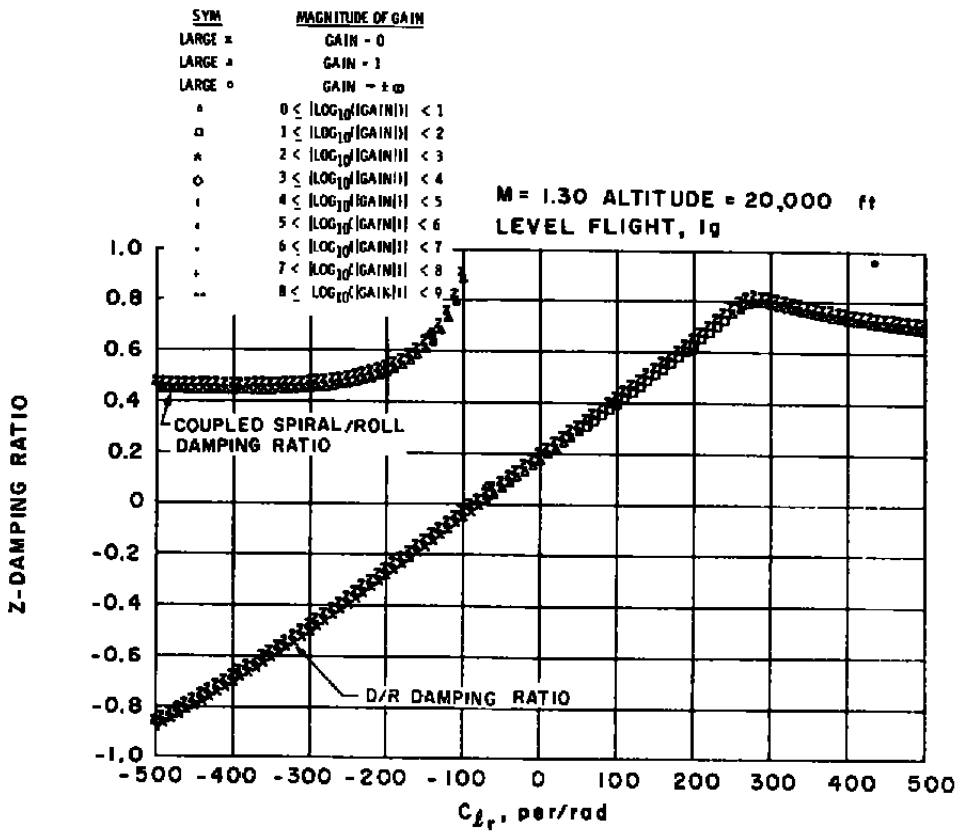

a. Damping ratio

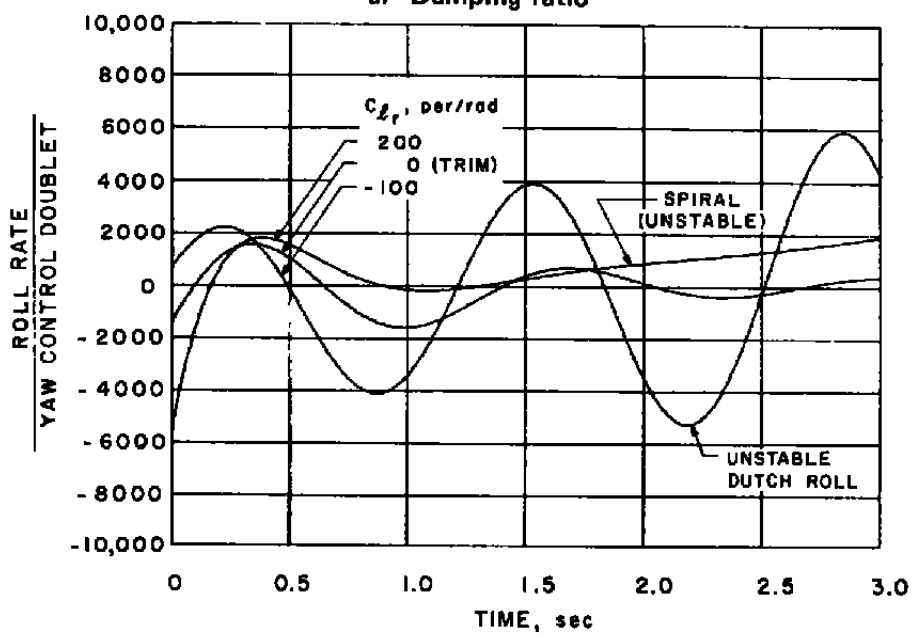

b. Time response

Figure 36. Yaw-to-turn configuration - effect of C_{ℓ_r} on damping ratio and time response.

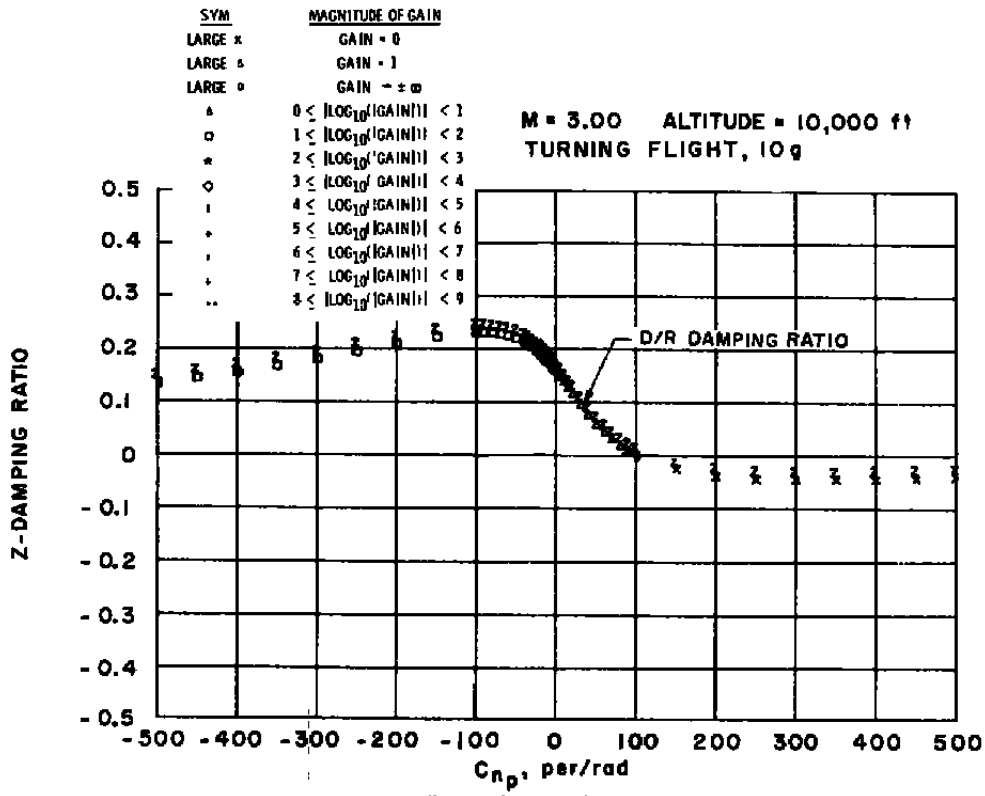

a. Damping ratio

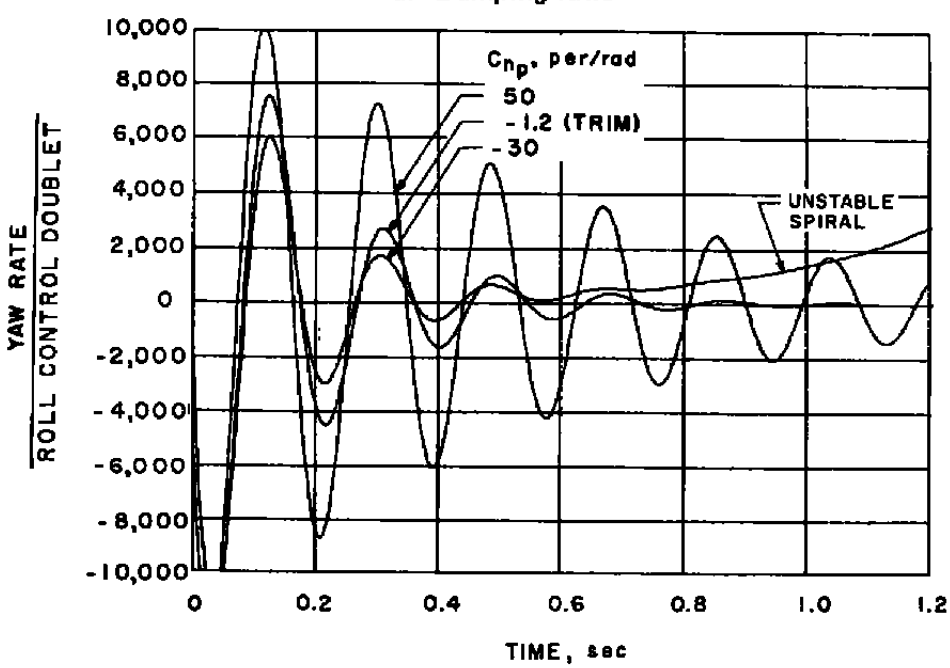

b. Time response

Figure 37. Yaw-to-turn configuration - effect of C_{n_p} on damping ratio and time response.

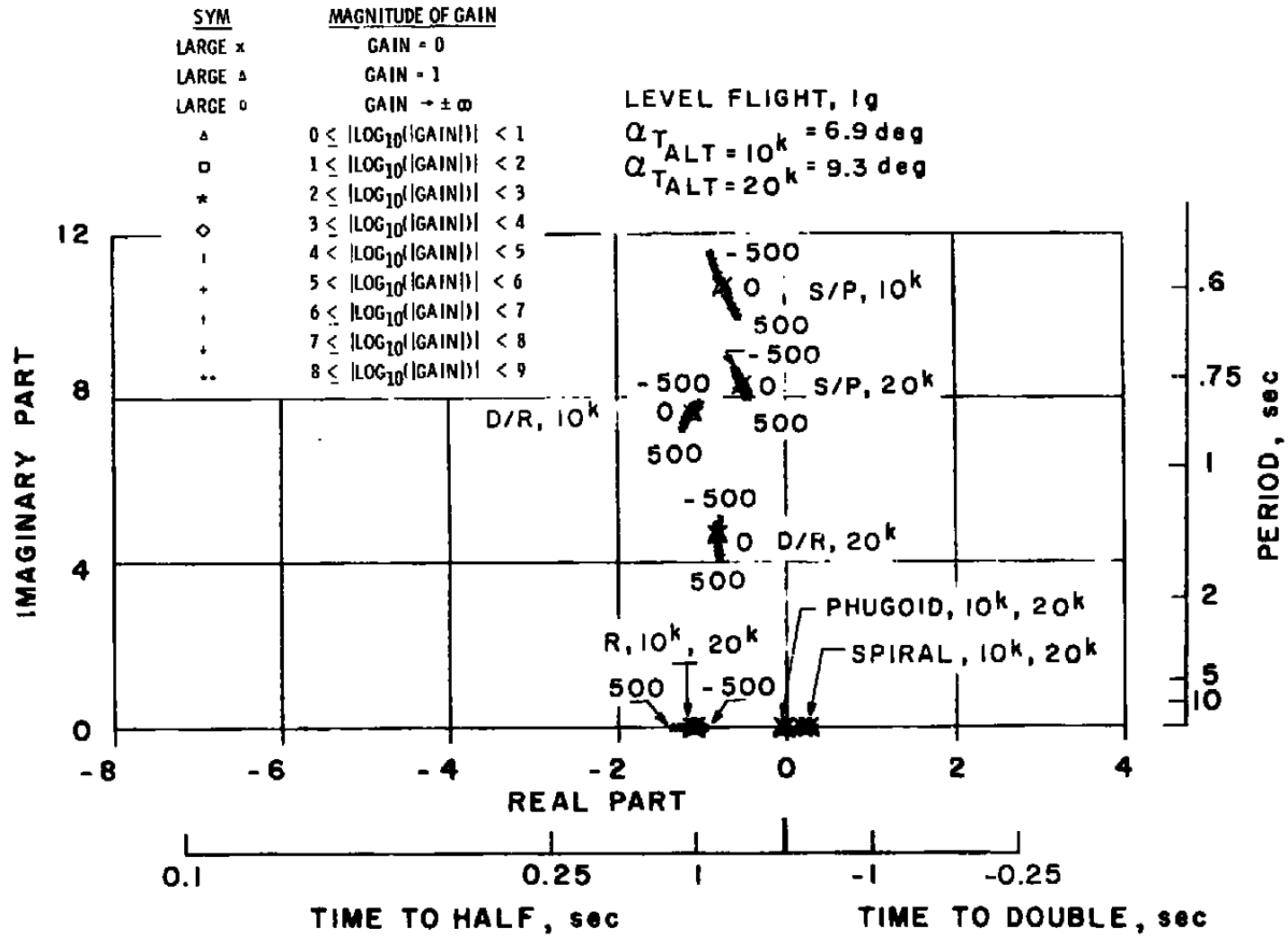

a. M = 1.3

Figure 38. Yaw-to-turn configuration - locus of roots with $C\ell_q$ variation.

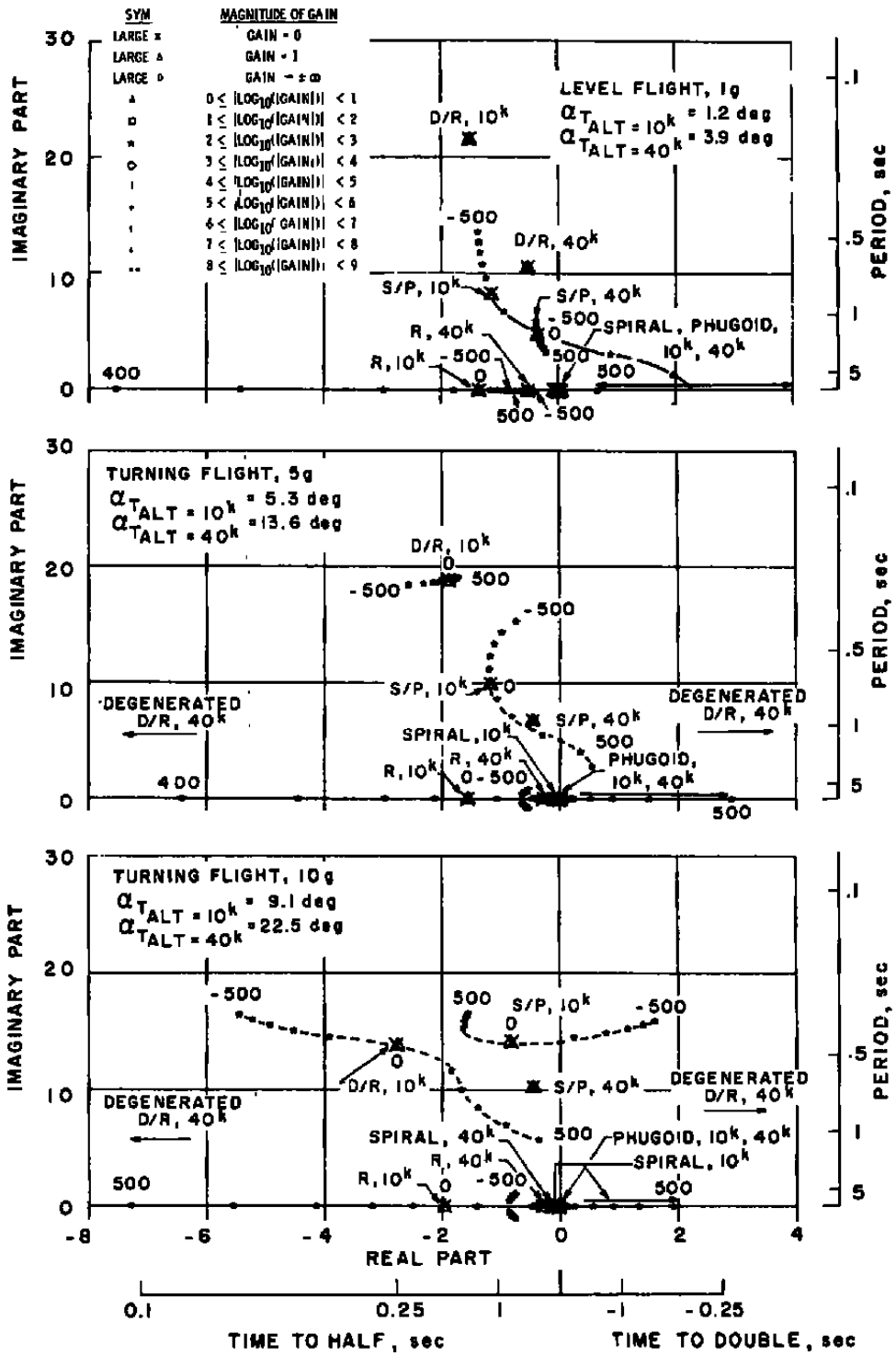

b. M = 3.0

Figure 38. Concluded.

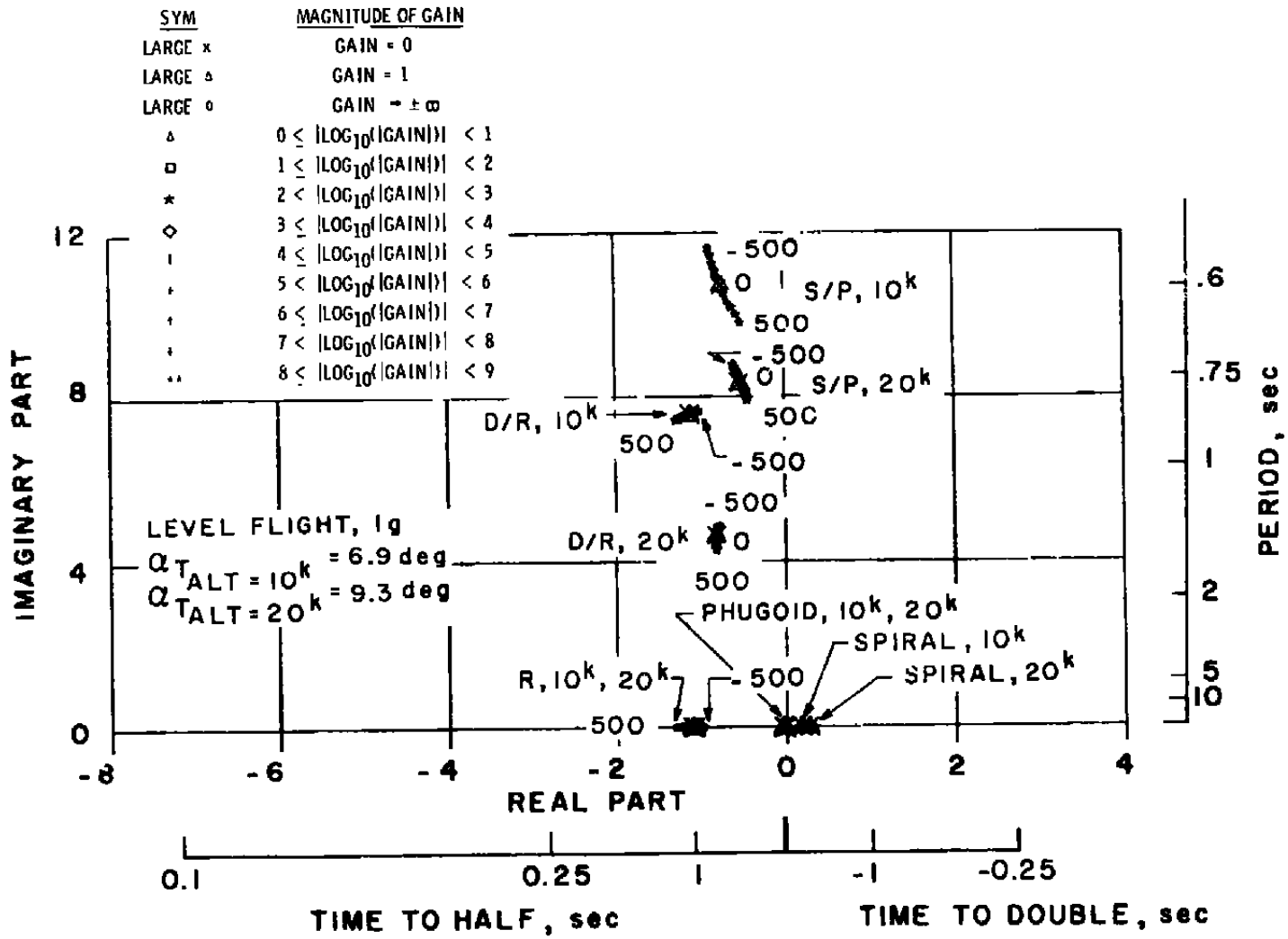

a. M = 1.3

Figure 39. Yaw-to-turn configuration - locus of roots with C_{m_p} variation.

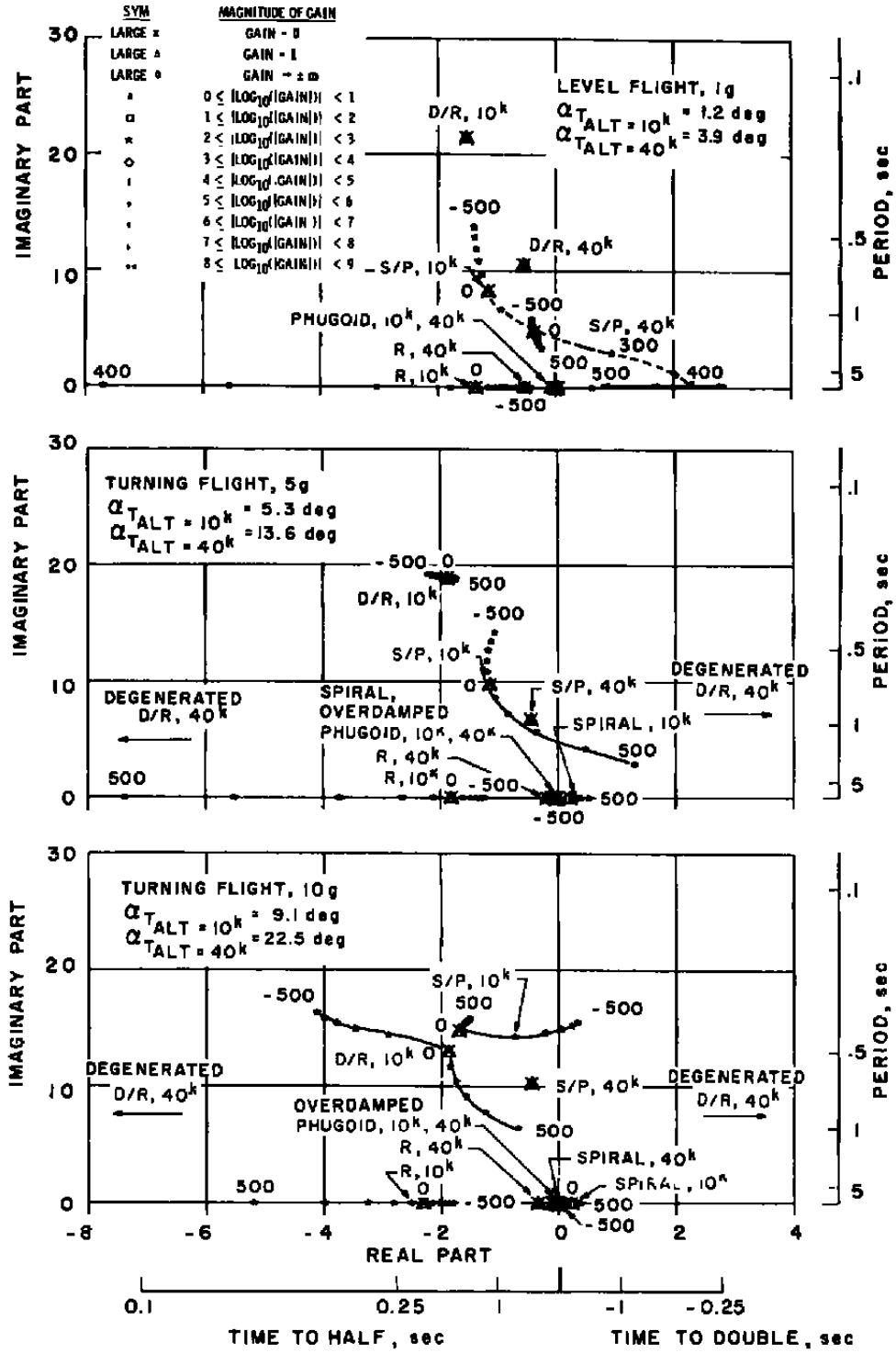

b. M = 3.0

Figure 39. Concluded.

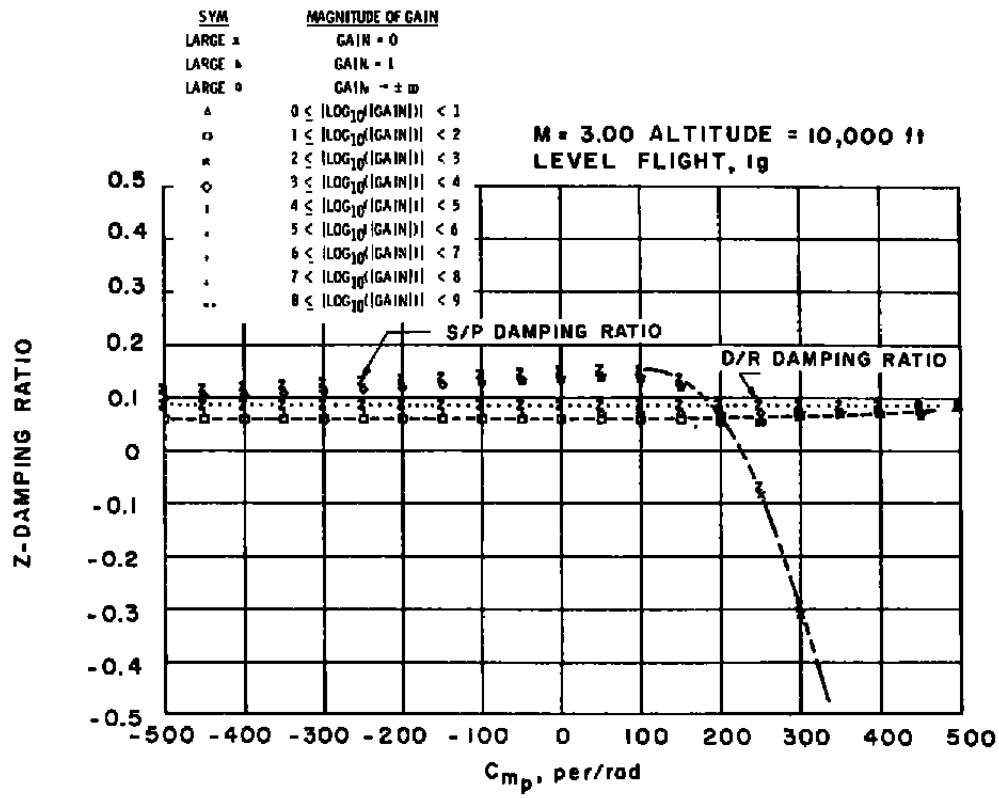

a. Damping ratio

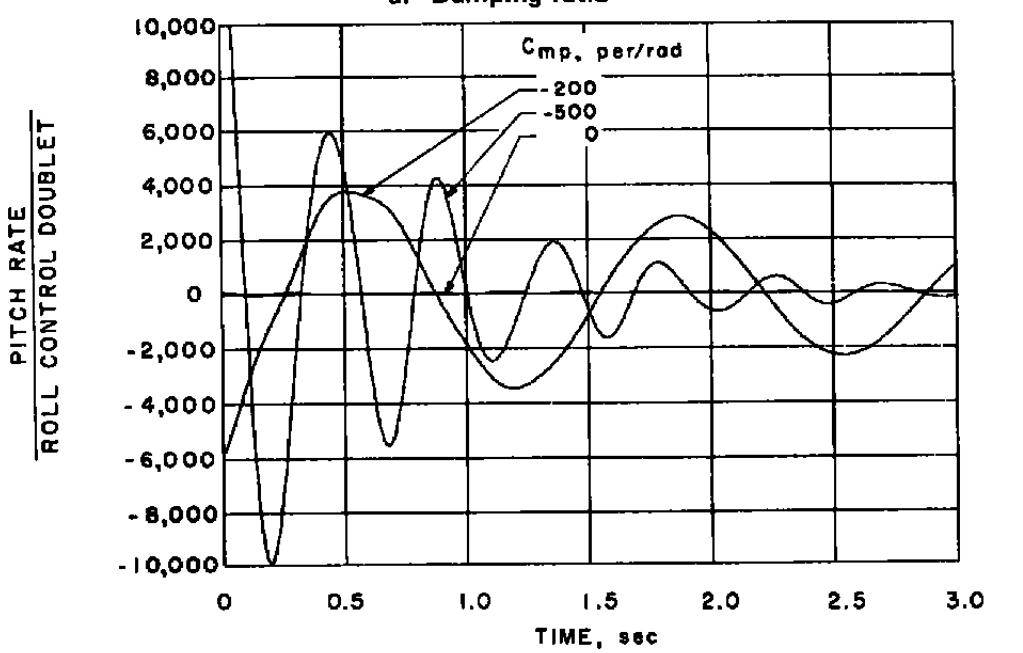

b. Time response

Figure 42. Yaw-to-turn configuration - effect of C_{m_p} on damping ratio and time response.

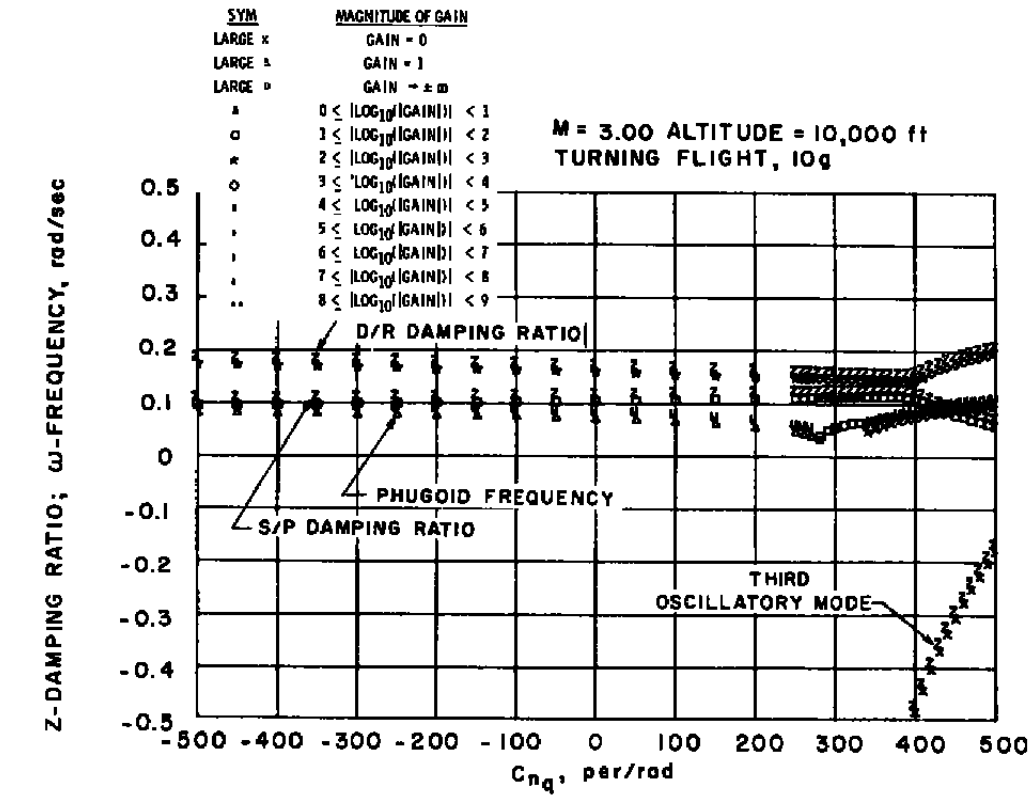

a. Damping ratio

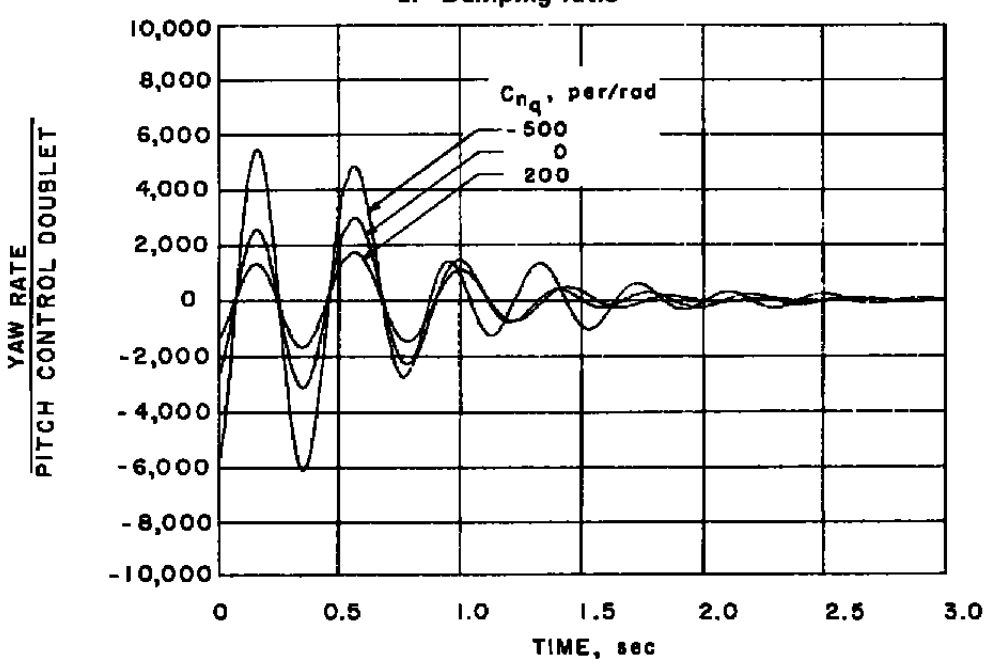

b. Time response

Figure 43. Yaw-to-turn configuration - effect of C_{n_q} on damping ratio and time response.

Table 1. Bank-To-Turn Configuration
a. M = 0.8, Altitude = 10,000 ft

Trim Values	Level Flight, 1 g	Turning Flight, 5 g	Turning Flight, 10 g
α(deg)	1.5	5.8	9.8
ϕ(deg)	0	78.5	84.3
$\dot{\psi}$(deg/sec)	0	10.5	21.3
C_{m_q} (per rad)	-264.9	-286.6	-301.3
$C_{m_{\dot{\alpha}}}$ (per rad)	0	0	0
C_{m_p} (per rad)	0	0	0
C_{m_r} (per rad)	0	0	0
C_{L_q} (per rad)	137.4	169.8	186.4
$C_{L_{\dot{\alpha}}}$ (per rad)	0	0	0
C_{n_r} (per rad)	-66.3	-67.0	-66.8
C_{n_p} (per rad)	-1.0	-7.4	-13.3
C_{n_q} (per rad)	0	0	0
C_{ℓ_r} (per rad)	13.4	13.8	14.3
C_{ℓ_p} (per rad)	-62.6	-62.8	-62.5
C_{ℓ_q} (per rad)	0	0	0
C_{y_r} (per rad)	0.3	0.2	0.2
C_{y_p} (per rad)	-0.7	0.6	1.8

Table 1. Continued
b. M = 0.8, Altitude = 40,000 ft

Trim Values	Level Flight, 1 g	Turning Flight, 5 g	Turning Flight, 10 g
α(deg)	4.4	15.1	24.7
ϕ(deg)	0	78.5	84.3
$\dot{\psi}$(deg/sec)	0	11.8	23.9
C_{m_q} (per rad)	-274.8	-311.2	-330.5
$C_{m_{\dot{\alpha}}}$ (per rad)	0	0	0
C_{m_p} (per rad)	0	0	0
C_{m_r} (per rad)	0	0	0
C_{L_q} (per rad)	157.6	205.4	231.0
$C_{L_{\dot{\alpha}}}$ (per rad)	0	0	0
C_{n_r} (per rad)	-66.9	-65.4	-60.8
C_{n_p} (per rad)	-5.3	-20.9	-33.3
C_{n_q} (per rad)	0	0	0
C_{ℓ_r} (per rad)	13.7	15.2	17.0
C_{ℓ_p} (per rad)	-62.7	-59.7	-58.7
C_{ℓ_q} (per rad)	0	0	0
C_{y_r} (per rad)	0.3	0.1	-0.1
C_{y_p} (per rad)	0.2	3.5	6.3

Table 1. Continued
c. M = 1.10, Altitude = 10,000 ft

Trim Values	Level Flight, 1 g	Turning Flight, 5 g	Turning Flight, 10 g
α(deg)	0.1	3.5	6.0
ϕ(deg)	0	78.5	84.2
$\dot{\psi}$(deg/sec)	0	7.6	15.4
C_{m_q} (per rad)	-335.7	-343.3	-367.3
$C_{m_{\dot{\alpha}}}$ (per rad)	0	0	0
C_{m_p} (per rad)	0	0	0
C_{m_r} (per rad)	0	0	0
C_{L_q} (per rad)	153.0	167.4	184.6
$C_{L_{\dot{\alpha}}}$ (per rad)	0	0	0
C_{n_r} (per rad)	-64.6	-65.1	-65.3
C_{n_p} (per rad)	-0.1	-3.3	-6.6
C_{n_q} (per rad)	0	0	0
C_{ℓ_r} (per rad)	10.0	10.2	10.5
C_{ℓ_p} (per rad)	-55.8	-56.4	-57.1
C_{ℓ_q} (per rad)	0	0	0
C_{Y_r} (per rad)	0.3	0.3	0.3
C_{Y_p} (per rad)	-1.0	-1.0	0.6

Table 1. Continued
d. M = 1.10, Altitude = 40,000 ft

Trim Values	Level Flight, 1 g	Turning Flight, 5 g	Turning Flight, 10 g
α(deg)	2.6	9.3	16.2
ϕ(deg)	0	78.5	84.2
$\dot{\psi}$(deg/sec)	0	8.5	17.4
C_{m_q} (per rad)	-339.7	-406.0	-425.8
$C_{m_{\dot{\alpha}}}$ (per rad)	0	0	0
C_{m_p} (per rad)	0	0	0
C_{m_r} (per rad)	0	0	0
C_{L_q} (per rad)	161.2	203.4	216.3
$C_{L_{\dot{\alpha}}}$ (per rad)	0	0	0
C_{n_r} (per rad)	-65.0	-65.0	-62.7
C_{n_p} (per rad)	-2.2	-10.8	-19.2
C_{n_q} (per rad)	0	0	0
C_{ℓ_r} (per rad)	10.1	10.9	12.4
C_{ℓ_p} (per rad)	-56.1	-58.0	-53.6
C_{ℓ_q} (per rad)	0	0	0
C_{y_r} (per rad)	0.3	0.2	0
C_{y_p} (per rad)	-0.3	1.5	3.4

Table 1. Continued
e. M = 3.50, Altitude = 10,000 ft

Trim Values	Level Flight, 1 g	Turning Flight, 10 g	Turning Flight, 25 g
α(deg)	0.2	1.1	2.6
ϕ(deg)	0	84.3	87.7
$\dot{\psi}$(deg/sec)	0	4.9	12.2
C_{m_q} (per rad)	-227.0	-228.1	-230.4
$C_{m_{\dot{\alpha}}}$ (per rad)	0	0	0
C_{m_p} (per rad)	0	0	0
C_{m_r} (per rad)	0	0	0
C_{L_q} (per rad)	122.0	122.4	123.5
$C_{L_{\dot{\alpha}}}$ (per rad)	0	0	0
C_{n_r} (per rad)	-31.7	-31.8	-32.0
C_{n_p} (per rad)	0.7	0.1	-0.9
C_{n_q} (per rad)	0	0	0
C_{ℓ_r} (per rad)	4.5	4.6	4.6
C_{ℓ_p} (per rad)	-40.5	-40.6	-40.8
C_{ℓ_q} (per rad)	0	0	0
C_{y_r} (per rad)	0.2	0.2	0.2
C_{y_p} (per rad)	-0.7	-0.6	-0.3

Table 1. Concluded
f. M = 3.50, Altitude = 40,000 ft

Trim Values	Level Flight, 1 g	Turning Flight, 10 g	Turning Flight, 25 g
α(deg)	.5	3.6	8.4
ϕ(deg)	0	84.3	87.7
$\dot{\psi}$(deg/sec)	0	5.5	13.7
C_{m_q} (per rad)	-227.4	-232.3	-252.2
$C_{m_{\dot{\alpha}}}$ (per rad)	0	0	0
C_{m_p} (per rad)	0	0	0
C_{m_r} (per rad)	0	0	0
C_{L_q} (per rad)	122.1	124.7	131.4
$C_{L_{\dot{\alpha}}}$ (per rad)	0	0	0
C_{n_r} (per rad)	-31.7	-32.1	-32.4
C_{n_p} (per rad)	0.6	-1.6	-4.9
C_{n_q} (per rad)	0	0	0
C_{ℓ_r} (per rad)	4.5	4.7	4.9
C_{ℓ_p} (per rad)	-40.5	-41.0	-42.0
C_{ℓ_q} (per rad)	0	0	0
C_{y_r} (per rad)	0.2	0.2	0.3
C_{y_p} (per rad)	-0.7	-0.1	1.0

Table 2. Yaw-To-Turn Configuration
a. M = 1.3

Trim Values	Altitude = 10,000 ft, Level Flight, 1 g	Altitude = 20,000 ft, Level Flight, 1 g
α	6.5	9.3
φ	0	0
$\dot{\psi}$	0	0
C_{m_q}	-409.7	-398.7
$C_{m_{\dot{\alpha}}}$	0	0
C_{m_p}	0	0
C_{m_r}	0	0
C_{L_q}	0	0
$C_{L_{\dot{\alpha}}}$	0	0
C_{n_r}	-389.3	-309.7
C_{n_p}	-4.1	-5.1
C_{n_q}	0	0
C_{ℓ_r}	0	0
C_{ℓ_p}	-4.9	-5.1
C_{ℓ_q}	0	0
C_{Y_r}	0	0
C_{Y_p}	0.8	0.8

Table 2. Continued
b. M = 3.0, Altitude = 10,000 ft

Trim Values	Level Flight, 1 g	Turning Flight, 5 g	Turning Flight, 10 g
α	1.2	5.3	9.1
ϕ	0	78.5	84.3
$\dot{\psi}$	0	2.8	5.7
C_{m_q}	-298.0	-287.7	-302.9
$C_{m_{\dot{\alpha}}}$	0	0	0
C_{m_p}	0	0	0
C_{m_r}	0	0	0
C_{L_q}	0	0	0
$C_{L_{\dot{\alpha}}}$	0	0	0
C_{n_r}	-309.7	-307.0	-244.5
C_{n_p}	-0.8	-0.5	-1.2
C_{n_q}	0	0	0
C_{ℓ_r}	0	0	0
C_{ℓ_p}	-3.2	-3.6	-3.7
C_{ℓ_q}	0	0	0
C_{y_r}	0	0	0
C_{y_p}	-0.6	-0.2	-0.1

Table 2. Concluded
c. M = 3.0, Altitude = 40,000 ft

Trim Values	Level Flight, 1 g	Turning Flight, 5 g	Turning Flight, 10 g
α	3.9	13.6	22.5
ϕ	0	78.5	84.3
$\dot{\psi}$	0	3.2	6.4
C_{m_q}	-287.9	-303.8	-301.8
$C_{m_{\dot{\alpha}}}$	0	0	0
C_{m_p}	0	0	0
C_{m_r}	0	0	0
C_{L_q}	0	0	0
$C_{L_{\dot{\alpha}}}$	0	0	0
C_{n_r}	-310.0	-182.7	-172.6
C_{n_p}	-0.5	-3.0	-6.5
C_{n_q}	0	0	0
C_{ℓ_r}	0	0	0
C_{ℓ_p}	-3.5	-3.7	-4.1
C_{ℓ_q}	0	0	0
C_{y_r}	0	0	0
C_{y_p}	-0.2	0.1	1.0

Table 3. Missile Physical and Mass Characteristics

	Bank-to-Turn	Yaw-to-Turn
Mass	5.75 slugs	43.80 slugs
I_X(body axis)	0.34 slug-ft^2	9.4 slug-ft^2
I_Y(body axis)	34.1 slug-ft^2	745 slug-ft^2
I_Z(body axis)	34.15 slug-ft^2	745 slug-ft^2
I_{XZ}(body axis)	0.0 slug-ft^2	0.0 slug-ft^2
s	0.458 ft^2	1.54 ft^2
d	0.7633 ft	1.4 ft
ℓ	8.9 ft	14 ft
cg	50 percent body length	50 percent body length

APPENDIX

EQUATIONS DEFINING THE TOTAL AERODYNAMIC DATA IN THE STABILITY AXIS SYSTEM

Longitudinal

$$F_X = \bar{q}S\left[C_D(\alpha, \delta_p, M)\right]$$

$$F_Z = \bar{q}S\left[C_L(\alpha, \delta_p, M) + C_{L_q}\left(\frac{qd}{2V}\right) + C_{L_{\dot{\alpha}}}\left(\frac{\dot{\alpha}d}{2V}\right)\right]$$

$$M_Y = \bar{q}Sd\left[C_m(\alpha, \delta_p, M) + C_{m_q}(\alpha, M)\left(\frac{qd}{2V}\right) + C_{m_{\dot{\alpha}}}\left(\frac{\dot{\alpha}d}{2V}\right) + C_{m_p}\left(\frac{pd}{2V}\right) + C_{m_r}\left(\frac{rd}{2V}\right)\right]$$

Lateral-Directional

$$F_Y = \bar{q}S\left[C_{y_\beta}(\alpha, M)\beta + C_{y_{\delta_y}}(\alpha, M)\delta_y + C_{y_p}(\alpha,M)\left(\frac{pd}{2V}\right) + C_{y_r}(\alpha,M)\left(\frac{rd}{2V}\right)\right]$$

$$M_Z = \bar{q}Sd\left[C_{n_\beta}(\alpha, M)\beta - C_{n_{\delta_y}}(\alpha,M)\delta_y + C_{n_{\delta_r}}(\alpha,M)\delta_r - C_{n_p}(\alpha,M)\left(\frac{pd}{2V}\right)\right.$$

$$\left. + C_{n_r}(\alpha,M)\left(\frac{rd}{2V}\right) + C_{n_q}\left(\frac{qd}{2V}\right)\right]$$

$$M_X = \bar{q}Sd\left[C_{\ell_\beta}(\alpha,M)\beta + C_{\ell_{\delta_y}}(\alpha, M)\delta_y + C_{\ell_{\delta_r}}(\alpha,M)\delta_r - C_{\ell_p}(\alpha,M)\left(\frac{pd}{2V}\right)\right.$$

$$\left. + C_{\ell_r}(\alpha,M)\left(\frac{rd}{2V}\right) + C_{\ell_q}\left(\frac{qd}{2V}\right)\right]$$

where

δ_p = Pitch Control

δ_R = Roll Control

δ_Y = Yaw Control

Bank-to-Turn Missile		Yaw-to-Turn Missile	
	Data Matrix Variables		
α	-6 to 26 deg	α	0 to 24 deg
M	0.8 to 3.5	M	0.6 to 3.0
δ_p	-10 to 20 deg	δ_p	-20 to 20 deg
	Control Authority		
δ_p	-10 to 20 deg	δ_p	-20 to 20 deg
δ_R	-20 to 20 deg	δ_R	-20 to 20 deg
δ_y	-20 to 20 deg	δ_y	-20 to 20 deg

NOMENCLATURE

(Note: All aerodynamic data are referenced to the stability axis system.)

C_D Drag-force coefficient, drag force/$\bar{q}S$

C_L Lift-force coefficient, lift force/$\bar{q}S$

C_{L_q} Derivative of lift-force coefficient with respect to pitch rate, $\partial C_L/\partial(qd/2V)$, per radian

$C_{L_{\dot{\alpha}}}$ Derivative of lift-force coefficient with respect to $\dot{\alpha}$, $\partial C_L/\partial(\dot{\alpha}d/2V)$, per radian

C_{ℓ_p} Derivative of rolling-moment coefficient with respect to roll rate, $\partial C_\ell/\partial(pd/2V)$, per radian

C_{ℓ_q} Derivative of rolling-moment coefficient with respect to pitch rate, $\partial C_\ell/\partial(qd/2V)$, per radian

C_{ℓ_r} Derivative of rolling-moment coefficient with respect to yaw rate, $\partial C_\ell/\partial(rd/2V)$, per radian

$C_{\ell_{\dot{\alpha}}}$ Derivative of rolling-moment coefficient with respect to $\dot{\alpha}$, $\partial C_\ell/\partial(\dot{\alpha}d/2V)$, per radian

C_{ℓ_β} Derivative of rolling-moment coefficient with respect to angle of sideslip, $\partial C_\ell/\partial\beta$, per radian

$C_{\ell_{\dot{\beta}}}$ Derivative of rolling-moment coefficient with respect to $\dot{\beta}$, $\partial C_\ell/\partial(\dot{\beta}d/2V)$, per radian

$C_{\ell_{\delta_R}}$ Derivative of rolling-moment coefficient with respect to δ_R, $\partial C_\ell/\partial\delta_R$, per radian

$C_{n_{\delta_y}}$ Derivative of rolling-moment coefficient with respect to δ_Y, $\partial C_\ell/\partial\delta_y$, per radian

C_m Pitching-moment coefficient, pitching moment/$\bar{q}Sb$

C_{m_p} Derivative of pitching-moment coefficient with respect to roll rate, $\partial C_m/\partial(pd/2V)$, per radian

C_{m_q} Derivative of pitching-moment coefficient with respect to pitch rate, $\partial C_m/\partial(qd/2V)$, per radian

C_{m_r} Derivative of pitching-moment coefficient with respect to yaw rate, $\partial C_m/\partial(rd/2V)$, per radian

$C_{m_{\dot{\alpha}}}$ Derivative of pitching-moment coefficient with respect to $\dot{\alpha}$, $\partial C_m/\partial(\dot{\alpha}d/2V)$, per radian

$C_{m_{\dot{\beta}}}$ Derivative of pitching-moment coefficient with respect to $\dot{\beta}$, $\partial C_m/\partial(\dot{\beta}d/2V)$, per radian

C_n Yawing-moment coefficient, yawing moment/$\bar{q}Sd$ about missile cg

C_{n_p} Derivative of yawing-moment coefficient with respect to roll rate, $\partial C_n/\partial(pd/2V)$, per radian

C_{n_q} Derivative of yawing-moment coefficient with respect to pitch rate, $\partial C_n/\partial(qd/2V)$, per radian

C_{n_r} Derivative of yawing-moment coefficient with respect to yaw rate, $\partial C_n/\partial(rd/2V)$, per radian

$C_{n_{\dot{\alpha}}}$ Derivative of yawing-moment coefficient with respect to $\dot{\alpha}$, $\partial C_n/\partial(\dot{\alpha}d/2V)$, per radian

C_{n_β} Derivative of yawing-moment coefficient with respect to angle of sideslip, $\partial C_n/\partial\beta$, per radian

$C_{n_{\dot{\beta}}}$ Derivative of yawing-moment coefficient with respect to $\dot{\beta}$, $\partial C_n/\partial(\dot{\beta}d/2V)$, per radian

$C_{n_{\delta_R}}$ Derivative of yawing-moment coefficient with respect to δ_R, $\partial C_n/\partial\delta_R$, per radian

$C_{n_{\delta_y}}$ Derivative of yawing-moment coefficient with respect to δ_Y, $\delta C_n/\partial\delta_y$, per radian

C_{y_p} Derivative of side-force coefficient with respect to roll rate, $\partial C_y/\partial(pd/2V)$, per radian

C_{y_r} Derivative of side-force coefficient with respect to yaw rate, $\partial C_y/\partial(rd/2V)$, per radian

C_{y_β} Derivative of side-force coefficient with respect to angle of sideslip, $\partial C_y/\partial\beta$, per radian

$C_{y_{\delta_y}}$ Derivative of side-force coefficient with respect to δ_y, $\partial C_y/\partial\delta_y$, per radian

cg	Center-of-gravity location, percent body length
D/R	Dutch roll
d	Reference body diameter, ft
F_X	Force acting along X-stability axis, lb
F_Y	Force acting along Y-stability axis, lb
F_Z	Force acting along Z-stability axis, lb
g	Acceleration of gravity, ft/sec^2
I_X, I_Y, I_Z	Moments of inertia about X-, Y-, and Z-body axes, respectively, slug-ft^2
I_{XZ}	Product of inertia, slug-ft^2
j	Imaginary number, -1
M	Mach number
M_X	Moment acting about X-stability axis, ft-lb
M_Y	Moment acting about Y-stability axis, ft-lb
M_Z	Moment acting about Z-stability axis, ft-lb
m	Mass, slugs
p,q,r	Components of $\vec{\Omega}$ about X-, Y-, and Z-body axes, respectively, radian/sec
$\bar{q}$	Dynamic pressure, $\varrho V^2/2$, lb/ft^2
S	Body reference area, ft^2
S/P	Short period
V	Total velocity, ft/sec
W_n, W	Undamped natural frequency, radian/sec
Z	Damping ratio
α	Angle of attack, deg
β	Angle of side force, deg

δ_p	Pitch control deflection, per radian
δ_R	Roll control deflection, per radian
δ_y	Yaw control deflection, per radian
ϱ	Air density, slug/ft^3
σ	Real part of complex variable
ϕ	Angle of roll, deg

SUPERSCRIPT

	Derivative with respect to time
K	1,000 of feet